9-2009

Intermolecular Electron Transfer Reactivity and Dynamics of Cytochrome c – Nanoparticle Adducts

Adrienne M. Carver
University of Massachusetts Amherst, agilbert@chem.umass.edu

INTERMOLECULAR ELECTRON TRANSFER REACTIVITY AND DYNAMICS OF CYTOCHROME *c* – NANOPARTICLE ADDUCTS

A Dissertation Presented

By

Adrienne M. Carver

Submitted to the Graduate School of the
University of Massachusetts Amherst in partial fulfillment
of the requirements for the degree of

DOCTOR OF PHILOSOPHY

September 2009

Chemistry

INTERMOLECULAR ELECTRON TRANSFER REACTIVITY AND DYNAMICS OF CYTOCHROME *c* – NANOPARTICLE ADDUCTS

A Dissertation Presented

By

Adrienne M. Carver

Approved as to style and content by:

_____
Michael J. Knapp, Chair

_____
Michael J. Maroney, Member

_____
Sankaran Thayumanavan, Member

_____
Gregory Tew, Member

_____
Bret Jackson, Department Head
Department of Chemistry

DEDICATION

To my loving, supportive, and very patient parents.

ACKNOWLEDGEMENTS

I would like to thank Dr. Michael Knapp for his dedication and encouragement throughout my graduate studies. Without your patience and guidance, I would have never finished. Whenever I strayed off the path, you guided me back in the correct direction. I realize I'm a tough sell, but you sold me on my second project that resulted in something I take pride in. I also want to thank the other Knapp group members, Meaghan, Halil, Robert, Shannon, and Evren, for your help and support. I particularly want to thank the other "girls" of the lab, Meaghan and Shannon. I enjoyed your company and greatly benefited from your encouragement and support.

I would also like to thank my committee members, Dr. Michael Maroney, Dr. Sankaran Thayumanavan, and Dr. Gregory Tew for their comments and constructive criticism that helped better shape my work. I'd also like to thank Dr. Michael Maroney for the use of the stopped-flow instrument. I'd also like to thank the Dr. Vincent Rotello lab for providing nanoparticle samples and the Dr. Charles Scholes lab for providing Cyt *c* mutants.

Finally, I want to thank my family for their love and support. My parents not only told me that I could achieve anything I wanted, but also granted me the encouragement, support, opportunity, and resources in which to pursue my goals. You were always patient with me, despite my seemingly constant, unconscious efforts to test its limits. I want to thank Dad for his late night talks of encouragement that I miss. I want to thank mom for being only a phone call away, for being a great listener, and for granting me good advice and good company. I miss you both. I want to thank you for being in the audience at my final defense, yet again supporting me in finishing another life chapter. I lastly want to thank my husband Jared for moving half way across the country for me to pursue my education, working hard and tirelessly to

support me, yet again following me to the next destination, and for providing me with a lovely home that you practically built with your bare hands (and a lot of tools!). I look forward to what lies ahead of us.

ABSTRACT

INTERMOLECULAR ELECTRON TRANSFER REACTIVITY AND DYNAMICS OF CYTOCHROME *c* – NANOPARTICLE ADDUCTS

SEPTEMBER 2009

ADRIENNE M. CARVER, B.S., PURDUE UNIVERSITY

Ph.D., UNIVERSITY OF MASSACHUSETTS AMHERST

Directed by: Professor Michael J. Knapp

Interprotein electron transfer (ET) is crucial for natural energy conversion and a fundamental reaction in the pursuit of understanding the broader problem of protein-protein interactions and reactivity. Simplifying the complicated nature of these natural systems has driven development of biomimetic approaches. Functionalized gold nanoparticles offer simplified, tunable surfaces that can serve as a proxy to study the reactivity and dynamics of proteins.

Amino-acid functionalized gold nanoparticles (**Au-TX**) served as a complementary partner to cytochrome *c* (Cyt *c*) and catalyzed its ET reactivity without altering the native structure. Redox mediator and EPR experiments confirmed that the redox potential and coordination environment of the heme were unaltered. Varying the functionality of **Au-TX** under limiting redox reagent concentrations resulted in distinct ET reactivity. These conditions reflected the collision of a small redox reagent with the Cyt *c*/**Au-TX** adduct, introducing the possibility of Cyt *c*/**Au-TX** dynamics to modulate ET. Under high ionic strength conditions, the rate enhancement ranged from 0.0870×10^{11} for Cyt *c*/**Au-TAsp** to 1.95×10^{11} M^{-1} s^{-1} for Cyt *c*/**Au-TPhe**. **Au-TAsp** binds to a larger surface of the front face of Cyt *c* than **Au-TPhe**, likely reducing heme access and resulting in attenuated ET reactivity.

Site-directed spin-labeling characterized the dynamic interactions and motion of Cyt *c* with **Au-TX**. Several mutants of Cyt *c* were utilized to extract information about the different dynamics of the Cyt *c*/**Au-TPhe** and Cyt *c*/**Au-TAsp** systems. Cyt *c* appeared to have a highly dynamic binding interaction with the surface of **Au-TPhe** while binding to **Au-TAsp** resulted in a more rigid interface, particularly at the heme crevice. The dynamic interaction of Cyt *c*/**Au-TX** at the heme crevice could promote a gated ET mechanism between Cyt *c* and its redox partner. Thus, the reduced reactivity of Cyt *c*/**Au-TAsp** is likely a result of both slower global dynamics and more rigid binding near the heme crevice.

CONTENTS

LIST OF TABLES

LIST OF FIGURES

LIST OF SCHEMES

LIST OF CHARTS

LIST OF ABBREVIATIONS

ACN	acetonitrile
bpy	2,2'-bipyridine
CAO	copper amine oxidase
CH_2Cl_2	dichloromethane
CH_3CN	acetonitrile
Cu(bppa)	copper(II) bis-pyridyl phenolamine
Cu(icoph)	copper (II) bis-iminocatechol *o*-phenylenediamine
Cu(salben)	copper (II) *N,N'*-disalicylidene-1,4-butylenediamine
Cu(salen)	copper (II) *N,N'*-disalicylidene-1,2-ethylenediamine
Cu(salophen)	copper (II) *N,N'*- *o*-phenylenebis(salicylideneimine)
Cu(salpen)	copper (II) *N,N'*-disalicylidene-1,3-propylenediamine
Cyt *c*	cytochrome *c*
DEPC	diethylpyrocarbonate
dmbpy	4,4'-dimethyl bipyridine
dombpy	4,4'-dimethoxy bipyridine
DTT	dithiothreitol
EPR	electron paramagnetic resonance spectroscopy
ET	electron transfer
GalOx	galactose oxidase
Hbppa	bis-pyridyl phenolamine
H_2icoph	bis-iminocatechol *o*-phenylenediamine
H_2salxn	bis-salicylidinediamine
MOPS	3-morpholinopropanesulfonic acid
MS	mass spectrometry

MTSSL	1-oxyl-2,2',5,5'-tetramethylpyrroline-3-methyl-methanethiosulfonate
MWCO	molecular weight cut-off
NP	nanoparticle
PCET	proton-coupled electron transfer
$PhO^{\bullet}$	phenoxyl radical
SDSL	site-directed spin labeling
SL	spin label
SL-Cyt *c*	spin-labeled cytochrome *c*
TBA	tetra-n-butylammonium hexafluorophosphate
TEG	tetra(ethylene glycol)
Tris	tris(hydroxymethyl)-aminomethane
Zn(salophen)	zinc (II) *N,N'*- *o*-phenylenebis(salicylideneimine)

CHAPTER 1

INTRODUCTION

1.1. Introduction

Nanoparticles (NP) are increasingly utilized for many applications, including as artificial receptors, catalysts, sensors, and molecules that promote self assembly. These materials couple the optical, electronic, and magnetic properties of NPs to the specific function of proteins or other biomacromolecules.[1] NPs offer size and material dependent chemical properties that are tunable to the desired system or function.[2,3] Despite the heavy interest in these systems, much is still unknown about the interactions and interface between NPs and proteins. NPs can have a large surface covered with dynamic ligands, which complicates the interface between the two macromolecules and often promotes non-specific, protein denaturing interactions. Minimizing unproductive and even detrimental interactions is key in the utilization of NPs in materials and biological systems. There is much potential for NPs in medical applications because their size grants them access into cells. However, increasing awareness of the possible negative ramifications of these relatively poorly characterized systems within the body is severely limiting.[4,5] Understanding and manipulating the interface and interactions of NPs with biological molecules will greatly increase their potential in the fields of medicine, catalysis, molecular recognition, sensing, and bioassembly.

1.2. Molecular recognition and catalysis using nanoparticles

Nanoparticles influence the interactions and reactivity of proteins and other biological molecules. NPs are promising candidates for proxies or biomolecular receptors because their similar size and large surface area that provides a tunable

interface for binding biomacromolecules.[2,6,7] Various examples exist, showcasing different properties and advantages of NPs as artificial receptors.[8] Pasquato and Scrimin et al. synthesized gold nanoclusters covered with thiol-terminated amino acids which served as multivalent catalysts for the cleavage of carboxylic esters and phosphate esters.[9] Confinement of the monomers by the monolayer resulted in altered binding and catalysis. Rotello et al. demonstrated a more general and less synthetically demanding approach in which amino acid functionalized gold NPs altered the reactivity of α-chymotrypsin by electrostatically controlling substrate capture and product release. The specificity of positive substrates was increased while anionic substrates decreased.[10] Lastly, work contained within this thesis reported the enhancement of intermolecular electron transfer rate of Cyt *c* with a small redox reagent in which a gold NP catalytically increased the rate by 10^5 M^{-1} s^{-1}, the largest NP assisted rate enhancement yet reported (Figure 1.1).[11] The surface functionalization and electrostatic attraction of the NP can greatly influence biological systems.

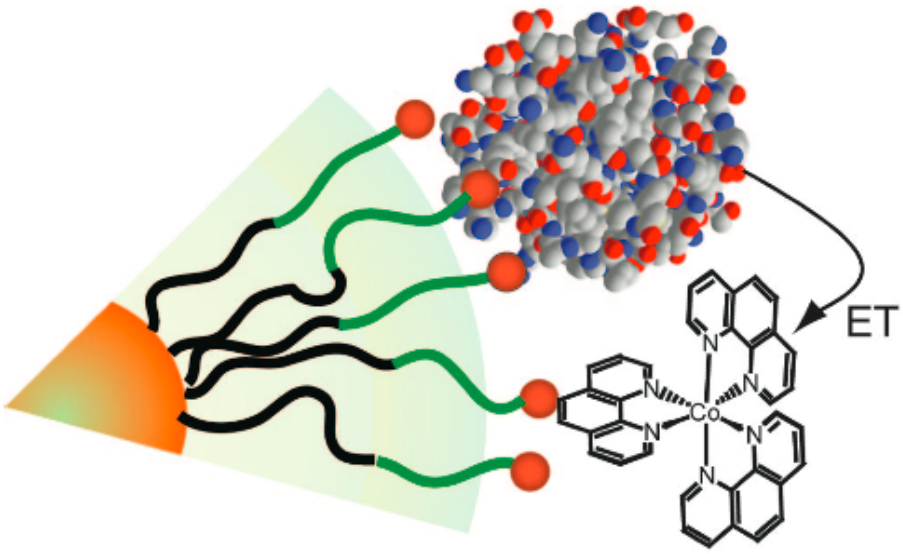

Figure 1.1. Encounter complex for ET from Cyt *c* to $Co(phen)_3^{3+}$ on the surface of **Au-TX**. Illustration reprinted from *J. Am. Chem. Soc.* **2009**, *131*, 3798-9.

Nanoparticles also disrupt or serve as proxies in protein-protein interactions. The Knapp group demonstrated that functionalized gold NPs disrupt the interaction between cytochrome *c* and cytochrome *c* peroxidase and bind to either protein selectively based upon the charges of the NP surface layer.[12] This extended into facial selectivity of NP binding to Cyt *c*, again influenced by the identity of the NP surface layer. A gold NP functionalized with hydrophilic aspartic acid groups bound to the front face of Cyt *c*, similar to Cyt *c* oxidase. However, hydrophobic phenylalanine groups shifted this binding interface to a smaller area around Lys^{72}, similar to Cyt *c* peroxidase.[13]

There is growing concern over the negative ramifications of the often strong, nonspecific interactions between various types of NPs and proteins, leading to a large increase in toxicity studies. NPs have large surface areas that quickly become covered with numerous proteins when they enter biological fluids. The outer layer, or "corona," determines the biological response to the NP (Figure 1.2). To complicate the matter, the corona is not static as many proteins have different binding and exchange rates with the surface.[4,14,15] Additionally, several types of NPs, including quantum dots, cerium oxide particles, and carbon nanotubes, have been shown to increase the rate of protein fibrillation, which is involved in numerous diseases. The surfaces increase the probability of protein fibril nucleation.[16] While the potential of NPs in molecular recognition and catalysis is great, clearly the interactions between many NPs and proteins are still ill defined and further characterization is necessary before widespread use, particularly in medicine.

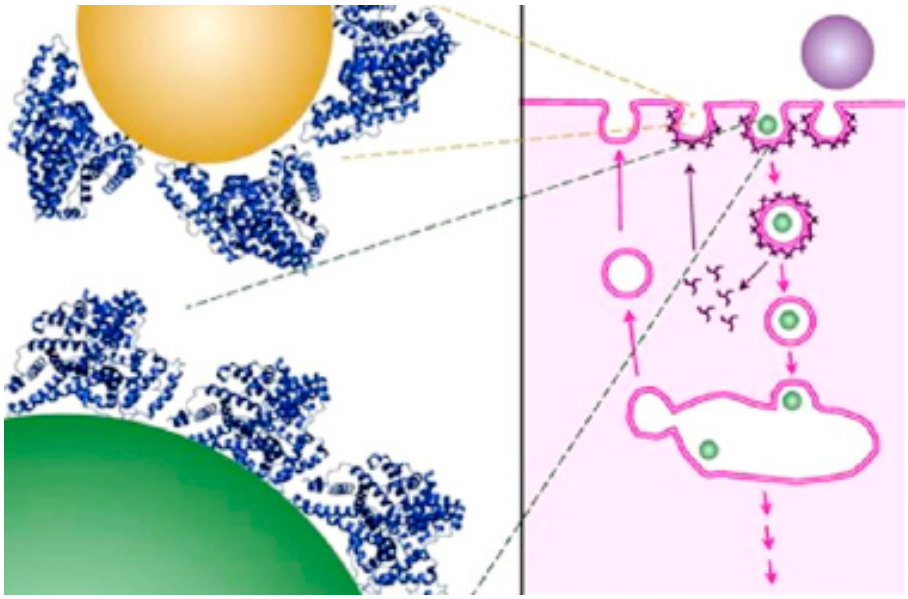

Figure 1.2. Nanoparticles coated by a protein "corona" undergoing receptor mediated endocytosis. Illustration reprinted with permission from *Adv. Colloid Interface Sci.* **2007**, *134-135*, 167-74.

1.3. Nanoparticle-based biological sensors

Many biological sensors exploit the unique optical and electronic properties of NPs and how they change in the presence of biological macromolecules. Yi Liu et al. designed a gold NP based colormetric sensor in which the Cu^{2+} dependent DNAzyme catalyzed ligation products that directed the assembly of DNA functionalized gold NP to detect Cu^{2+} concentrations.[17] The Mirkin group also used a DNA functionalized gold NPs in a competition assay that screens the sequence selectivity of DNA-binding molecules for potential drug candidates.[18] Another assay developed by Scrimin et al. again uses the unique optical properties of gold colloids to visually detect a protease at the low nanomolar range. The simplicity of using commercially available NPs for visual detection is appealing over the ELISA assay that requires high affinity protein specificity and receptors.[19] Colormetric approaches take advantage of the high extinction coeffcient

of gold NPs and how its optical properties are influenced through binding other molecules.

Many sensors rely on specific surface functionalization with biological molecules or the intrinsic optical properties of NPs to detect biomacromolecules. Mirkin et al. designed a PCR-free assay for the enzyme telomerase, which is an important biomarker in cancer diagnosis. The oligonucleotide-NP conjugates bind and amplify substrates to detect telomerase activity.[20] Another sensor involves oligonucleotide-NP and magnetic microparticles with antibodies as bio-barcodes to target specific proteins.[21] Aptamer-functionalized gold NPs are used as protein sensors, including one that amplifies the detection of thrombin. When the aptamers bind thrombin, the NPs aggregate and the absorbance spectra shifted and intensified. The catalytic enlargement of the NPs had a sensitivity limit of 2 nM. Another approach uses a fluorescence resonance energy transfer based inhibition assay that relies upon the photoluminescence quenching of streptavidin-conjugated quantum dots by biotin-labeled gold NPs. This assay detects molecules that inhibit specific biomolecular interactions and could be adapted for high throughput screening.[22] NPs can either serve as scaffolds or directly bind and interact with proteins for sensing applications.

1.4. Bioassembly using nanoparticles

The assembly of hybrid materials containing NPs and proteins aims to combine the size-dependent electronic, optical, and magnetic properties of NPs with the biological functionality of proteins and other biomacromolecules. The interactions between NPs and biological molecules template these structures. Rotello et al. used functionalized gold NPs to catalyze the ligation of peptide fragments by providing complementary

electrostatic interactions on the NP surface.[23] The Rotello group also designed structured aggregates of gold NPs with the proteins α-ChT and Cyt *c* which had controlled interparticle spacing, relying on molecular recognition to drive the self assembly.[24]

Protein-nanoparticle complexes with precisely controlled geometry, orientation, and stiochiometry can be formed using strategically placed genetic tags in proteins. Gold NPs functionalized with nitrilotriacetic acid groups bound histidine tags in proteins to form a structurally controlled protein-NP complex.[25] Another system used gold NP catalysts to template vertical Ge nanowires with controlled size and orientation.[26] NPs offer a tailorable scaffold or a large functionalizable surface to template biomolecules. More precisely controlled assembly strategies will lead to valuable self-assembling hybrid materials.

1.5. Reactivity of copper(II) coordinated phenolates

The second project presented within this thesis (Chapter 5) was earlier work that involved synthetic catalysts based upon stabilized phenoxyl radicals directly coordinated to Cu(II) centers and resulted in a single publication.[27] Redox-active amino acids are an important class of redox cofactors,[28-30] such as the tyrosyl-radical cofactors found in galactose oxidase (GalOx) and copper amine oxidase (CAO) that are covalently modified at the phenolic ring and require Cu(II) for normal function.[31-34] The reactivity of metal coordinated phenolates was investigated as a model of the proposed copper-tyrosine precursors from the oxidation of GalOx and CAO cofactors.

1.6. Effects of structure and dynamics on biological ET

The two projects presented within this thesis share the common theme of using electron transfer (ET) reactions to study protein reactivity and biomimetic models. ET is

important in fundamental biological processes such as metabolism, respiration, and photosynthesis. ET rates depend upon the driving force ($\Delta G°$), reorganization energy (λ), and the electronic coupling between reactants and products (H_{AB}).[35,36] Proteins present complicated systems because non-ET processes, such as chemical transformations or conformational changes, might influence the observed rate constant, obscuring the true ET rate.[37] Much work is focused on elucidating how structure and dynamics of proteins influence ET reactivity.[38-41]

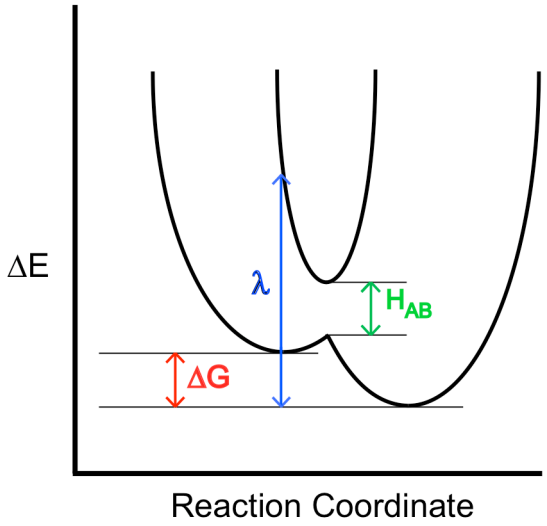

Figure 1.3. Potential energy diagrams for electron transfer reactions illustration the reorganization energy (λ) and the electronic coupling between reactants and products (H_{AB}).

There are several kinetic models that describe how non-ET events influence ET rates.[37,42,43] There is simple ET, in which the ET step is the slowest step in the overall reaction. The $\Delta G°$, λ, and H_{AB} parameters behave as outlined by Marcus theory. Coupled ET occurs when k_{ET} is still the rate-limiting step, but it is influenced by a preceding non-ET step. Lastly, gated ET occurs when the preceding non-ET process is the rate-determining step, resulting in a rate that reflects a non-ET process, such as a

relatively slow conformational change necessary to form a reactive complex. Parameters such as $\Delta G°$ and λ will not vary predictably since the rate-limiting step is not ET. Both simple and gated ET reactions will presented in this body of work.

Some gated ET reactions involve conformational changes that optimize the reactive configuration of redox partners to achieve ET. Since unimolecular ET rates should not be affected by solution conditions aside from solvation contributions to λ_{outer}, one way to confirm an ET event is gated is to vary the ionic strength and viscosity of the solution and see how k_{obs} is affected.[39] One early viscosity study showed that the electron transfer rate from Cyt *c* to bacteriochlorophyll dimer P840 Decreased linearly as viscosity was increased. The simple Brownian diffusion model couldn't account for the abnormally high dependence and it was suggested that a conformational fluctuation of Cyt *c* was a rate-determining step.[44]

In one notable example, Durham and Millet et al. found that the physiologically relevant complex of yeast Cyt *c* and CcP underwent simple ET, but the horse heart Cyt *c*/CCP complex experienced gated ET.[45] For yeast Cyt *c*/CCP, the rate constant was independent of viscosity and temperature and resulted in an observed rate consistent with ET as predicted from the crystal structure. In contrast, the horse heart Cyt *c*/CcP observed rate did not coincide with theoretical predictions and was dependent upon viscosity and temperature. The horse heart Cyt *c*/CCP complex bound differently and had an inefficient ET pathway. A conformational change to a binding mode similar to yeast Cyt *c*/CCP was necessary, resulting in a gated ET rate. This study illustrated how the specific binding interaction between Cyt *c* and CCP influenced observed ET rates.

Electrostatic interactions are important as well, as shown by a study in which the most electrostatically stable complex between Cyt *c* and CCP was not optimized for ET and was dependent upon a proceeding conformational reorganization. Increases in ionic strength or deletion of key charged Arg or Lys residues needed for orientation at the interface resulted in faster ET rates.[46] Deconvoluting the contribution of conformational changes to the rate-limiting step is essential in identifying the intrinsic k_{ET} rate. The effects from ionic strength on ET rates be addressed in these studies.

How structure and dynamics within protein-protein complexes influence ET rates is still not well understood.[47] One approach involved measuring photochemical ET and charge recombination between Zn-porphyrin-substituted CCP and Cyt *c* in single crystals, relating reactivity to the defined structures of the associated configurations. Different mutations at the interface greatly affected protein orientation. However, these structurally distinct complexes displayed similar ET reactivity, despite having different donor-to-acceptor distances. Temperature dependence suggested low amplitude conformational changes at the protein-protein interface promote interprotein ET.[48] Crystallographic data showed that the Cyt *c*/CCP interface was well-ordered, thus these structural changes at the interface were low in amplitude, yet influenced the ET rates enough to differentiate between yeast and horse heart Cyt *c*/CCP complexes.[48]

Another model referred to as "dynamic docking" involves an energy landscape that is filled with many weakly bound protein-protein configurations in which only a few are ET active and are not necessarily the most stable configurations. This model was developed to explain why the tightest bound complex between cytochrome b_5 (Cyt b_5) and myoglobin (Mb) did not have the fastest ET rate.[49-51] A study of the electrostatic

contributions to binding and ET within this system showed that neutralizing negative charges at the heme increased the bimolecular rate by two orders of magnitude, but the binding constants remained unchanged. This model involves a large sampling of conformations that doesn't require changes in binding affinities to modulate ET within a protein-protein complex.

Although the effect of structure and dynamics within protein-protein complexes on ET is still not well understood, evidence displays how low amplitude protein-protein interactions may have large effects on ET rates. The work presented within this thesis uses a nanoparticle surface as a proxy to characterize the binding interactions and dynamics within a protein/nanoparticle complex, investigating how local and global dynamics affect ET reactivity.

1.7. References Cited

(1) Niemeyer, C. M. *Angew. Chem. Int. Ed.* **2001**, *40*, 4128-4158.

(2) Aubin-Tam, M. E.; Hamad-Schifferli, K. *Biomed. Mater.* **2008**, *3*, 034001.

(3) Katz, E.; Willner, I. *Angew. Chem. Int. Ed.* **2004**, *43*, 6042-6108.

(4) Lynch, I.; Cedervall, T.; Lundqvist, M.; Cabaleiro-Lago, C.; Linse, S.; Dawson, K. A. *Adv. Colloid Interface Sci.* **2007**, *134-135*, 167-74.

(5) Klein, J. *Proc. Natl. Acad. Sci. U. S. A.* **2007**, *104*, 2029-30.

(6) You, C. C.; De, M.; Rotello, V. M. *Curr. Opin. Chem. Biol.* **2005**, *9*, 639-46.

(7) Daniel, M. C.; Astruc, D. *Chem. Rev.* **2004**, *104*, 293-346.

(8) Verma, A.; Rotello, V. M. *Chem. Commun.* **2005**, 303-312.

(9) Guarise, C.; Manea, F.; Zaupa, G.; Pasquato, L.; Prins, L. J.; Scrimin, P. *J. Pept. Sci.* **2008**, *14*, 174-83.

(10) You, C. C.; De, M.; Han, G.; Rotello, V. M. *J. Am. Chem. Soc.* **2005**, *127*, 12873-12881.

(11) Carver, A. M.; De, M.; Bayraktar, H.; Rana, S.; Rotello, V. M.; Knapp, M. J. *J. Am. Chem. Soc.* **2009**, *131*, 3798-9.

(12) Bayraktar, H.; Ghosh, P. S.; Rotello, V. M.; Knapp, M. J. *Chem. Commun.* **2006**, 1390-1392.

(13) Bayraktar, H.; You, C. C.; Rotello, V. M.; Knapp, M. J. *J. Am. Chem. Soc.* **2007**, *129*, 2732-2733.

(14) Cedervall, T.; Lynch, I.; Lindman, S.; Berggard, T.; Thulin, E.; Nilsson, H.; Dawson, K. A.; Linse, S. *Proc. Natl. Acad. Sci. U. S. A.* **2007**, *104*, 2050-5.

(15) Lundqvist, M.; Stigler, J.; Elia, G.; Lynch, I.; Cedervall, T.; Dawson, K. A. *Proc. Natl. Acad. Sci. U. S. A.* **2008**, *105*, 14265-70.

(16) Linse, S.; Cabaleiro-Lago, C.; Xue, W. F.; Lynch, I.; Lindman, S.; Thulin, E.; Radford, S. E.; Dawson, K. A. *Proc. Natl. Acad. Sci. U. S. A.* **2007**, *104*, 8691-6.

(17) Liu, J.; Lu, Y. *Chem. Commun.* **2007**, 4872-4.

(18) Hurst, S. J.; Han, M. S.; Lytton-Jean, A. K.; Mirkin, C. A. *Anal. Chem.* **2007**, *79*, 7201-5.

(19) Guarise, C.; Pasquato, L.; De Filippis, V.; Scrimin, P. *Proc. Natl. Acad. Sci. U. S. A.* **2006**, *103*, 3978-82.

(20) Zheng, G.; Daniel, W. L.; Mirkin, C. A. *J. Am. Chem. Soc.* **2008**, *130*, 9644-5.

(21) Cao, Y. C.; Jin, R.; Nam, J. M.; Thaxton, C. S.; Mirkin, C. A. *J. Am. Chem. Soc.* **2003**, *125*, 14676-7.

(22) Oh, E.; Hong, M. Y.; Lee, D.; Nam, S. H.; Yoon, H. C.; Kim, H. S. *J. Am. Chem. Soc.* **2005**, *127*, 3270-1.

(23) Fillon, Y.; Verma, A.; Ghosh, P.; Ernenwein, D.; Rotello, V. M.; Chmielewski, J. *J. Am. Chem. Soc.* **2007**, *129*, 6676-6677.

(24) You, C. C.; Agasti, S. S.; De, M.; Knapp, M. J.; Rotello, V. M. *J. Am. Chem. Soc.* **2006**, *128*, 14612-14618.

(25) Hu, M.; Qian, L.; Brinas, R. P.; Lymar, E. S.; Hainfeld, J. F. *Angew. Chem. Int. Ed.* **2007**, *46*, 5111-4.

(26) Sierra-Sastre, Y.; Choi, S.; Picraux, S. T.; Batt, C. A. *J. Am. Chem. Soc.* **2008**, *130*, 10488-9.
(27) Carver, A. M.; Knapp, M. J. *Polyhedron* **2008**, *27*, 3313-3317.
(28) Stubbe, J.; van der Donk, W. A. *Chem. Rev.* **1998**, *98*, 705-762.
(29) Davidson, V. L. *Biochemistry* **2007**, *46*, 5283-5292.
(30) Klinman, J. P. *Biochim. Biophys. Acta, Proteins Proteomics* **2003**, *1647*, 131-137.
(31) Okeley, N. M.; van der Donk, W. A. *Chemistry & Biology* **2000**, *7*, R159-R171.
(32) Rogers, M.; Firbank, S.; Knowles, P.; McPherson, M.; Phillips, S.; Dooley, D. *J. Inorg. Biochem.* **2001**, *86*, 404-404.
(33) Moore, R. H.; Spies, M. A.; Culpepper, M. B.; Murakawa, T.; Hirota, S.; Okajima, T.; Tanizawa, K.; Mure, M. *J. Am. Chem. Soc.* **2007**, *129*, 11524-11534.
(34) Dubois, J. L.; Klinman, J. P. *Biochemistry* **2005**, *44*, 11381-11388.
(35) Gray, H. B.; Winkler, J. R. *Proc. Natl. Acad. Sci. U. S. A.* **2005**, *102*, 3534-9.
(36) Gray, H. B.; Winkler, J. R. *Q. Rev. Biophys.* **2003**, *36*, 341-72.
(37) Davidson, V. L. *Acc. Chem. Res.* **2000**, *33*, 87-93.
(38) Gray, H. B.; Winkler, J. R. *Annu. Rev. Biochem.* **1996**, *65*, 537-61.
(39) Canters, G. W.; Dennison, C. *Biochimie* **1995**, *77*, 506-15.
(40) Juan, H.-F.; Liu, H.-L.; Hsu, J.-P. *Curr. Proteomics* **2004**, *1*, 183-197.
(41) Redfern, O. C.; Dessailly, B.; Orengo, C. A. *Curr. Opin. Struct. Biol.* **2008**, *18*, 394-402.
(42) Davidson, V. L. *Acc. Chem. Res.* **2008**, *41*, 730-738.
(43) Davidson, V. L. *Biochemistry* **2002**, *41*, 14633-6.
(44) OhOka, H.; Iwaki, M.; Itoh, S. *Biochemistry* **1997**, *36*, 9267-9272.
(45) Mei, H. K.; Wang, K. F.; Peffer, N.; Weatherly, G.; Cohen, D. S.; Miller, M.; Pielak, G.; Durham, B.; Millett, F. *Biochemistry* **1999**, *38*, 6846-6854.
(46) Hazzard, J. T.; Mclendon, G.; Cusanovich, M. A.; Das, G.; Sherman, F.; Tollin, G. *Biochemistry* **1988**, *27*, 4445-4451.
(47) Jeuken, L. J. *Biochim. Biophys. Acta* **2003**, *1604*, 67-76.
(48) Kang, S. A.; Crane, B. R. *Proc. Natl. Acad. Sci. U. S. A.* **2005**, *102*, 15465-15470.
(49) Liang, Z. X.; Kurnikov, I. V.; Nocek, J. M.; Mauk, A. G.; Beratan, D. N.; Hoffman, B. M. *J. Am. Chem. Soc.* **2004**, *126*, 2785-2798.
(50) Liang, Z. X.; Nocek, J. M.; Huang, K.; Hayes, R. T.; Kurnikov, I. V.; Beratan, D. N.; Hoffman, B. M. *J. Am. Chem. Soc.* **2002**, *124*, 6849-59.
(51) Liang, Z. X.; Jiang, M.; Ning, Q.; Hoffman, B. M. *J. Biol. Inorg. Chem.* **2002**, *7*, 580-8.

CHAPTER 2

INTERMOLECULAR ELECTRON-TRANSFER CATALYZED ON NANOPARTICLE SURFACES

2.1. Introduction

Interprotein electron transfer (ET) is crucial for natural energy conversion and a fundamental reaction in the pursuit of understanding the broader problem of protein-protein interactions and reactivity.[1] Simplifying the complicated nature of these natural systems has driven development of biomimetic approaches. Nanoparticles have been widely used as artificial receptors,[2-4] catalysts,[5-8] biological sensors,[9-14] and directors of bioassembly.[6,15-17] For this study, the catalytic ability of NPs is of particular interest, such as those used to catalyze peptide ligation,[6] phosphodiester cleavage,[18] and the reactivity of α-chymotrypsin.[8] A common limitation of many NP systems is that the structure or function of a protein is often altered when it binds to the NP surface.[19] Thus, we aim to design a tunable protein/NP macromolecule in which the NP acts as a complementary partner to a protein without altering its native structure such that we can study the link between protein dynamics and ET function.

ET reactions are often used to study protein-protein reactivity.[20,21] Cytochrome *c* (Cyt *c*) is a well-studied model system that reacts with many proteins and small molecules in a highly predictable manner. The artificial receptor of the proposed system is a water-soluble gold nanoparticle with varied L-amino acid terminal groups and tetra-ethyleneglycol tethers that minimize protein denaturation in protein/nanoparticle adducts.[8] Side chain functionalities of **Au-TX** will be varied in charge, size, and hydrophobicity to influence the binding and reactivity of Cyt *c* while non-covalently bound to **Au-TX**.

Several parameters affect ET reactivity: driving force, reorganization energy, electronic coupling between reactants and products, through pathways, collision

frequencies, and the probability of achieving an ET reactive configuration.[21] The possible effect of **Au-TX** on some of these parameters and subsequently the ET reactivity of Cyt *c* will be studied by utilizing a small redox reagent and monitoring ET kinetics via stopped-flow spectroscopy. A redox mediator will probe the redox potential of Cyt *c* while absorbed to the surface of **Au-TX**, indicating if reactivity differences are a result of altered thermodynamics. Finally, the coordination environment and electronic structure of the active site of Cyt *c* will be characterized using EPR spectroscopy, showing any change in the coordination of the heme that might result from binding to the NP surface. If these conditions are met, then the nanoparticle acts as a catalyst with a tunable surface without altering the native structure or function as a protein.

2.2. Experimental Methods

2.2.3. General Considerations

Horse heart Cyt *c* and Tris(hydroxymethyl)-aminomethane (Tris) were obtained from Sigma-Aldrich. Sodium dithionite was used to reduce Cyt *c* and separated using a G-25 Sephadex column. Cyt *c*(Fe^{3+}) samples were also run through a Sephadex column, concentrated, and pH adjusted. When noted, solutions of Cyt *c* were made anaerobic by gently passing hydrated N_2 over their surfaces while stirring for 60 minutes.

Anionic gold nanoparticles were functionalized with ligands containing a tetra-ethyleneglycol segment attached via an amide bond to the amine group of an L-amino acid (Chart 2.1). The ligands are denoted according to which amino acid is presented on the surface: L-aspartic acid (**Au-TAsp**), L-phenylalanine (**Au-TPhe**), L-valine (**Au-TVal**), and L-leucine (**Au-TLeu**). The ligands and **Au-TX** nanoparticles were prepared following previously published procedures.[8] Concentrations were

determined using a Hetlett-Packard 8453 UV-Vis spectrophotometer. A small amount of **Au-TX** (less than 1% total volume) was added to a Cyt *c* solution of known concentration (ε_{550} 27,700 M^{-1} cm^{-1}). The calculated absorbance of Cyt *c* at 506 nm (ε_{506} 7500 M^{-1} cm^{-1})[22] was subtracted from the Cyt *c*:**Au-TX** solution absorbance; the remaining absorbance was attributed to **Au-TX** using ε_{506} 488,350 M^{-1} cm^{-1} which was determined experimentally and coincided with similar reports.

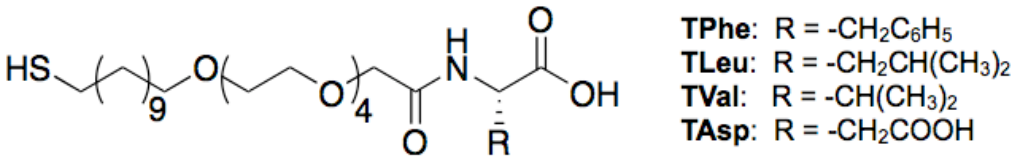

Chart 2.1. Ligand structure (TX) for surface functionalized **Au-TX** nanoparticles (R = **L -Phe**, **L -Leu**, **L-Val**, or **L-Asp**).

$Co(phen)_3(ClO_4)_3$ was synthesized and recrystallized according to literature.[23] Analytical grade potassium ferrocyanide and potassium ferricyanide were obtained commercially and used without further purification. Concentrations were verified using UV-Vis for $Co(phen)_3^{3+}$ (ε_{330} 4680 M^{-1} cm^{-1}),[24] ferrocyanide (ε_{325} 300 M^{-1} cm^{-1}), and ferricyanide (ε_{325} 1100 M^{-1} cm^{-1}).[25] $Co(phen)_3^{3+}$ and $Fe(CN)_6^{3-/4-}$ solutions were made anaerobic by sparging with hydrated N_2 for 20-30 minutes.

2.2.2. Stopped-flow reactivity studies

Kinetic experiments were performed on an OLIS RSM-100 stopped-flow spectrophotometer. The OLIS scandisk collected absorbance data from 390 – 610 nm for several seconds with a 20 mm observation cell pathlength. The temperature of the drive syringes and observation cell was maintained at 25.0º C by a Neslab RTE-211 recirculating water bath.

$Co(phen)_3^{3+}$ reactivity experiments were derived from previous literature methods.[24] All solutions were prepared using 10 mM Tris base, which was pH

adjusted using HCl (12 mM or 0.1 M NaCl, pH 7.4), and were degassed with N_2 prior to loading drive syringes via 3-way stopcocks. One drive syringe contained the oxidant $Co(phen)_3^{3+}$ in excess (0.1– 2.0 mM) while the other contained Cyt *c* (10.0 μM) pre-incubated with the appropriate **Au-TX** (0.2 – 1.0 μM). These solutions were rapidly mixed in a 1:1 ratio and the absorbance change monitored. For each observed rate, 4-5 individual shots were averaged for the reported k_{obs} and the standard deviations were taken as error estimations.

Data collection and processing was handled using Globalworks software (Olis, Inc., Georgia, USA) and subsequent fitting in Igor Pro (Wavemetrics Inc., Oregon, USA). Absorbance change traces as a function of time at 550 nm were fit using single exponential decays to determine k_{obs}; global SVD fits using the A→B kinetic model concurred with these single-wavelength fits. The apparent rate constants for electron transfer, k_{ET}(app) and k_{ET}/K_D(app), were determined using equations 1-2 where $[Co]_0$ is the initial concentration of $Co(phen)_3^{3+}$, K_D(app) is the kinetically determined dissociation constant for $Co(phen)_3^{3+}$ binding with Cyt *c*/**Au-TX**, and k_{ET}/K_D(app) is the apparent bimolecular rate for $Co(phen)_3^{3+}$ reacting with Cyt *c*/**Au-TX.**

$$k_{obs} = \left(k_{ET}\right)_{app} \frac{[Co]_0}{[Co]_0 + K_D} \tag{1}$$

$$k_{obs} = \left(\frac{k_{ET}}{K_D}\right)_{app} \left(\frac{[Co]_0}{{}^{[Co]_0}\!/_{K_D} + 1}\right) \tag{2}$$

Au-TX concentration was varied from approximately 0.1 to 0.5 μM for each individual particle over several experiments. The resulting k_{obs} values were plotted as k_{ET} versus [**Au-TX**] where the slope represents a bimolecular rate constant for that particular Cyt *c*/**Au-TX** complex with $Co(phen)_3^{3+}$.

2.2.3. Redox Potential of Cyt *c*

Absorption measurements were collected on a Hewlett-Packard 8453 UV-Vis spectrophotometer using degassed solutions. Solutions contained Cyt *c*(Fe^{3+}) (5 μM) and **Au-TX** (1.5 μM) in Tris buffer (10 mM, pH 7.4). Under these conditions, the mole fraction of Cyt *c* bound to **Au-TX** was approximately 0.97 (Appendix A). Ferricyanide (~0.05 M) and ferrocyanide (~0.7 M) stocks were prepared and degassed. 2.7 mL samples of Cyt *c*/**Au-TX** were loaded into UV-Vis quartz cells fitted with screwcaps and degassed. 0.3 mL aliquots of degassed ($Fe(CN)_6^{3-}$) or ($Fe(CN)_6^{4-}$) were then added using a gas-tight Hamilton syringe.

The redox potentials of the Cyt *c*/**Au-TX** adducts were determined using the "methods of mixtures" developed by Davenport and Hill[26] and later modified by a number of groups.[25,27,28] The ratio of Cyt *c*(Fe^{2+}) / Cyt *c*(Fe^{3+}) was measured by monitoring absorbance change at 550 nm, where Cyt *c*($Fe^{2+/3+}$) are the only absorbing species. Equations 3-4 describe the relationship between absorbance at 550nm (*Abs*), the redox potential of Cyt *c* (E_{Cytc}), and solution poise (E_{poise}).

$$Abs = \frac{(A_{ox}10^{n(E_{poise}-E_{Cytc})/59} + A_{red})}{1+10^{n(E_{poise}-E_{Cytc})/59}} \tag{3}$$

$$\Delta Abs = \frac{A_{ox}10^{n(E_{poise}-E_{Cytc})/59}}{1+10^{n(E_{poise}-E_{Cytc})/59}} \tag{4}$$

The sample of $(Fe(CN)_6^{3-})$/Cyt *c*/**Au-TX** was used to determine A_{ox}. Sodium dithionite was added to a third Cyt *c*/**Au-TX** sample to determine A_{red}. Aliquots of $(Fe(CN)_6^{3-})$/Cyt *c*(Fe^{3+})/**Au-TX** were added to $(Fe(CN)_6^{4-})$/Cyt *c*(Fe^{2+})/**Au-TX** via a gas-tight Hamilton syringe. A fraction of Cyt *c* oxidized and the solution rapidly reached equilibrium. The 550 nm absorption peak was monitored as it decreased relative to an isosbestic point (557 nm). Using known concentrations of

$(Fe(CN)_6^{3-})/(Fe(CN)_6^{4-})$ at each point and the redox potential of ferricyanide (E_{fcn} = 0.43 V), E_{poise} was calculated according to equation 5. A titration curve was generated and fitted to equation 4 to determine E_{Cytc}.

$$E_{poise} = E_{FCN} - \frac{2.303RT}{nF}\log\frac{[Fe(CN)_6^{4-}]}{[Fe(CN)_6^{3-}]} \quad (5)$$

2.2.4. Electron Paramagnetic Resonance Spectroscopy

X-band (9.62 GHz) EPR spectra were obtained using a Bruker E-500-10/12 spectrometer equipped with an Oxford instruments ER-9000 LHe cryostat. The modulation amplitude was 10 gauss and the frequency was 100 kHz. Spectra were collected at approximately 10 K with 2 mW power. Samples were prepared in 10 mM Tris buffer and 50% glycerol and frozen in liquid nitrogen. Sample pH (7.4) was confirmed using a Mettler Toledo Inlab 423 Combination pH and Metallic electrode after the addition of **Au-TX**. Protein and **Au-TX** concentrations for the Cyt *c*/**Au-TPhe**, Cyt *c*/**Au-TLeu**, and Cyt *c*/**Au-TVal** samples were 1.25 mM and 60 μM respectively. Under these conditions, the mole fraction of Cyt *c* bound to **Au-TX** is 0.34. The Cyt *c*/**Au-TAsp** sample was 1 mM and 30 μM, leading to a Cyt *c*/**Au-TX** mole fraction of 0.15[29] (Appendix A). The control experiment containing only Cyt *c* was 1.5 mM.

2.3. Results and Discussion

2.3.1. Midpoint reduction potential of Cyt *c*/Au-TX

The redox potential of Cyt *c*/**Au-TX** was measured, due to the importance of driving force on ET rates. Varied ratios of ferricyanide/ferrocyanide were used to set the solution redox poise, because they react rapidly with Cyt *c* and do not interfere with the absorbance at 550 nm.[30] A solution containing Cyt *c*(Fe^{3+}) (5 μM), **Au-TX** (1.5 μM), and $Fe(CN)_6^{3-}$ (5 mM) was titrated into a cuvette containing Cyt *c*(Fe^{2+}) (5

μM), **Au-TX** (1.5 μM), and $Fe(CN)_6^{4-}$ (70 mM), which maintained a constant Cyt *c* concentration while increasing the redox poise of the solution. As the redox poise of the solution was increased, the Cyt $c(Fe^{3+}) + e^- \rightleftharpoons$ Cyt $c(Fe^{2+})$ equilibrium shifted to favor Cyt $c(Fe^{3+})$. The $Fe(CN)_6^{3-}$ and $Fe(CN)_6^{4-}$ concentrations determined E_{poise} at each point according to equation 5. The increase in mole-fraction of Cyt $c(Fe^{3+})$ was detected by the decrease in A_{550} and fit to equation 4 to yield E_{Cytc}. A representative data set is given in Figure 2.1.

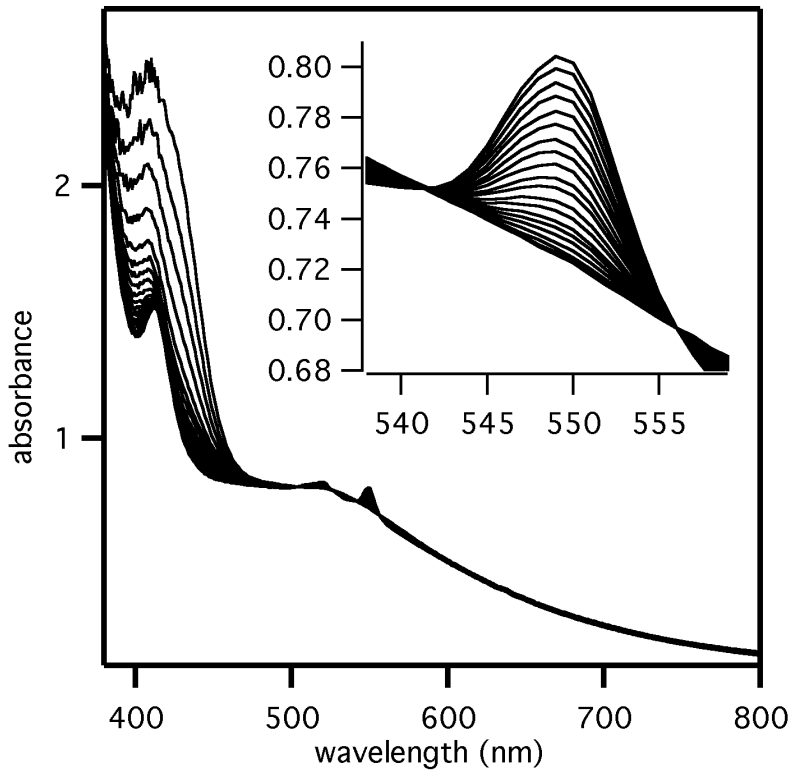

Figure 2.1. UV-Vis traces of the titration of small aliquots of a solution with Cyt $c(Fe^{3+})$ (5 μM), **Au-TLeu** (1.5 μM), and $Fe(CN)_6^{3-}$ (5 mM) into a cuvette containing Cyt $c(Fe^{2+})$ (5 μM), **Au-TLeu** (1.5 μM), and $Fe(CN)_6^{4-}$ (70 mM).

The titration curve shown in Figure 2.2 (●) was fit to equation 4, yielding the redox potential of Cyt *c* as E_{Cytc} = 260 mV, This value closely agreed with previously reported values, which ranged from 256 – 266 mV (table 2.1).[25,31-33] The redox potentials of Cyt *c*/**Au-TX** were slightly less positive, 245 – 253 mV, however these values were within the experimental uncertainty of the redox potential of unbound Cyt

c, indicating that the driving force for ET reactions with Cyt *c* was independent of **Au-TX** binding.

Microperoxidases provide an estimation of how the redox potential could change if Cyt *c* was structurally altered. Microperoxidases are heme-containing peptides from Cyt *c* digests that retain His axial ligation while the second axial site is occupied by a labile H_2O ligand.[34] This five coordinate model heme system has a dramatically different redox potential of -160 mV, supporting that Cyt *c*/**Au-TX** retained a 6 coordinate environment.[35]

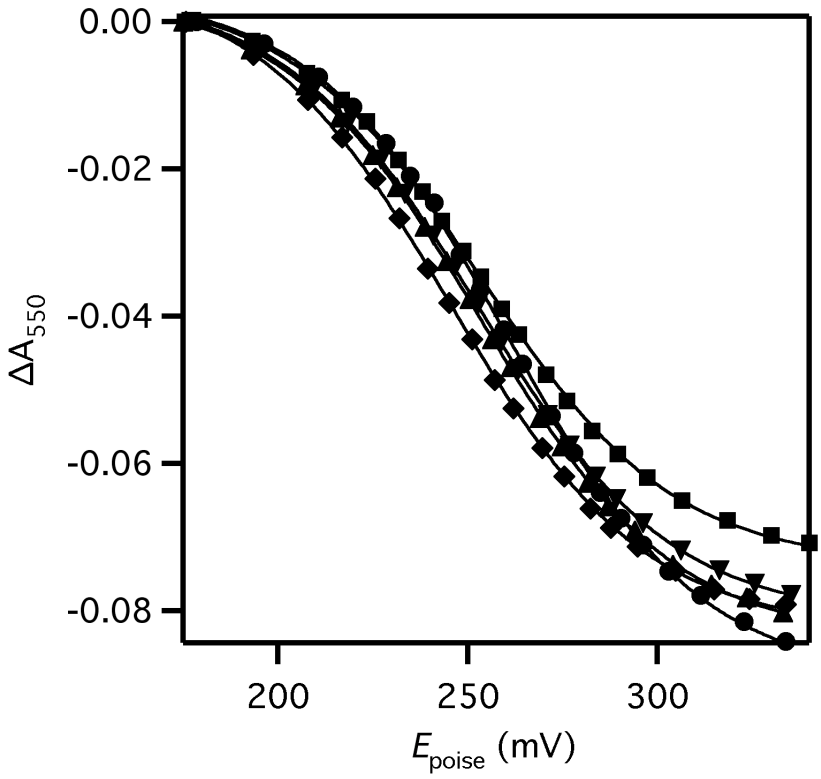

Figure 2.2. Redox mediator titration results for free Cyt *c* (●), Cyt *c*/**Au-TPhe** (▼), Cyt *c*/**Au-TLeu** (◆), Cyt *c*/**Au-TVal** (▲), and Cyt *c*/**Au-TAsp** (■) show absorbance changes as a function of solution redox poise, E_{poise}. Cyt *c* (5 μM) and **Au-TX** (1.5 μM) were in 10 mM Tris, pH 7.4. Lines represent fits to the Nerst equation 4.

Table 2.1. Redox potentials of free Cyt *c* and Cyt *c*/**Au-TX.**

	E_{Cytc} (mV)
Cyt *c*	260 ± 18
Cyt *c*/**Au-TPhe**	252 ± 19

Cyt *c*/**Au-TLeu**	245 ± 19
Cyt *c*/**Au-TVal**	253 ± 18
Cyt *c*/**Au-TAsp**	253 ± 20

Data fitted to equation 4. A_{ox} and A_{red} were determined using fully oxidized and reduced samples respectively. E_{poise} was calculated according to equation 5. n was fixed to 1. Error assumed 2% uncertainty in data points.

2.3.2. Electronic Structure of Cyt *c*/Au-TX using EPR

EPR was used to monitor the active-site structure and coordination geometry of Cyt *c*(Fe^{3+}) when bound as Cyt *c*(Fe^{3+})/**Au-TX**. Cyt *c*(Fe^{3+}) exhibits a unique EPR signal due to the 6-coordinate, low-spin heme with axial His and Met ligation, with signals at g_{eff} = 3.07 and 2.23.[36] The EPR lineshape of Cyt *c*(Fe^{3+}) is a sensitive probe for the structural integrity of Cyt *c*, as the Met ligand is readily lost upon partial unfolding, resulting in a high-spin Fe^{3+} heme with His/H_2O ligands which exhibit EPR signals at g_{eff} ~ 6 and 2.00.[37] The X-band EPR spectra of free and **Au-TX**-bound Cyt *c*(Fe^{3+}) were acquired at 10 K (Figure 2.3). Cyt *c*(Fe^{3+}) exhibited signals at g_{eff} = 3.06 or 3.07 and 2.23, as expected for natively structured Cyt *c*. Cyt *c*(Fe^{3+})/**Au-TX** exhibited similar EPR lineshapes to native Cyt *c*(Fe^{3+}), with additional low-intensity features in the g_{eff} = 4 – 6 region. Under the same experimental conditions and instrumental settings, a 100 μM **Au-TVal** sample was EPR silent (data not shown).

The Cyt *c*(Fe^{3+})/**Au-TAsp** sample appeared to be a mixture of low-spin and high-spin Cyt *c*(Fe^{3+}). It should be noted that the high-spin Fe^{3+} signals from His/H_2O hemes typically are more easily observed than low-spin Fe^{3+} from this His/H_2O heme. Simple double integration of the spectrum indicated that the high-spin component at g ~6 accounted for less than 10% of the total area. As the low-spin state of Cyt c undergoes rapid relaxation, making it a difficult to observe signal, this

indicates that the mole-fraction of high-spin state in these EPR samples was much less than this, perhaps by a factor of five.

Although the Cyt *c*(Fe^{3+})/**Au-TX** samples were physical mixtures of unbound Cyt *c* (66 – 75 %) and **Au-TX**-bound Cyt *c* (15 – 34 %), the high-spin component did not correlate with bound fraction, indicating that Fe^{3+} of Cyt *c*(Fe^{3+})/**Au-TX** is predominantly in the low-spin state.

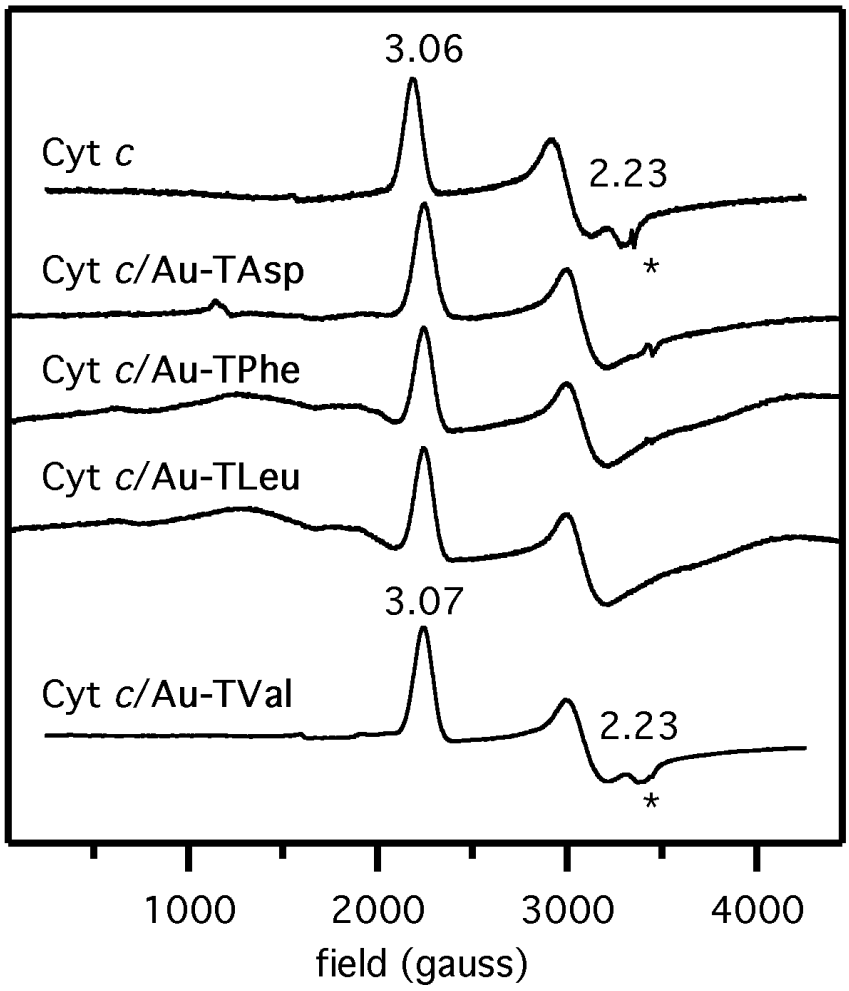

Figure 2.3. X-band EPR spectra (10 K) of Cyt *c* (1.5 mM), Cyt *c*/**Au-TAsp** (1 mM/30 μM), Cyt *c*/**Au-TPhe** (1.25 mM/60 μM), Cyt *c*/**Au-TLeu** (1.25 mM/60 μM), and Cyt *c*/**Au-TVal** (1.25 mM/60 μM) in 10mM Tris buffer (pH 7.4) and 50% glycerol. Power was 2 mW, modulation amplitude was 10 gauss, and modulation frequency was 100 kHz. Cavity noise is marked by (*).

2.3.3. $Co(phen)_3^{3+}$ oxidizes Cyt *c*(Fe^{2+})/Au-TX

In order to study the reactivity of Cyt *c* when bound to **Au-TX**, the small redox reagent $Co(phen)_3^{3+}$ was chosen because it undergoes an electron transfer reaction with Cyt *c* and could be easily altered synthetically to vary the driving force if needed to generate a Marcus curve.[38] In trial hand-mixed experiments, this reaction was completed within four seconds, requiring the stopped-flow method for kinetic measurements. Cyt *c*(Fe^{2+}) was rapidly oxidized by excess $Co(phen)_3^{3+}$ under pseudo-first order kinetics conditions. Optical changes were in accord with those expected for the oxidation of Cyt *c*(Fe^{2+}) to Cyt *c*(Fe^{3+}); the Soret shifted from 412 to 407 nm, while the α/β bands shifted from resolved peaks at 519 and 550 nm to an unresolved peak at 529 nm.[22,39] Single-exponential reactions were observed under all conditions.

Free Cyt *c* oxidation by $Co(phen)_3^{3+}$ exhibited second order kinetics, as shown by reacting fixed concentrations of Cyt *c*(Fe^{2+}) with varied concentrations of $Co(phen)_3^{3+}$. Linear fitting of k_{obs} versus the concentration of $Co(phen)_3^{3+}$ produced a bimolecular rate constant of $k_{ET}/K_D = 1.33\times10^3 \pm 40\ M^{-1}\ s^{-1}$, which is comparable to previously reported values under similar conditions.[24]

The effect of **Au-TX** binding on Cyt *c* oxidation was tested by pre-incubating Cyt *c*(Fe^{2+}) with **Au-TX**, followed by rapid mixing and reaction with $Co(phen)_3^{3+}$. Oxidations of the Cyt *c*(Fe^{2+})/**Au-TX** adduct by $Co(phen)_3^{3+}$ exhibited an optically turbid phase which lasted for tens of milliseconds, followed by a single-exponential phase on the seconds timescale. The early phase was attributed to mixing artifacts known as Schlering effects while the latter phase corresponded in amplitude and absorption changes with that expected for Cyt *c*(Fe^{2+}) oxidation. The unshifted α/β bands in this example are initial indicators that Cyt *c* is not structurally altered. The

Soret and α/β bands of Cyt *c* are known to shift upon denaturation,[40] including when bound to a nanoparticle surface that perturbs protein structure.[41] The kinetics of Cyt *c*(Fe^{2+})/**Au-TX** oxidation were considerably faster than those of unbound Cyt *c*(Fe^{2+}). A typical dataset is shown in Figure 2.4.

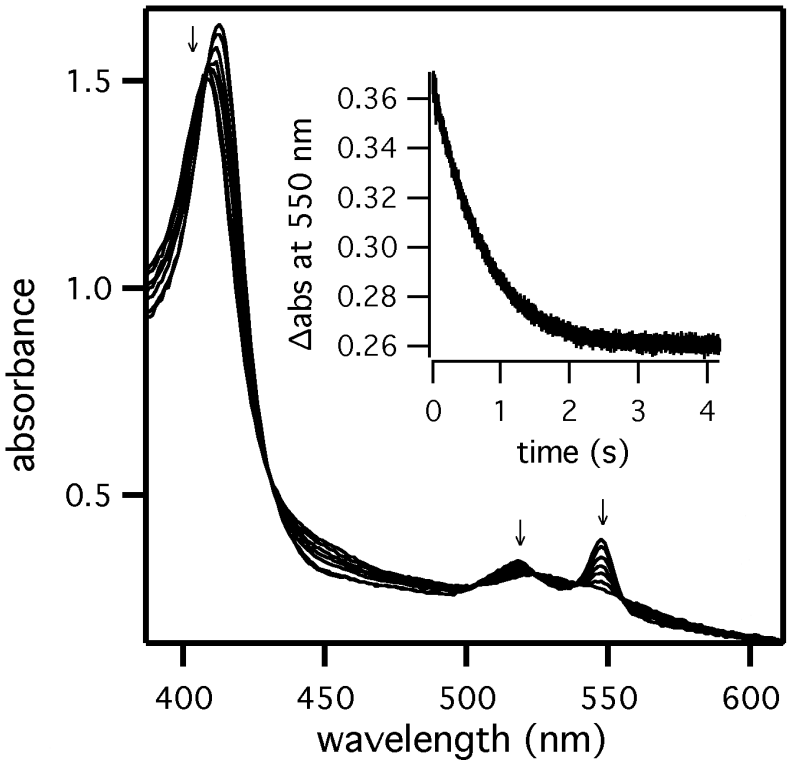

Figure 2.4. Stopped-flow UV-Vis traces following reaction of Cyt *c*/**Au-TLeu** with $Co(phen)_3^{3+}$ in 10 mM Tris (pH 7.40, 0.1 M NaCl). Syringe A: 10 μM Cyt *c*, 0.34 μM **Au-TLeu**; Syringe B: 0.502 mM $Co(phen)_3^{3+}$. Inset: decay trace at 550 nm, fitted to a single exponential decay (k_{obs} = 1.42 s^{-1}).

The single exponential oxidation of the Cyt *c*/**Au-TX** adduct indicated the binding for Cyt *c* to the **Au-TX** surface was rapid and that there was a single type of reactive Cyt *c* site. The observed oxidation rate is the sum of the free Cyt *c* fraction and the Cyt *c*/**Au-TX** fraction. Since the coupled observed rate is much greater than that of free Cyt *c*, the dominant reaction is that of Cyt *c*/**Au-TX**.

The kinetic model in Scheme 2.1 outlines a random order mechanism in which k_{obs} is a product of encounter complex formation and subsequent ET. At lower, limiting $Co(phen)_3^{3+}$ concentrations, the dominant pathway is likely that in which the

Cyt *c*/**Au-TX** adduct collides with $Co(phen)_3^{3+}$ to form the encounter complex. Conversely, under saturating $Co(phen)_3^{3+}$ concentrations, the dominant pathway is likely that in which the **Au-TX**/$Co(phen)_3^{3+}$ adduct collides with Cyt *c* to form the encounter complex. The relevant step under saturating $Co(phen)_3^{3+}$ concentrations is k_{ET}(app) while k_{ET}/K_D(app) reflects limiting $Co(phen)_3^{3+}$ concentrations. Both will later elucidate the importance of columbics and protein dynamics under different [$Co(phen)_3^{3+}$] and ionic strength conditions.

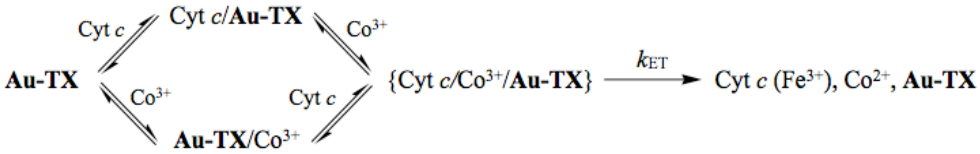

Scheme 2.1. The kinetic model that outlines the formation and subsequent reaction of the encounter complex {Cyt *c*/Co^{3+}/**Au-TX**}. The top route represents the adduct that forms under limiting $Co(phen)_3^{3+}$ concentrations while the bottom route reflects saturating $Co(phen)_3^{3+}$ concentrations.

2.3.4. Diffusion and electrostatics dominate ET rates at low ionic strength

Electrostatic interactions are a major influence on reactivity, so exploring different ionic strength experimental conditions yields information about the nature of the ET reaction. Several factors determine the rate at which Cyt *c* reacts with small redox reagents. The collision frequency between the two reagents is important and is affected by charge screening. Additionally, the heme must be spatially accessible to achieve ET with a small molecule like $Co(phen)_3^{3+}$ that reacts at the heme edge.[24] It has also been shown that under low ionic strength conditions, an intrinsic heme crevice opening is a rate-limiting process.[42] Experimental conditions that are sensitive to accessibility of the heme to $Co(phen)_3^{3+}$ could reveal the importance of columbics.

The presence of a large macromolecule like **Au-TX** can influence the aforementioned rate-limiting processes. **Au-TX** can affect diffusion by either binding

and concentrating reagents on its surface or actually slowing down the tumbling rate by binding Cyt *c*, creating a significantly larger adduct with a different diffusional rate. Additionally, depending on the binding interface, **Au-TX** can block access to the heme. Heme access was restricted in Cyt *c*/**Au-TPhe** and Cyt *c*/**Au-TAsp** as shown by H/D amide exchange,[29] thus the dynamics of these complexes could influence reactivity under these conditions.

The oxidation of Cyt *c* by $Co(phen)_3^{3+}$ alone was performed in 10 mM Tris buffer (pH 7.40, 12 mM NaCl, I = 20 mM, 25.0 °C) as shown in Figure 2.5. The kinetic data was fit according to equation 6, where k_∞ and k_o represent the reaction rate at high and low $Co(phen)_3^{3+}$ concentrations respectively. The inhibition constant K_i was fixed at $1x10^7$ M^{-2}.

$$k_{obs} = k_o - \frac{K_i[Co]_o^{\,2}(k_o - k_\infty)}{1 + K_i[Co]_o^{\,2}} \qquad (6)$$

The free Cyt *c* experiment coincides with literature in which the rate of oxidation is independent of oxidant concentration.[42] At low ionic strength and low oxidant concentrations, the rate determining step is a conformational change in Cyt *c* in which the heme crevice opens. The rate of heme crevice opening depends on the average number of associated anions which is also shown by the inhibition of Cyt *c* oxidation at higher $Co(phen)_3^{3+}$ concentrations (Figure 2.5). These experimental conditions (12 mM NaCl, I = 20 mM) and resulting rates will reflect the importance of columbics and heme accessibility and the effect of **Au-TAsp** and **Au-TPhe** on these processes.

Kinetic experiments using Cyt *c* adducts of **Au-TAsp** and **Au-TPhe** were performed to investigate reactivity differences under conditions that emphasize heme accessibility. The experimental procedure is exactly the same as described in the earlier example, except less salt is added for charge screening. Under these

conditions, Cyt *c* binds tightly to **Au-TAsp** with $K_S \sim 10^7$ M^{-1}.[5] The resulting kinetic curves are shown in Figure 2.6 and the data tabulated in Table 2.2. Note that the Cyt *c* adducts of **Au-TAsp** and **Au-TPhe** saturate similarly with respect to $Co(phen)_3^{3+}$ concentration.

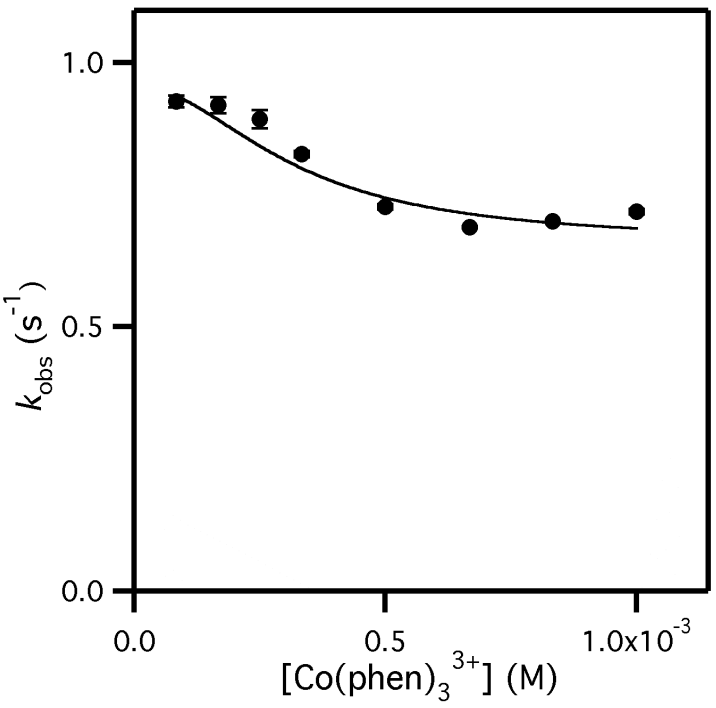

Figure 2.5. Cyt *c* (5 µM) oxidation by $Co(phen)_3^{3+}$ in 10 mM Tris buffer (pH 7.40, 12 mM NaCl, I = 20 mM, 25.0 °C). The curve was fit according to equation 6 with the inhibition constant K_i fixed at 1x10^7 M^{-2}, resulting in $k_\infty = 0.66 \pm 0.0018$ and $k_o = 0.96 \pm 0.0076$.

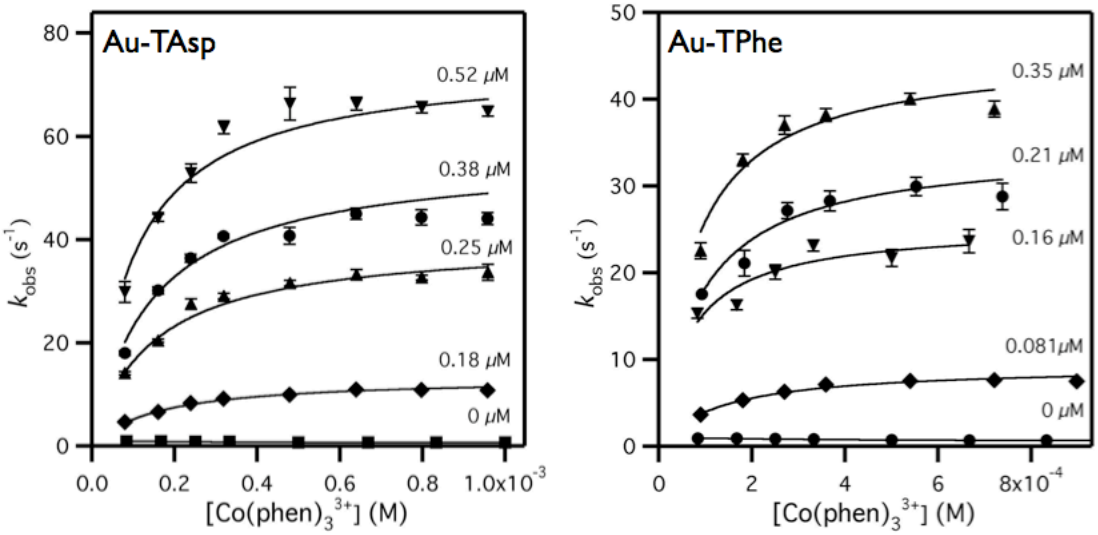

Figure 2.6. Cyt *c* (10 μM) oxidation by $Co(phen)_3^{3+}$ (0.1 – 2 mM) in the presence of varied **Au-TAsp** (0 – 1.04 μM; left) or **Au-TPhe** (0 – 0.7 μM; right) in 10 mM Tris buffer (pH 7.40, 12 mM NaCl, I = 20 mM, 25.0 °C).

Table 2.2. Apparent rate constants for the oxidation of Cyt *c*/**Au-TX** by $Co(phen)_3^{3+}$ in the presence of varied [**Au-TX**] under low salt conditions.

	[**Au-TX**] (μM)	k_{ET}(app) (s^{-1})	$[k_{ET}/K_D]$(app) (M^{-1} s^{-1})	K_D ($\times 10^4$ M^{-1})
Cyt *c*/**Au-TAsp**				
	0.18	13 ± 0.31	0.85 ± 0.020	1.4 ± 0.12
	0.25	39 ± 1.3	2.8 ± 0.085	1.3 ± 0.17
	0.38	52 ± 2.1	4.0 ± 0.14	1.2 ± 0.19
	0.52	77 ± 3.1	7.2 ± 0.33	1.1 ± 0.19
Cyt *c*/**Au-TPhe**				
	0.081	8.9 ± 0.32	0.70 ± 0.021	1.2 ± 0.17
	0.16	26 ± 1.7	4.0 ± 0.43	0.66 ± 0.21
	0.21	34 ± 1.8	3.9 ± 0.13	0.88 ± 0.20
	0.35	45 ± 2.0	6.1 ± 0.47	0.77 ± 0.16

Data fit to equations 1-2.

Au-TX concentration was varied for each particle over several experiments to determine a bimolecular rate constant. The first bimolecular rate plot in Figure 2.7 reflects k_{ET}(app) under saturating $Co(phen)_3^{3+}$ concentrations, resulting in rates of 1.35×10^8 for Cyt *c*/**Au-TAsp** and 1.20×10^8 M^{-1} s^{-1} for Cyt *c*/**Au-TPhe**. There was no dependence on the identity of **TX**. Under these conditions of saturating $[Co(phen)_3^{3+}]$, the reaction likely followed the pathway in which Cyt *c* collides with **Au-TX**/$Co(phen)_3^{3+}$, and the bimolecular rate constants reported here are those for this collision and the subsequent ET.

The collision of Cyt *c* with the preformed **Au-TX**/$Co(phen)_3^{3+}$ adduct could be limited by diffusion, heme crevice accessibility, or intrinsic ET kinetic. Although these rate constants are very fast, they are significantly slower that the calculated rate of diffusion (2.54×10^{11} M^{-1} s^{-1}; Appendix B). However, note that diffusional encounters between large molecules must also incorporate an orientational factor, as a small fraction of collisions will have the correct spatial orientation for a reaction to

occur. This process is likely limited by diffusion because Cyt *c* reacts from solution, where heme accessibility of the unbound protein is unaffected by **Au-TX**.

The second bimolecular rate plot in Figure 2.8 is that of k_{ET}/K_D(app), observed under limiting $Co(phen)_3^{3+}$ concentrations. This apparatent rate constant depends linearly on [**Au-TX**], yielding slopes equal to the absolute rate constant for collision and ET of $Co(phen)_3^{3+}$ with Cyt c/**Au-TX**: $k_{ET}/K_D = 1.86\ (\pm 0.05) \times 10^{12}$ (**Au-TAsp**) and $2.39\ (\pm 0.09) \times 10^{12}\ M^{-1}\ s^{-1}$ (**Au-TPhe**). This bimolecular rate constant is very close to the calculated rate of diffusion ($2.54 \times 10^{11}\ M^{-1}\ s^{-1}$) for both **Au-TAsp** and **Au-TPhe**, suggesting that diffusion may be rate-limiting. This further implies that heme access is equally facile for each Cyt *c*/**Au-TX**, despite differences in their binding footprints.

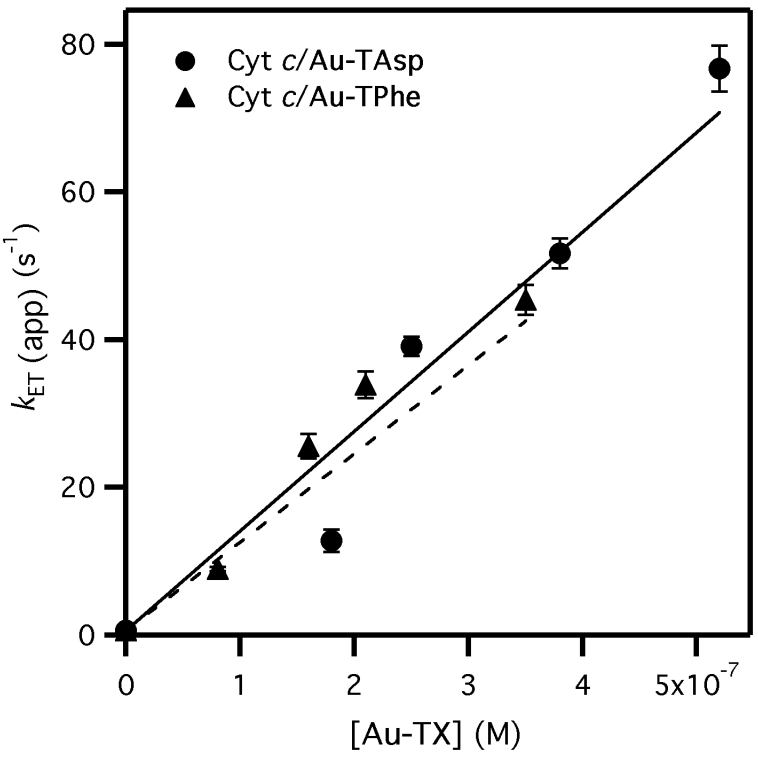

Figure 2.7. Bimolecular rate plot for Cyt *c* oxidation (5 μM, 10 mM Tris, pH 7.4, I = 20 mM, 25.0 °C) by $Co(phen)_3^{3+}$ in the presence of **Au-TX** (X = Asp, Phe). Linear fitting to equation 1 yielded $k_{ET} = 1.35\ (\pm 0.03) \times 10^8$ (X = Asp) and $1.20\ (\pm 0.03) \times 10^8\ M^{-1}\ s^{-1}$ (X = Phe).

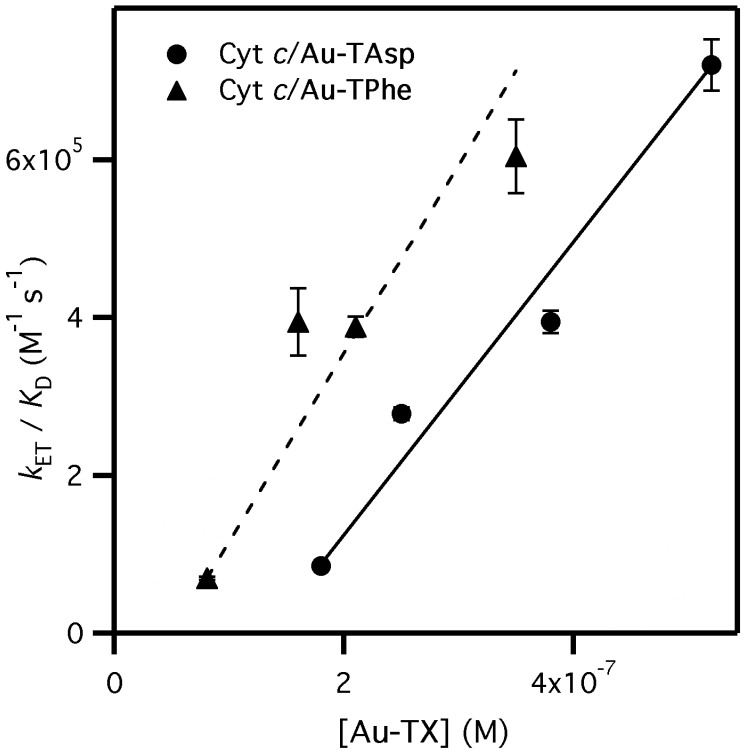

Figure 2.8. Bimolecular rate plot for Cyt *c* oxidation (5 μM, 10 mM Tris, pH 7.4, I = 20 mM, 25.0 °C) by $Co(phen)_3^{3+}$ in the presence of **Au-TX** (X = Asp, Phe). Linear fitting to equation 2 yielded $k_{ET}/K_D = 1.86\ (\pm 0.05) \times 10^{12}$ (X = Asp) and $2.39\ (\pm 0.09) \times 10^{12}\ M^{-1}\ s^{-1}$ (X = Phe).

The reaction at low ionic strength appeared diffusion controlled. The bimolecular rate constants under both limiting and saturating $Co(phen)_3^{3+}$ concentrations showed no distinction between **TX** functionalities. This may reflect the combination of a heme crevice that is preferentially open, and the electrostatic attraction between **Au-TX** and both Cyt *c* and $Co(phen)_3^{3+}$. Notably, when Cyt *c* is bound to **Au-TX**, heme accessibility is not rate limiting, despite differences in the binding footprints.[29]

2.3.5. Au-TX **selectively enhances oxidation rates under higher ionic strength**

Increased ionic strength was used to de-emphasize the effect of electrostatics on the ET reactivity of Cyt *c* in the presence of **Au-TX**. When the ionic strength is increased to 0.1 M NaCl, Cyt *c* binds weakly to **Au-TX** with a K_S of $\sim \times 10^5\ M^{-1}$

(Appendix D), which makes the binding of Cyt c/Au-TX more transient. Higher ionic strength also results in a closed heme crevice configuration[42] which will emphasize the dynamics and heme accessibility in the Cyt *c*/**Au-TX** adducts.

The side chain functionalities of **Au-TX** were varied to manipulate the reactivity of Cyt *c*. Pseudo-first order kinetics datasets were collected in the presence of varied **Au-TX** concentrations, with k_{obs} saturating at elevated $Co(phen)_3^{3+}$ concentrations as shown in Figure 2.9. The datasets were fitted to equation 2, providing the apparent bimolecular rate constants $[k_{ET}/K_D]$(app) and K_D for Co^{3+} binding to the ternary complex that are collected in Table 2.3. As the apparent bimolecular rate constant $[k_{ET}/K_D]$(app) is the tangent to each curve in the limit of low $[Co^{3+}]$, it is clear that the apparent bimolecular ET increased significantly for each Cyt *c*/**Au-TX** adduct. These apparent bimolecular rate constants ranged from 10^3 – 10^6 M^{-1} s^{-1} for increasing concentrations of **Au-TX**. Oxidation rates for bound Cyt *c* were sensitive to the concentration of **Au-TX** and the identity of the functional groups.

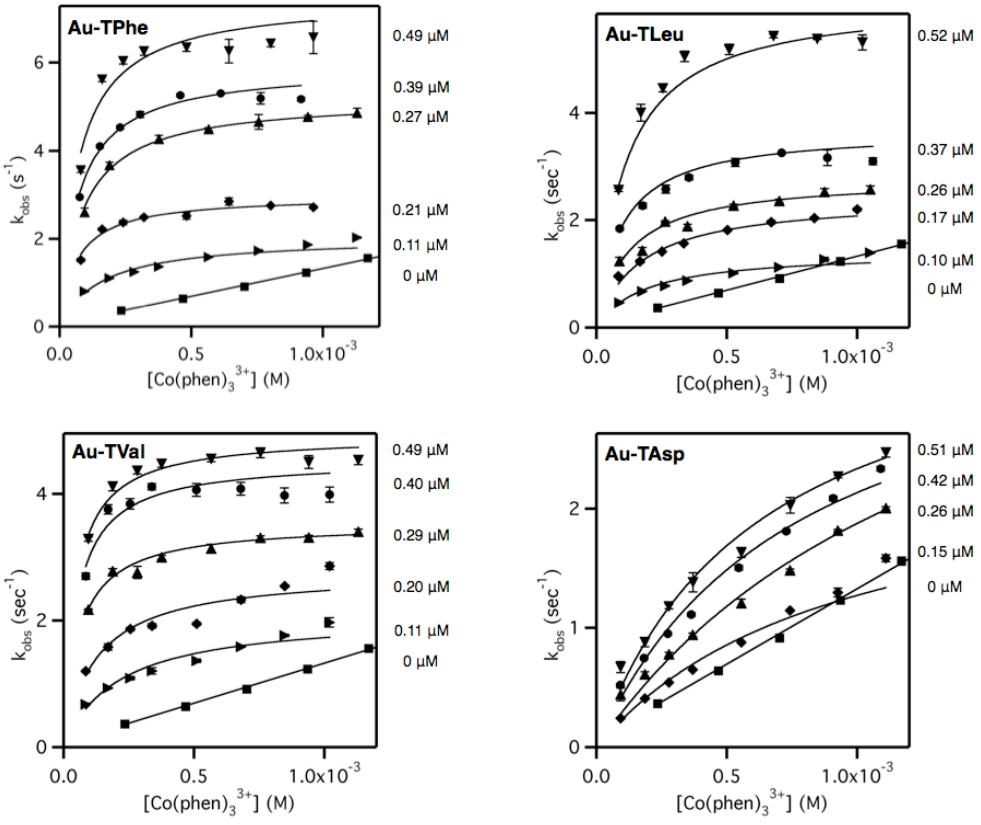

Figure 2.9. Second-order plots of k_{obs} for the $Co(phen)_3^{3+}$ oxidation of Cyt $c(Fe^{2+})$/**Au-TX** in 10 mM Tris (pH 7.40, 0.1 M NaCl, 25 °C); **X** = **Phe**, **Leu**, **Val**, and **Asp**. Syringe A: 10 μM Cyt *c*, 0.2 – 1 μM **Au-TX**. Syringe B: 0.1 – 2 mM $Co(phen)_3^{3+}$. Data was fit to equation 2. The reaction of free Cyt *c* is indicated by (■).

Table 2.3. Apparent rate constants for the oxidation of Cyt $c(Fe^{2+})$ by $Co(phen)_3^{3+}$ in the presence of varied [**Au-TX**].

	[**Au-TX**] (μM)	k_{ET}(app) (s^{-1})	$[k_{ET}/K_D]$(app) (M^{-1} s^{-1})	K_D ($\times 10^{-4}$ M)	fraction bound
Cyt *c*/**Au-TPhe**					
	0.11	2.04 ± 0.107	13181 ± 140	1.54 ± 0.0237	0.0158
	0.21	2.98 ± 0.0791	46007 ± 1750	0.647 ± 0.0274	0.0298
	0.27	5.20 ± 0.0565	60861 ± 3520	0.854 ± 0.0565	0.0381
	0.39	5.91 ± 0.123	82778 ± 1280	0.714 ± 0.0136	0.0544
	0.49	7.47 ± 0.264	105590 ± 3150	0.707 ± 0.0273	0.0676
Cyt *c*/**Au-TLeu**					
	0.10	1.42 ± 0.106	7785 ± 70.7	1.82 ± 0.0320	0.0148
	0.17	2.43 ± 0.0911	14618 ± 398	1.66 ± 0.0630	0.0250
	0.26	2.79 ±0.124	23929 ± 1180	1.20 ± 0.0794	0.0379
	0.37	3.68 ±0.0793	39435 ± 1180	0.932 ± 0.0318	0.0535
	0.52	6.14 ±0.189	54227 ± 995	1.13 ± 0.0243	0.0742
Cyt *c*/**Au-TVal**					
	0.11	2.09 ±0.182	10100 ± 215	2.07 ± 0.0637	0.0090
	0.20	2.79 ±0.221	22635 ± 614	1.23 ± 0.0423	0.0162
	0.29	3.54 ±0.0602	60139 ± 1370	0.588 ± 0.0165	0.0234
	0.40	4.54 ±0.135	90617 ± 5380	0.501 ± 0.0353	0.0321
	0.49	4.93 ±0.0814	110710 ± 4490	0.445 ± 0.0209	0.0391
Cyt *c*/**Au-TAsp**					
	0.15	2.47 ±0.0409	2632 ± 23.2	9.38 ± 0.232	0.0161
	0.26	4.54 ± 0.140	3201 ± 62.1	14.1 ± 0.705	0.0279
	0.42	3.78 ± 0.0521	4913 ± 42.4	7.69 ± 0.165	0.0447
	0.51	3.78 ± 0.0803	6123 ± 179	6.17 ± 0.307	0.0541

Pseudo-first-order rates (k_{obs}) were fit to equations 1-2. Cyt $c(Fe^{2+})$ (5.0 μM) was preincubated with **Au-TX** (10 mM Tris, pH = 7.40, 0.10 M NaCl). Fraction bound was calculated using the ITC data collected in Appendix D and equation D.1.

Free Cyt *c* oxidation by $Co(phen)_3^{3+}$ exhibited second order kinetics in Figure 2.9 (■) with a bimolecular rate constant of $k_{ET}/K_D = 1.33\times10^3 \pm 40$ M^{-1} s^{-1}. In contrast, the Cyt *c*/**Au-TX** adducts exhibited saturation kinetics, with the apparent rate constants, k_{ET}(app) and k_{ET}/K_D(app), increasing with increasing **Au-TX** concentration. k_{ET}/K_D(app) fell in the range of either 10^3 or 10^5 M^{-1} s^{-1}, depending upon **Au-TX** concentration and functionality, unlike the low ionic strength experiments that

displayed no **TX** discrimination. Based upon the apparent Cyt *c*(Fe^{2+}) oxidation rates, the nanoparticles fell into two classes. The hydrophilic **Au-TAsp** particle was noticeably different than those with surfaces functionalized by hydrophobic amino acid side chains (**Phe**, **Leu**, and **Val**). Cyt *c*/**Au-TAsp** exhibited a k_{ET}/K_D(app) near 10^3 $M^{-1}s^{-1}$, whereas this rate constant was in the range of 10^5 $M^{-1}s^{-1}$ for the more hydrophobic **Au-TX** groups.

The apparent rate constant at saturating [$Co(phen)_3^{3+}$], k_{ET}(app), increased linearly with **Au-TX** concentration (Figure 2.10) showing a weak dependence on **TX** identity with slopes of approximately 1×10^7 $M^{-1}s^{-1}$ (Table 2.4). As stated previously, the rate should be determined by heme accessibility, collisional frequency, or intrinsic ET rates. As k_{ET} represents the rate for Cyt *c* reacting with the **Au-TX**/$Co(phen)_3^{3+}$ adduct, heme accessibility should be governed by the status of Cyt c in solution, and show no dependence on Cyt *c*/**Au-TX** binding footprint – this was borne out by the similarity of k_{ET} for both **Au-TAsp** and **Au-TPhe**. The fast rates observed suggest that diffusion may be rate-limiting; however, intrinsic ET cannot be ruled out.

Under limiting $Co(phen)_3^{3+}$ concentrations, the reaction of Cyt *c*/**Au-TX** adduct with $Co(phen)_3^{3+}$ displayed dependence on the functional groups of **Au-TX**. The $k_{ET}/K_{D(app)}$ plot (Figure 2.11) resulted in bimolecular rate constants ranging from 0.0870×10^{11} $M^{-1}s^{-1}$ to 1.95×10^{11} $M^{-2}s^{-1}$ (Table 2.5) in which $k_{ET}/K_{D(app)}$ is the rate constant in the limit of very low [$Co(phen)_3^{3+}$], representing the **Au-TX**/Cyt *c* adduct reacting with $Co(phen)_3^{3+}$. The high rate constant likely is limited by diffusional rates. The dependence on **TX** functionality probably results from the distinct heme access afforded by Au-TX binding to Cyt *c*. This is supported by a previously published amide H/D exchange experiment in which **Au-TAsp** was shown to strongly bind to the front face of Cyt *c*, which would effectively block heme access to small

molecules.[29] In contrast, **Au-TPhe** bound to a slightly shifted, smaller face of Cyt *c*. As **Au-TAsp** binds to a large surface of Cyt c, this would reduce heme access, leading to slower ET kinetics. Under these conditions, **Au-TX** provides a tunable surface that catalyzes the ET reactivity of Cyt *c*. Since Cyt *c* is bound to **Au-TX** when it collides and reacts with $Co(phen)_3^{3+}$, the possibility of protein dynamics on the surface of **Au-TX** modulating ET reactivity will be addressed in a later study.

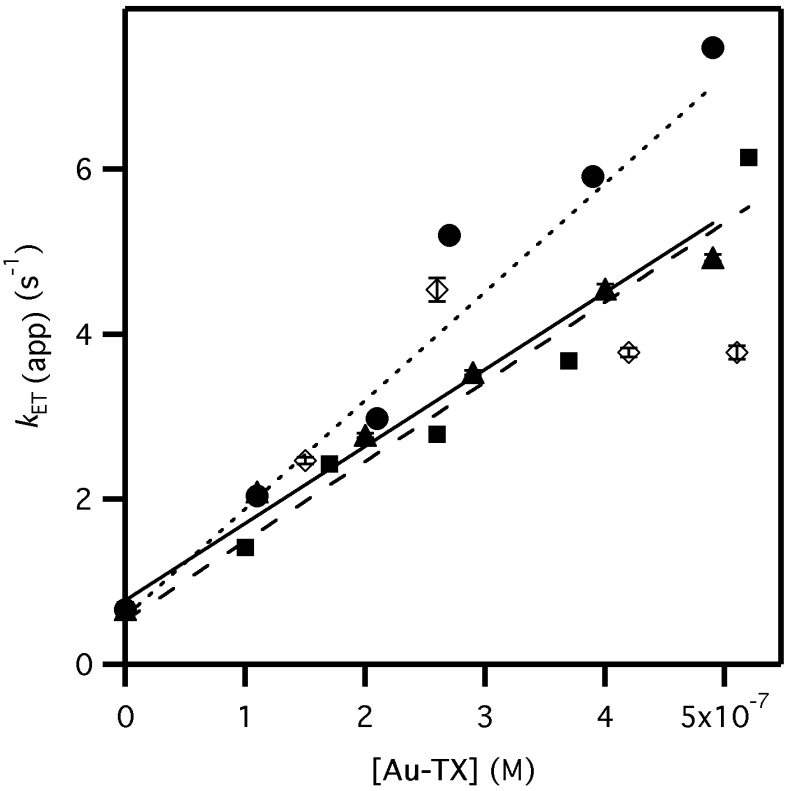

Figure 2.10. Cyt *c* oxidation (5 μM, 10 mM Tris, pH 7.4, 0.1 M NaCl) by $Co(phen)_3^{3+}$ in the presence of **Au-TX** and the dependence of apparent electron transfer rate, k_{ET}/K_D, on concentration of **Au-TPhe** (●), **Au-TLeu** (■), **Au-TVal (▲), and Au-TAsp** (◆). Data fit to equation 1.

Table 2.4. Absolute bimolecular rate constants for the reaction of Cyt *c*:**Au-TX** with $Co(phen)_3^{3+}$.

	k_{ET} ($\times 10^7$ s^{-1})
Cyt *c*:**Au-TPhe**	1.31 ±(0.0129)
Cyt *c*:**Au-TLeu**	0.963 ±(0.00870)

Cyt *c*:**Au-TVal**	0.932 ± (0.0129)
Cyt *c*:**Au-TAsp**	---

The data in Table 2.4 was plotted as k_{ET}(app) against [**Au-TX**]. The linear to give the estimated error of the tabulated bimolecular rate constants , k_{ET}. The Cyt *c*/**Au-TAsp** data was too scattered to result in a satisfactory fit.

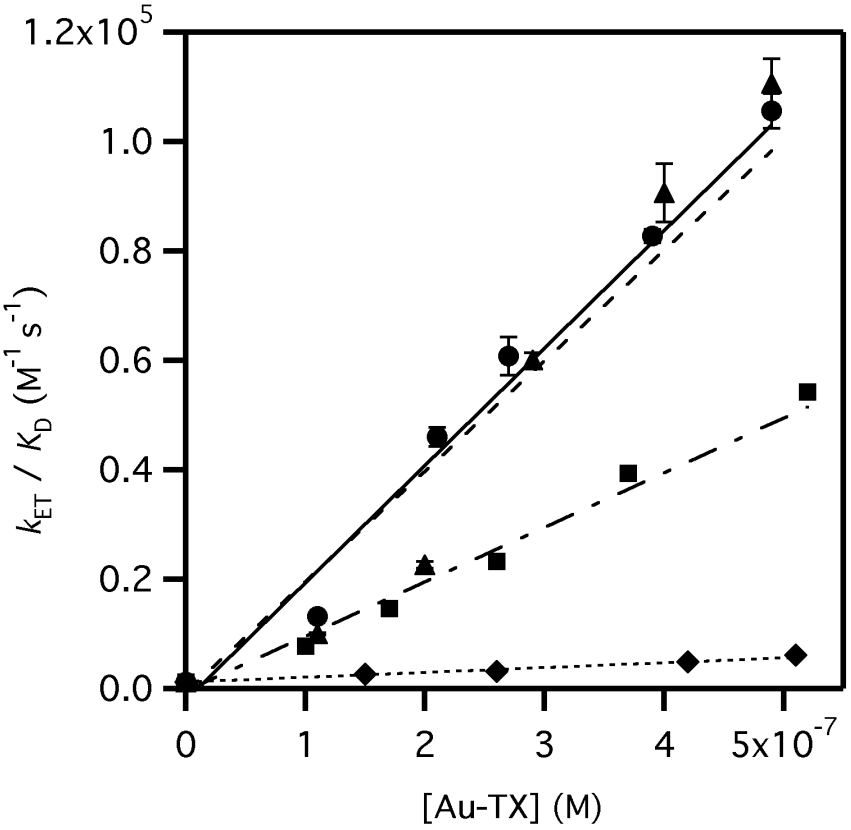

Figure 2.11. Cyt *c* oxidation (5 μM, 10 mM Tris, pH 7.4, 0.1 M NaCl) by $Co(phen)_3^{3+}$ in the presence of **Au-TX** and the dependence of apparent electron transfer rate, k_{ET}/K_D, on concentration of **Au-TPhe** (●), **Au-TLeu** (■), **Au-TVal (▲), and Au-TAsp** (◆).

Table 2.5. Absolute bimolecular rate constants for the reaction of Cyt *c*/**Au-TX** with $Co(phen)_3^{3+}$.

	k_{ET}/K_D ($\times 10^{11}$ M^{-1} s^{-1})
Cyt *c*	0.00133
Cyt *c*/**Au-TPhe**	2.02 ± 0.0569
Cyt *c*.**Au-TLeu**	0.996 ± .0383
Cyt *c*/**Au-TVal**	2.14 ± .0976
Cyt *c*/**Au-TAsp**	0.0866 ± .00203

The data in Table 2.5 was plotted as k_{ET}/K_D against [**Au-TX**]. The linear fits were weighted by 2σ to give the estimated error of the tabulated bimolecular rate constants, k_{ET}/K_D.

2.3.6. Interpreting the ET catalysis mechanism

The model presented in Scheme 2.1 outlines a random mechanism in which Cyt *c* reacts with $Co(phen)_3^{3+}$ in the presence of **Au-TX**. The two extreme cases, Cyt *c*/**Au-TPhe** and Cyt *c*/**Au-TAsp** are directly compared in Figure 2.12 to highlight the rate determining factors.

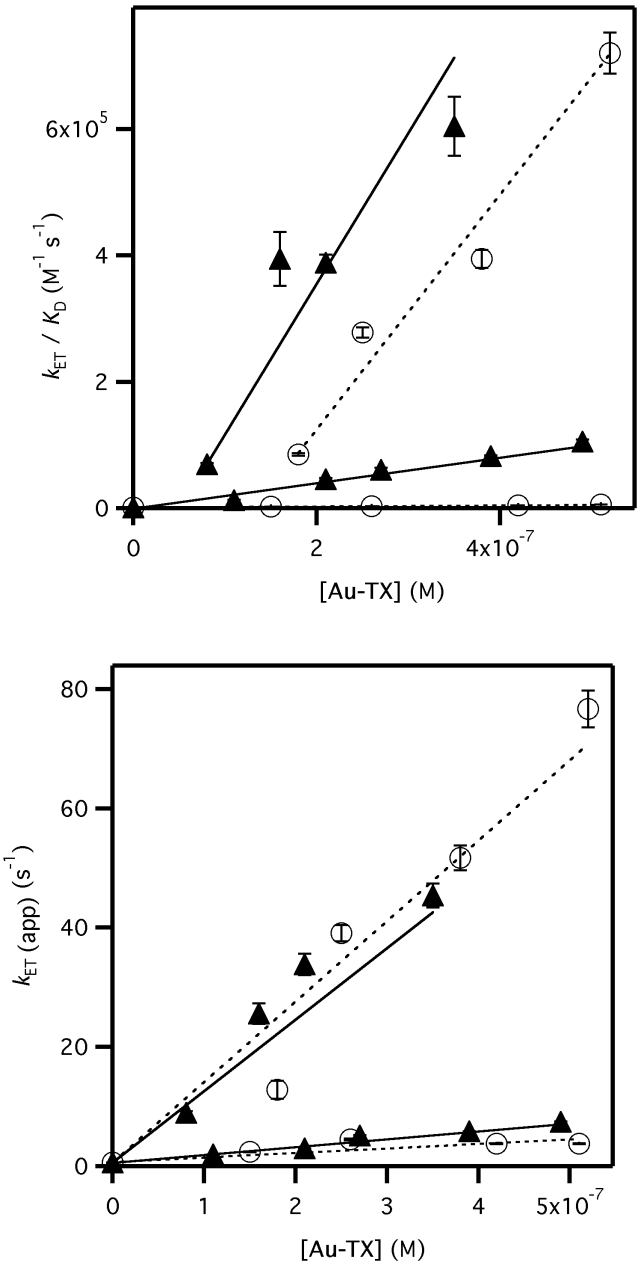

Figure 2.12. Bimolecular rate plots of Cyt *c* oxidation by $Co(phen)_3^{3+}$ in the presence of **Au-TPhe** (▲) and **Au-TAsp** (○) under low (*I* = 20 mM) and high (0.1 M NaCl) conditions in 10 mM Tris (pH 7.4, 25.0 °C)

$k_{ET(app)}$ is the apparent rate constant that reflects Cyt *c* reacting with **Au-TX**/$Co(phen)_3^{3+}$. Since heme access is determined by the solution properties of Cyt *c*, no TX selectivity was apparent under both low and high salt conditions (Figure 2.12). The diffusional collisions of Cyt *c* with **Au-TX**/$Co(phen)_3^{3+}$ is likely to be the rate determining step and may be attenuated by orientation factors.

k_{ET}/K_D is the apparent rate constant for $Co(phen)_3^{3+}$ reacting with Cyt *c*/**Au-TX**. Since Cyt *c* is bound to **Au-TX** during the collision and reaction with $Co(phen)_3^{3+}$, TX selectivity was expected due to the different **Au-TX** binding faces. It was previously shown that **Au-TAsp** binds to a larger area located at the front face of Cyt *c*. Thus, the binding interaction likely transiently blocks heme access, reducing reactivity. In contrast, **Au-TPhe** binds in a smaller area that is shifted further away from the heme crevice.[29] The dynamics necessary to expose the heme crevice must be considered. Under low salt conditions, there was little difference in the bimolecular rates while high salt conditions resulted in a significant 100-fold difference in k_{ET}/K_D (Figure 2.11). Under low ionic strength, Cyt *c* favors an open heme crevice conformation not seen under higher, physiological salt conditions.[42] This resulted in the k_{ET} rates for low salt conditions to be faster with attenuated TX selectivity. The high salt conditions favored a closed heme crevice conformation and resulted in slower rates that were sensitive to **Au-TX**'s effect on heme accessibility.

2.4. Conclusions

Anionic gold nanoparticles catalyzed the ET reactivity of Cyt *c* without altering the native structure. The reaction rates should depend upon heme accessibility, collisional frequency, or intrinsic ET rates. Under high [$Co(phen)_3^{3+}$], there was little to no dependence of k_{ET} on TX functionalization under both low and high ionic strength conditions. Since these rates represented the collision of Cyt *c*

with **Au-TX**/$Co(phen)_3^{3+}$, the heme accessibility of Cyt *c* in solution was not dependent on **Au-TX**, suggesting a diffusion-limited process.

Extremely fast, efficient enzymes like triose-phosphate isomerases (TIM) and Cu, Zn-superoxide dismutases (SOD), rely on electrostatics to steer substrates into the active site, resulting in a diffusion limited rate-determining step.[43] TIM, which has been described as a "perfect enzyme,[44]" has catalytic rates of $\sim 10^8$ $M^{-1}s^{-1}$ at 0.1 M ionic strength.[45] Eight species of SOD have catalytic rates of $\sim 3 \times 10^9$ $M^{-1}s^{-1}$ at 0.02 M ionic strength.[46] The enzyme/NP systems presented here near diffusion reaction rates that ranged from $\sim 10^{11}$ - 10^{12} $M^{-1}s^{-1}$ depending upon ionic strength conditions. The NP efficiently catalyzed the ET reaction near diffusion and about 10^5 times faster than the free protein[5]. In addition, the redox potential and coordination geometry of the heme was monitored using redox mediators and EPR spectroscopy, respectively. These properties were unaltered when Cyt *c* was bound to **Au-TX**, indicating that **Au-TX** acts a catalyst, yet doesn't compromise the native structure or function of Cyt *c*.

Limiting [$Co(phen)_3^{3+}$] resulted in distinct ET reactivity. k_{ET}/K_D reflected the collision of $Co(phen)_3^{3+}$ with Cyt *c*/**Au-TX**, which introduced the possibility of Cyt *c*/**Au-TX** dynamics to modulate ET. Under high ionic strength conditions, the k_{ET}/K_D enhancement was tunable by varying the substituents of **Au-TX**, ranging from 0.0870 $\times 10^{11}$ for Cyt *c*/**Au-TAsp** to 1.95×10^{11} M^{-1} s^{-1} for Cyt *c*/**Au-TPhe**. The larger binding interface between **Au-TAsp** and Cyt *c* is located at the heme crevice and likely transiently blocked heme access, resulting in attenuated ET reactivity.

The distinct **Au-TX**/Cyt *c* binding interface and ET reactivity is analogous to how differences in binding result in different ET mechanisms for CCP with either horse heart Cyt *c* or yeast Cyt *c*. Horse heart Cyt *c* experiences gated ET because the rotated binding interface produces an inefficient ET pathway.[47] Similarly, if the

binding interaction between Cyt *c* and **Au-TX** transiently blocks heme access, a different ET mechanism could be favored. Strong **TX** selectivity was present for conditions that represented the reaction of **Au-TX**/Cyt *c* with $Co(phen)_3^{3+}$. If bound to **Au-TX** at the time of reaction, Cyt *c* is subject to any differences in binding or dynamics caused by different **Au-TX** functionality.

There are several possible mechanisms behind the catalysis. This chapter mainly addresses electrostatic effects in which **Au-TX** brings together the two positive reactants, thus increasing the local concentration. The Circe effect predicts a 100-fold increase in effective concentration for each reagent (Appendix C). Under high ionic strength conditions with excess oxidant concentrations, the ET reactivity was sensitive to **TX** functionality, possibly due to differences in binding and dynamics. Later studies will directly address possible dynamic changes of Cyt *c* when bound to the surface of **Au-TX** and its effect on reactivity.

2.5. References Cited

(1) Gray, H. B.; Winkler, J. R. *Q. Rev. Biophys.* **2003**, *36*, 341-72.

(2) Verma, A.; Rotello, V. M. *Chem. Commun.* **2005**, 303-312.

(3) You, C. C.; De, M.; Rotello, V. M. *Curr. Opin. Chem. Biol.* **2005**, *9*, 639-46.

(4) Daniel, M. C.; Astruc, D. *Chem. Rev.* **2004**, *104*, 293-346.

(5) Carver, A. M.; De, M.; Bayraktar, H.; Rana, S.; Rotello, V. M.; Knapp, M. J. *J. Am. Chem. Soc.* **2009**, *131*, 3798-9.

(6) Fillon, Y.; Verma, A.; Ghosh, P.; Ernenwein, D.; Rotello, V. M.; Chmielewski, J. *J. Am. Chem. Soc.* **2007**, *129*, 6676-6677.

(7) Guarise, C.; Manea, F.; Zaupa, G.; Pasquato, L.; Prins, L. J.; Scrimin, P. *J. Pept. Sci.* **2008**, *14*, 174-83.

(8) You, C. C.; De, M.; Han, G.; Rotello, V. M. *J. Am. Chem. Soc.* **2005**, *127*, 12873-12881.

(9) Liu, J.; Lu, Y. *Chem. Commun.* **2007**, 4872-4.

(10) Hurst, S. J.; Han, M. S.; Lytton-Jean, A. K.; Mirkin, C. A. *Anal. Chem.* **2007**, *79*, 7201-5.

(11) Guarise, C.; Pasquato, L.; De Filippis, V.; Scrimin, P. *Proc. Natl. Acad. Sci. U. S. A.* **2006**, *103*, 3978-82.

(12) Zheng, G.; Daniel, W. L.; Mirkin, C. A. *J. Am. Chem. Soc.* **2008**, *130*, 9644-5.

(13) Cao, Y. C.; Jin, R.; Nam, J. M.; Thaxton, C. S.; Mirkin, C. A. *J. Am. Chem. Soc.* **2003**, *125*, 14676-7.

(14) Oh, E.; Hong, M. Y.; Lee, D.; Nam, S. H.; Yoon, H. C.; Kim, H. S. *J. Am. Chem. Soc.* **2005**, *127*, 3270-1.

(15) You, C. C.; Agasti, S. S.; De, M.; Knapp, M. J.; Rotello, V. M. *J. Am. Chem. Soc.* **2006**, *128*, 14612-14618.

(16) Hu, M.; Qian, L.; Brinas, R. P.; Lymar, E. S.; Hainfeld, J. F. *Angew. Chem. Int. Ed.* **2007**, *46*, 5111-4.

(17) Sierra-Sastre, Y.; Choi, S.; Picraux, S. T.; Batt, C. A. *J. Am. Chem. Soc.* **2008**, *130*, 10488-9.

(18) Zaupa, G.; Scrimin, P.; Prins, L. J. *J. Am. Chem. Soc.* **2008**, *130*, 5699-5709.

(19) Aubin-Tam, M. E.; Hamad-Schifferli, K. *Biomed. Mater.* **2008**, *3*, 034001.

(20) Gray, H. B.; Winkler, J. R. *Annu. Rev. Biochem.* **1996**, *65*, 537-61.

(21) Davidson, V. L. *Acc. Chem. Res.* **2000**, *33*, 87-93.

(22) Margoliash, E.; Frohwirt, N. *Biochem. J* **1959**, *71*, 570-578.

(23) Schilt, A. A.; Taylor, R. C. *J. Inorg. Nucl. Chem.* **1959**, *9*, 211-221.

(24) Holwerda, R. A.; Knaff, D. B.; Gray, H. B.; Clemmer, J. D.; Crowley, R.; Smith, J. M.; Mauk, A. G. *J. Am. Chem. Soc.* **1980**, *102*, 1142-1146.

(25) Wallace, C. J. A.; Corradin, G.; Marchiori, F.; Borin, G. *Biopolymers* **1986**, *25*, 2121-2132.

(26) Davenport, H. E.; Hill, R. *Proc. R. Soc. London, Ser. B* **1952**, *139*, 327-347.

(27) Craig, D. B.; Nichols, E. R. *J. Chem. Educ.* **2006**, *83*, 1325-1326.

(28) Bernhardt, P. V.; Chen, K. I.; Sharpe, P. C. *J. Biol. Inorg. Chem.* **2006**, *11*, 930-936.

(29) Bayraktar, H.; You, C. C.; Rotello, V. M.; Knapp, M. J. *J. Am. Chem. Soc.* **2007**, *129*, 2732-2733.
(30) Dutton, P. L. *Methods Enzymol.* **1978**, *54*, 411-435.
(31) Wallace, C. J. A.; Proudfoot, A. E. I. *Biochem. J* **1987**, *245*, 773-779.
(32) Myer, Y. P.; Saturno, A. F.; Verma, B. C.; Pande, A. *J. Biol. Chem.* **1979**, *254*, 1202-1207.
(33) Rodkey, F. L.; Ball, E. G. *J. Biol. Chem.* **1950**, *182*, 17-28.
(34) Marques, H. M. *Dalton Trans.* **2007**, 4371-85.
(35) Santucci, R.; Reinhard, H.; Brunori, M. *J. Am. Chem. Soc.* **1988**, *110*, 8536-8537.
(36) Pollock, W. B. R.; Rosell, F. I.; Twitchett, M. B.; Dumont, M. E.; Mauk, A. G. *Biochemistry* **1998**, *37*, 6124-6131.
(37) Peisach, J.; Blumberg, W. E.; Ogawa, S.; Rachmilewitz, E. A.; Oltzik, R. *J. Biol. Chem.* **1971**, *246*, 3342-3355.
(38) Marcus, R. A.; Sutin, N. *Biochim. Biophys. Acta* **1985**, *811*, 265-322.
(39) Kellogg, J. A.; Bren, K. L. *Biochim. Biophys. Acta* **2002**, *1601*, 215-221.
(40) Latypov, R. F.; Cheng, H.; Roder, N. A.; Zhang, J.; Roder, H. *J. Mol. Biol.* **2006**, *357*, 1009-25.
(41) Aubin-Tam, M. E.; Hamad-Schifferli, K. *Langmuir* **2005**, *21*, 12080-4.
(42) Rush, J. D.; Koppenol, W. H.; Garber, E. A. E.; Margoliash, E. *J. Biol. Chem.* **1988**, *263*, 7514-7520.
(43) Wade, R. C.; Gabdoulline, R. R.; Ludemann, S. K.; Lounnas, V. *Proc. Natl. Acad. Sci. U. S. A.* **1998**, *95*, 5942-9.
(44) Knowles, J. R. *Nature* **1991**, *350*, 121-4.
(45) Albery, W. J.; Knowles, J. R. *Biochemistry* **1976**, *15*, 5627-31.
(46) Sergi, A.; Ferrario, M.; Polticelli, F.; O'Neill, P.; Desideri, A. *J. Phys. Chem.* **1994**, *98*, 10554-10557.
(47) Mei, H. K.; Wang, K. F.; Peffer, N.; Weatherly, G.; Cohen, D. S.; Miller, M.; Pielak, G.; Durham, B.; Millett, F. *Biochemistry* **1999**, *38*, 6846-6854.

CHAPTER 3

THE DYNAMICS OF CYT *c* ON NANOPARTICLE SURFACES

3.1. Introduction

Site-directed spin labeling (SDSL) is a technique that attaches a spin label (SL) to a protein to probe local structure and conformational dynamics.[1,2] SDSL EPR has been applied to characterize dynamics within a wide range of systems, including protein backbone dynamics,[3] conformational changes,[4] helix mobility,[5] protein folding kinetics,[6] local structure and dynamics of ion channels,[7] conformational motion of transporters,[8-10] conformational changes of RNA at the individual nucleotide level,[11] as well as to map the molecular surface involved in protein-protein binding[12,13] and protein-membrane interactions.[14,15] The sensitivity of the SL to its local environment provides information on structure, dynamics, and conformational changes.

The EPR lineshape of spin labels are sensitive to nanosecond motion. When combined with site-directed cysteine mutagenesis, cysteine-specific spin labels such as nitroxide derivatives can be introduced at chosen locations within a protein, resulting in a stable organic radical that can be monitored using EPR. The SL EPR lineshape and rotational correlation times reflect both local structure and dynamics, as well as global tumbling of the protein. In one study, Scholes produced a series of Cyt *c* mutants with SLs located at various external sites that reported a global kinetic folding process.[16] SLs can also elucidate the interactions of spin-labeled proteins with other biomacromolecules. An investigation of the interaction of Cyt *c* with lipid bilayers showed that the EPR spectrum of spin-labeled apo-Cyt *c* was sensitive to the protein binding to negatively charged lipid bilayers and detergent micelles. Mixed lipid systems resulted in distinctly identifiable binding modes.[17] The purpose of this

study is to characterize the dynamics of Cyt *c* while non-covalently bound to surface-functionalized gold nanoparticles, **Au-TX**.

The location of a SL in a protein can be correlated to the type of local environment and interactions using EPR lineshape analysis.[18] Surface loops tend to be highly mobile, while buried sites or locations with local structure or residues that interfere or interact with a SL restrict dynamic motion. The previously mentioned study by Scholes attached SLs at external, solvent accessible positions. The structure of Cyt *c* was unperturbed by introducing SLs at these sites, unlike wild type Cyt *c*. Labeling the native C102 position distorted the hydrophobic packing, leading to a 20 °C lower melting temperature. The mutants showed no appreciable change in the far UV CD helical spectral signatures nor melting temperatures. All these SL locations reported a global 20-30 ms folding phase, showing that these positions reported common, not disconnected, kinetic events.[16] By selecting these mutants with varied locations throughout the protein, the dynamics of Cyt *c* at the nanoparticle surface can be monitored.

The ET kinetics study suggested that global dynamics and heme crevice access were important factors and under certain experimental conditions, resulted in a 100-fold difference in ET reactivity between Cyt *c*/**Au-TAsp** and Cyt *c*/**Au-TPhe**. The binding interface and dynamics of Cyt *c* on the surface of **Au-TX** will be probed by spin-labeled Cyt *c* and four specific mutants. The initial basis for selection was a study published by Bayraktar et al that characterized the binding interface and facial selectivity between Cyt *c* and **Au-TX** using amide H/D exchange.[19] The differences in solvent protection, which indicate either binding or dynamic movement of Cyt *c* on that area of the **Au-TX** surface, are illustrated in Figure 3.1. **Au-TAsp** has a larger solvent protected surface, suggesting either a larger binding interface or a less

dynamic binding interaction than **Au-TPhe**. This binding information will serve as reference in the interpretation of the dynamics of each SL-Cyt *c*/**Au-TX** adduct.

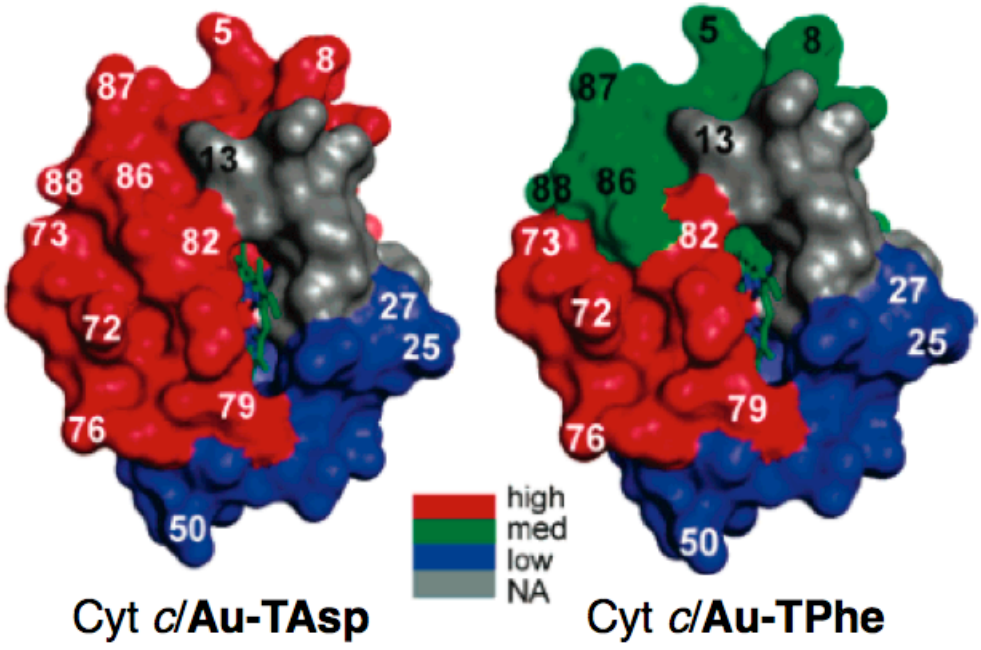

Figure 3.1. Solvent protection of wild type Cyt *c* peptides bound to **Au-TX** taken from a facial selectivity study performed by Bayraktar et al.[19]

The selected Cyt *c* mutants had mutation-tolerant positions located at external labeling sites that didn't destabilize the protein.[16] The mutants fell into several categories according to what type of information about binding and dynamics they will yield as outlined in Figure 3.2. Locations displaying distinct solvent protection (T8C, N92C, C102) should report unique dynamics sensitive to the surface functionalization of **Au-TX**. In contrast, areas of no or relatively low solvent protection (C102 and D50C) could report global dynamics. The medium solvent protection region for Cyt *c*/**Au-TPhe** (T8C and N92C) could yield information about dynamic movement of Cyt *c* at those locations. Finally, the position located near the heme crevice (K79C), where small molecules like $Co(phen)_3^{3+}$ react with Cyt *c*, will reflect heme accessibly of Cyt *c* when bound to **Au-TX**. Using all this information,

we aim to understand both the local and global dynamics of Cyt *c* on the surface of **Au-TX**.

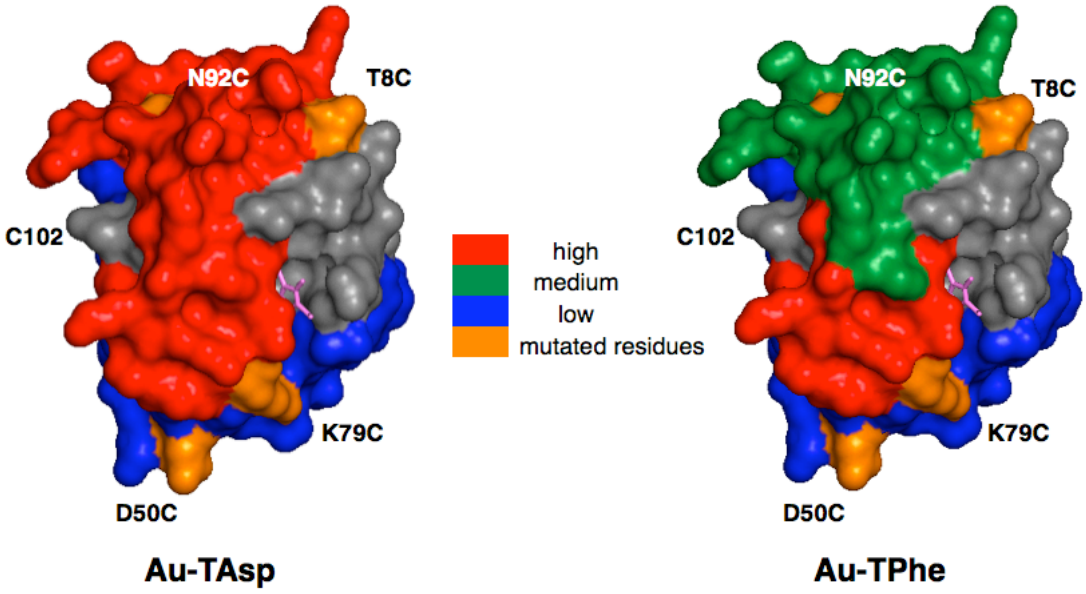

Au-TAsp **Au-TPhe**

distinct solvent protection	low solvent protection	key locations
T8C (higher on **Au-TAsp**)	D50C (possible global dynamics)	K79C (near heme crevice)
N92C (higher on **Au-TAsp**)	C102 (possible global dynamics)	T8C (dynamic location on **Au-TPhe**)
C102 (higher on **Au-TAsp**)		N92C (dynamic location on **Au-TPhe**)

Figure 3.2. The locations of the SL in wild type Cyt *c* and the selected mutants superimposed on the binding interface determined using H/D amide exchange.[19] The name and number of the mutants correspond to the residue that was replaced with cysteine. In the mutants, the cysteine residue C102 was replaced with serine. The table summarizes key features of each mutant selection.

In the previously presented intermolecular electron transfer study, it was shown that the Cyt *c*/**Au-TPhe** adduct has a bimolecular rate constant 100 times larger than the corresponding **Au-TAsp** adduct. This discrepancy could result from several things, including local concentration effects or dynamics. Using both wild type and selected mutants of yeast Cyt *c*, the local dynamics of key locations and global motion of SL-Cyt *c*/**Au-TX** adducts will be characterized, linking the binding and dynamic interactions of SL-Cyt *c* with **Au-TX** to ET reactivity.

3.2. Experimental Methods

3.2.1. General Considerations

Wild type yeast (*Saccharomyces cerevisiae*) Cyt *c* and tris(hydroxymethyl)-aminomethane (Tris) were obtained from Sigma Aldrich. As yeast Cyt *c* contains a single surface reactive Cys residue at position 102, it will be denoted as C102. A series of Cyt *c* double mutants were provided by C. P. Scholes, et al.[16] These double mutants each contained a $Cys^{102} \rightarrow$ Ser mutation, with a single surface reactive Cys as follows: $Asp^{50} \rightarrow$ Cys (D50C); $Thr^{8} \rightarrow$ Cys (T8C); $Lys^{79} \rightarrow$ Cys (K79C); $Asn^{92} \rightarrow$ Cys (N92C). The nitroxide spin label 1-oxyl-2,2',5,5'-tetramethylpyrroline-3-methyl-methanethiosulfonate (MTSSL) was purchased from Toronto Research Chemicals; this particular spin label reacts with accessible cysteine residues. Cyt *c* was incubated with excess dithiothreitol (DTT) for one hour at room temperature under N_2 to reduce any disulfides, then the DTT was then removed via multiple buffer exchanges. A two-fold excess of MTSSL was added and incubated for an hour under N_2 at room temperature, then the sample was concentrated and excess MTSSL removed by centrifugal concentrators. Surface-functionalized gold nanoparticles (**Au-TX**) were prepared as previously described.[20] The **TX** ligands are thiols containing a free-carboxylate form of an amino acid.

3.2.2. Electron Paramagntic Resonance Spectroscopy

50 μM Cyt *c* samples were prepared in 10 mM Tris buffer (pH 7.4). **Au-TX** concentrations were 11 μM, resulting in >99% percent bound protein.[19] Sample pH was measured using a Mettler Toledo Inlab 423 Combination pH and Metallic electrode following the addition of **Au-TX**. Two quartz capillaries were filled via Hamilton syringe, sealed using either a flame or teflon tape, and placed in a standard EPR tube.

X-band (9.62 GHz) EPR spectra were obtained using a Bruker E-500-10/12 spectrometer with a Super-high-Q X-band single cavity and equipped with a Bruker ER 4131 nitrogen flow insert temperature controller. Temperature was controlled by a flow of cool nitrogen gas across heaters. Spectra were collected at 298 K with 8 mW power. A power saturation experiment confirmed 8 mW was non-saturating. The modulation amplitude was 0.5 gauss and the frequency was 100 kHz. Multiple scans (32) were averaged to increase signal integrity. Rotational correlation times, τ_B and τ_C, were calculated according to equations 1 and 2 and averaged to τ_{iso} with equation 3, where the *B* and *C* terms are determined by equations 4 and 5.[2,16,21]

$$\tau_B = 4.26 * 10^{-6} * \frac{B}{H} \quad (1)$$

$$\tau_C = 1.02 * 10^{-6} * C \quad (2)$$

$$\tau_{iso} = (\tau_B + \tau_C)/2 \quad (3)$$

$$B = 0.5 * \Delta H(0) * \left\{ \sqrt{\frac{H(0)}{H(+1)}} - \sqrt{\frac{H(0)}{H(-1)}} \right\} \quad (4)$$

$$C = 0.5 * \Delta H(0) * \left\{ \sqrt{\frac{H(0)}{H(+1)}} + \sqrt{\frac{H(0)}{H(-1)}} \right\} \quad (5)$$

ΔH(0) is the peak-to-trough width of the center peak and H(-1), H(0), and H(+1) are the peak-to-trough heights of the left, middle, and right hyperfine peaks respectively.

3.3. Results and Discussion

3.3.1. SL-Cyt *c*/Au-TX experiences restricted motion

Dynamic motion of SL probes provided information about local protein structure and conformational dynamics. MTSSL is a stable nitroxide radical spin label that reacted specifically with cysteine residues. When MTSSL attached to the C102 residue in wild type yeast Cyt *c*, the EPR spectrum reported a mobile environment

(Figure 3.3; A) with an average rotational correlation time of 1.63 ns that was calculated using equations 1-5. The unequal line heights and widths indicated anisotropic motion, a feature common to SLs when attached to bulky proteins. The low intensity, subtle bump features are ^{13}C satellite peaks.[22,23]

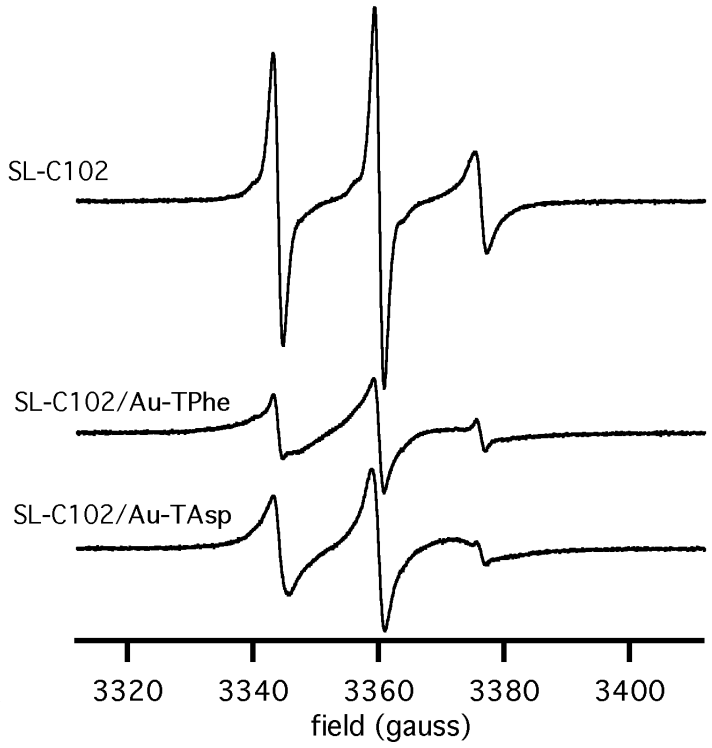

Figure 3.3. EPR spectra of spin labeled wild type Cyt *c* SL-C102 Cyt *c*, SL-C102 Cyt *c*/**Au-Phe**, and SL-C102 Cyt *c*/**Au-TAsp** in 10 mM Tris buffer, pH 7.4, 298 K. SL-Cyt *c* concentrations were 50 μM while **Au-TX** was 11 μM. Rotational correlation times are given in Table 3.1.

Table 3.1. Rotational correlation times and |C/B| of SL-C102 and **Au-TX**.

	τ_B (ns)	τ_C (ns)	τ_{iso} (ns)	|C/B|
SL(C102)	0.883	2.37	1.63	3.88
SL(C102)/**Au-TPhe**	0.676	2.73	1.70	5.85
SL(C102)/**Au-TAsp**	2.16	4.36	3.26	2.92

Values calculated using equations 1-5. Error was estimated at 0.1 ns (Appendix F).

When wild type Cyt *c* was bound to **Au-TX**, the interactions between the two macromolecules influenced both the EPR lineshape and rotational correlation times of the SL. The C102/**Au-TPhe** adduct (Figure 3.3; B) decreased in signal intensity and there was no change in τ_{iso}, suggesting Cyt *c* was still relatively dynamic. However,

there was a significant increase in the C/B ratio, meaning the SL motion was more anisotropic due to the SL interacting with the local environment.[18] The hydrophobic residues on the surface of **Au-TPhe** likely interacted with the hydrophobic SL, influencing its free rotation. In contrast, when C102 was bound to **Au-TAsp** (Figure 3.3; C), signal intensity was also lost, but τ_{iso} increased significantly from 1.63 ns to 3.26 ns. The C/B ratio decreased only slightly, indicating the SL directional motion was relatively unaffected as compared to unbound Cyt *c*. Binding C102 Cyt *c* to **Au-TX** resulted in distinct motion for both adducts, with the **Au-TAsp** adduct having the least dynamic behavior.

3.3.2. Varying SL location on Cyt *c* reflects local environment and binding interface interactions with Au-TX

The dynamics of Cyt *c*/**Au-TX** was characterized using a series of spin-labeled Cyt *c* mutants. The EPR spectra of wild type Cyt *c* and each mutant is pictured in Figure 3.4 and the rotational correlation times given in Table 3.2. Each sample was relatively mobile with SL-N92C Cyt *c* showing significant anisotropic motion. This is consistent with the Scholes study in which SL-N92C displayed probe immobilization, along with SL-K79C to a lesser extent.[16] However, it must be noted that the experimental conditions in that study emphasize different dynamics. Their samples were prepared in 30% sucrose, which significantly slowed the global protein tumbling to emphasize local probe motion.[18] The spectra presented here reflect both the correlation time associated with local dynamics of the probe, as well as the correlation time associated with global protein tumbling. The large |C/B| ratio of SL-N92C indicated that the probe was interacting strongly with its local environment, even though the overall correlation time was dominated by rapid protein tumbling.

This information reflects the SL interaction with the local protein environment and serves as a reference point for the Cyt *c*/**Au-TX** adducts.

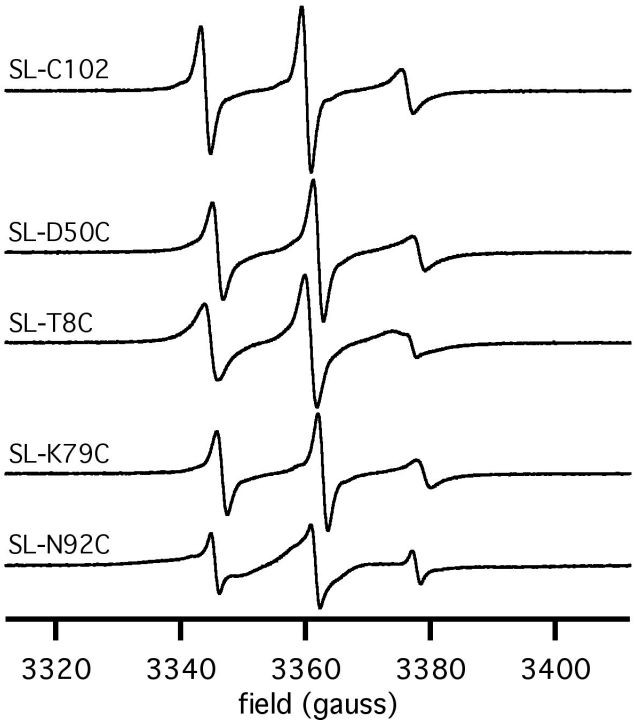

Figure 3.4. EPR spectra of spin labeled wild type and mutants of Cyt *c* in 10 mM Tris buffer, pH 7.4, 298 K. SL-Cyt *c* concentrations were 50 μM. Rotational correlation times are given in Table 3.2.

Table 3.2. Rotational correlation times and |C/B| of SL-C102 and the four mutants.

	τ_B (ns)	τ_C (ns)	τ_{iso} (ns)	|C/B|
SL(C102)	0.883	2.37	1.63	3.88
SL(D50C)	0.930	2.56	1.75	3.98
SL(T8C)	1.52	3.68	2.60	3.50
SL(K79C)	1.02	2.65	1.84	3.76
SL(N92C)	0.452	2.07	1.26	6.63

Values calculated using equations 1-5. Error was estimated at 0.1 ns (Appendix F).

The average rotational correlation times of SL-Cyt *c* were relatively unchanged upon binding Cyt *c* to **Au-TPhe**. Although the anisotropy of the SL increased in most cases, τ_{iso} remained relatively unchanged between free SL-Cyt *c* and SL-Cyt *c*/**Au-TPhe** for all the samples with the exception of SL-K79C. This

indicates that Cyt *c* undergoes rapid tumbling in the Cyt *c*/**Au-TPhe** adduct, but that the SL can experience specific contacts within the **Au-TPhe** ligand environment.

K79C is unique because this is the only mutation which introduces a SL at the solvent-protected binding interface of Cyt *c* and **Au-TPhe**.[19] τ_{iso} increased when SL-Cyt *c* was bound to **Au-TPhe**, suggesting that the heme crevice was less accessible. The longer τ_{iso} values were consistent with **Au-TPhe** restricting the SL motion due to strong binding interactions at this location. The SL-Cyt *c*/**Au-TAsp** adducts presented later (Figure 3.6) had a even longer τ_{iso} value because of a more rigid binding interaction.

Several SL-Cyt *c* mutants displayed spectral features which indicated a highly anisotropic SL environment, or a fractional population in which the SL was immobilized in Cyt *c*/**Au-TPhe**. The |C/B| ratio increased for C102 and every mutant except K79C, indicating that the SL motion was strongly influenced by its local environment. Being at the primary binding interface (Figure 3.1), K79C experienced a significant increase in both τ_B and τ_C values, which was reflected in the smaller |C/B| ratio. N92C had the largest |C/B| ratio due to probe immobilization, as indicated by the far left spectral feature.[24,25] This common indicator of probe immobilization is typically defined from the rest of the spectral features.[26] The two component spectra found for SL-T8C, SL-K79C, and SL-N92C in Figure 3.5 reflected two distinct conformations of the SL that were described by an average rotational correlation time. The SL-T8C and SL-K79C/**Au-TPhe** adducts clearly showed that the SL experienced significant motion restriction, as evidenced by the two component spectra and highly anisotropic movement. The slower component in SL-K79C was much less defined. This is often characteristic of a partially buried binding site, caused by the hydrophobic TPhe groups of **Au-TPhe** interacting or directly binding the SL itself,

affecting the rotational freedom in a fraction of the sample. Thus, a spectrum like SL-T8C reflects strong interactions and restricted movement of the SL due to TPhe interactions, versus just SL immobilization.

SL-C102 and SL-D50C were the least affected when bound to **Au-TPhe**, as predicted by the solvent protection data, with little to no change in rotational correlation times. Both SL locations are removed from the binding footprint, thus the SLs cannot interact directly with the **Au-TPhe** functional groups.

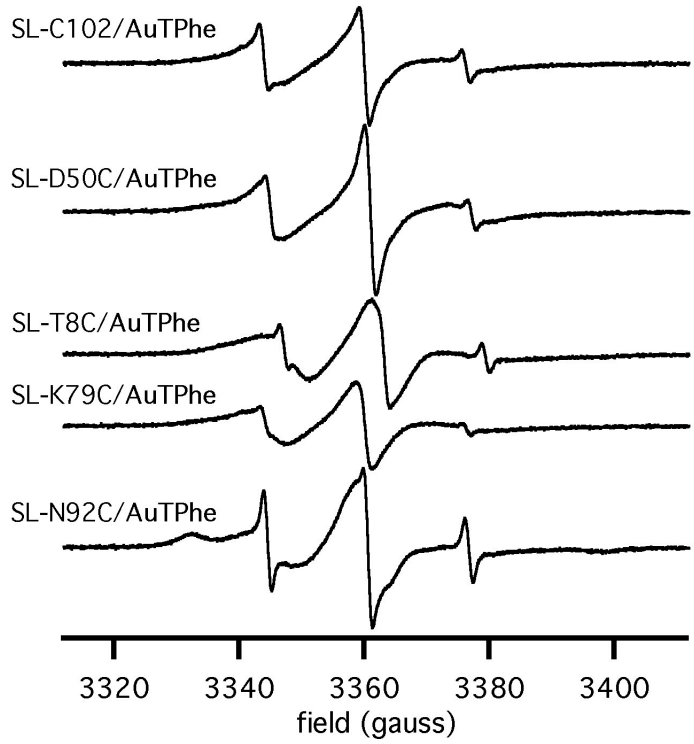

Figure 3.5. EPR spectra of spin labeled wild type and mutants of Cyt *c* bound to **Au-TPhe** in 10 mM Tris buffer, pH 7.4, 298 K. SL-Cyt *c* concentrations were 50 μM while **Au-TPhe** was 11 μM. Rotational correlation times are given in Table 3.3.

Table 3.3. Rotational correlation times and |C/B| of the adducts of SL-C102 and the four mutants with **Au-TPhe**.

	τ_B (ns)	τ_C (ns)	τ_{iso} (ns)	|C/B|
SL(C102)/**Au-TPhe**	0.676	2.73	1.70	5.85
SL(D50C)/**Au-TPhe**	0.997	3.69	2.34	5.35
SL(T8C)/Au-TPhe**	1.21	5.03	3.12	6.03
SL(K79C)/Au-TPhe**	2.12	5.51	3.82	3.76
SL(N92C)/Au-TPhe**	0.339	2.12	1.23	9.05

**indicates a significant slow component present in the spectrum. Values for the faster component were calculated using equations 1-5. Error was estimated at 0.1 ns (Appendix F).

Each of the SL-Cyt *c*/**Au-TAsp** adducts exhibited longer τ_{iso} compared to both free SL-Cyt *c* and SL-Cyt *c*/**Au-TPhe** samples. This indicated that Cyt *c* experienced restricted motion when bound within the Cyt *c*/**Au-TAsp** adduct. Each of the SL-Cyt *c*/**Au-TAsp** spectra in Figure 3.6 have similar EPR lineshapes, with no additional features distorting the three-line, broadened nitroxyl radical signals.

Three of the five SL sites are located within the solvent-protected surface identified as the Cyt *c*/**Au-TAsp** binding interface (Figure 3.3). Despite this, there are no signs of probe immobilization in the spectral lineshapes. The unique locations C102 and SL-D50C reported longer τ_{iso} times even though they were positioned well outside of the binding footprint, suggesting that the global motion of the entire protein was less dynamic in Cyt *c*/**Au-TAsp** in comparison to Cyt *c*/**Au-TPhe**.

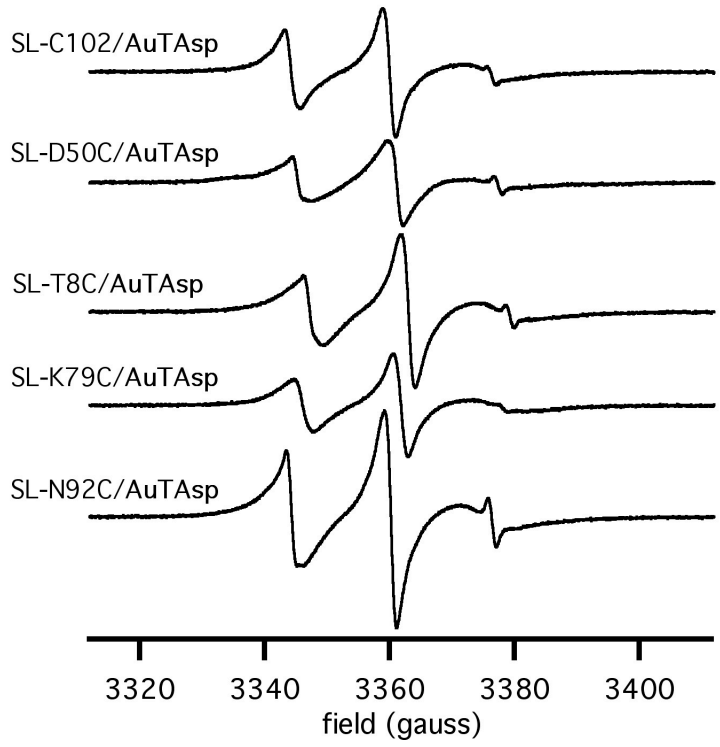

Figure 3.6. EPR spectra of spin labeled wild type and mutants of Cyt *c* bound to **Au-TAsp** in 10 mM Tris buffer, pH 7.4, 298 K. SL-Cyt *c* concentrations were 50 μM while **Au-TAsp** was 11 μM. Rotational correlation times are given in Table 3.4.

Table 3.4. Rotational correlation times and |C/B| of the adducts of SL-C102 and the four mutants with **Au-TAsp**.

	τ_B (ns)	τ_C (ns)	τ_{iso} (ns)	|C/B|
SL(C102)/**Au-TAsp**	2.16	4.36	3.26	2.92
SL(D50C)/**Au-TAsp**	1.39	4.52	2.96	4.72
SL(T8C)/**Au-TAsp**	1.88	4.74	3.31	3.65
SL(K79C)/**Au-TAsp**	3.36	5.49	4.43	2.37
SL(N92C)/**Au-TAsp**	1.10	3.62	4.78	4.78

Values calculated using equations 1-5. Error was estimated at 0.1 ns (Appendix F).

The SLs on Cyt *c* experienced less restricted movement when bound to **Au-TAsp**. The more isotropic movement indicated by the lower C/B ratios and the lack of multiple component spectra indicated that the SL didn't interact strongly with the ligand environment found on **Au-TAsp**. This suggested that the hydrophobic SL was more likely to directly interact with the mutually hydrophobic benzyl groups found in the **Au-TPhe** ligands.

3.3.3. Dynamic binding of Cyt *c*/Au-TX

The EPR lineshapes, rotational correlation times, and |C/B| ratios of each SL-Cyt *c* mutant bound to **Au-TPhe** and **Au-TAsp** illustrated the interaction and dynamics of the protein at that location with **Au-TX**. The dominant binding face for Cyt *c*/**Au-TX** was reflected by differences in τ_{iso} as shown in Figure 3.7. Residues in red represent longer τ_{iso} values with the largest differences located within the respective Cyt *c*/**Au-TX** primary binding footprints. The Cyt *c*/**Au-TPhe** adduct tumbled rapidly through solution as indicated by the unchanged τ_{iso} value for SL-C102, which was removed from the binding interface and reported global dynamics. In contrast, Cyt *c*/**Au-TAsp** experienced longer rotational correlation times at all locations, indicating a larger binding area with less dynamic interactions and slower global dynamics.

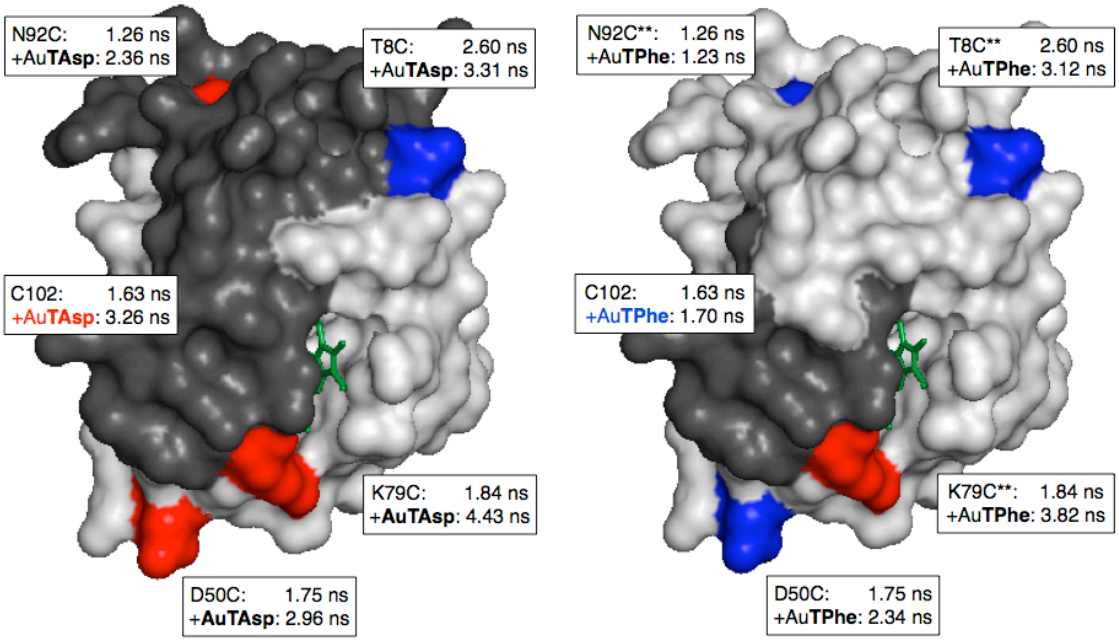

Figure 3.7. τ_{iso} illustrates how average rotational correlation times vary with SL location in the SL-Cyt *c*/**Au-TAsp** (left) and SL-Cyt *c*/**Au-TPhe** (right) adducts. The binding face data is included for reference, with gray representing higher solvent protection. Residues in red represent large increases in rotational correlation times while blue is little to no change relative to free SL-Cyt *c*. ** indicates spectra with two components. The SL-Cyt *c*/**Au-TAsp** adduct in general had longer τ_{iso} times including areas not associated with binding, suggesting slower global dynamics.

The anisotropic motion of the SL, |C/B|, and the immobilized spectral components reported how strongly the SL interacted with its local environment. The |C/B| ratio and two component spectra are indicated in Figure 3.8. Despite having a large binding interface, the |C/B| ratio never increased in the SL-Cyt *c*/**Au-TAsp** adducts and even decreased noticeably in several locations. The hydrophobic SL likely didn't strongly interact with the hydrophilic Asp functional groups. The binding between Cyt *c* and **Au-TAsp** might alleviate some interactions of the SL with the local protein structure, making the SL motion more isotropic. However, the hydrophobic Phe groups extensively interacted with the SLs. All locations besides K79C displayed significant increases in |C/B| and several were partially immobilized. The strong interactions between the SL and **Au-TPhe** suggested a dynamic binding interaction in Cyt *c*/**Au-TPhe**.

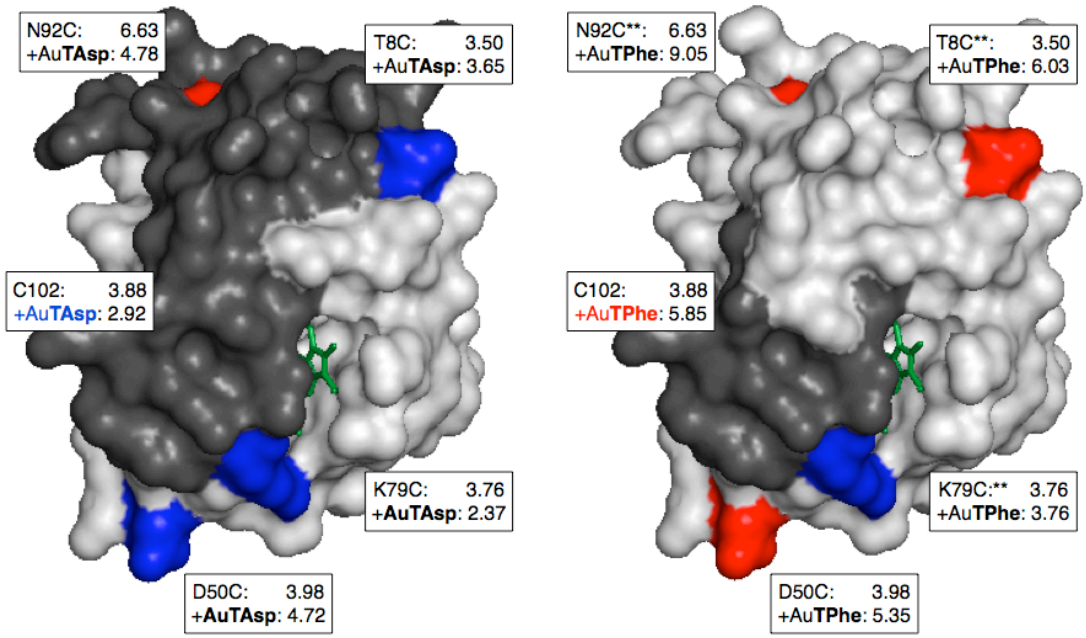

Figure 3.8. The |C/B| ratios reflect anisotropic motion in the SL-Cyt *c*/**Au-TAsp** (left) and SL-Cyt *c*/**Au-TPhe** (right) adducts. Residues in red represent large increases in |C/B| while blue is little to no change relative to free SL-Cyt *c*. ** indicates spectra with two components. The |C/B| ratios in SL-Cyt *c*/**Au-TPhe** indicate strong interactions between the SL and Phe groups.

The K79C mutant probed the heme crevice area, where a small redox reagent like $Co(phen)_3^{3+}$ is likely to react. Both the SL probe immobilization and shorter τ_{iso} values illustrated that **Au-TPhe** had a more dynamic interaction at this location. The τ_{iso} and |C/B| values suggested a more rigid interface in the SL-Cyt *c*/**Au-TAsp** adducts. All this evidence indicated that the SL-Cyt *c*/**Au-TPhe** adducts experienced more dynamic interactions than the **Au-TAsp** counterparts, particularly near the heme crevice.

3.3.4. Ramifications for ET reactivity of Cyt *c*/Au-TX

Key indicators for the bimolecular ET reaction of Cyt *c*/**Au-TX** adducts are global motion, as probed by D50C and C102, and heme crevice accessibility, as probed by K79C. There was little to no change in τ_{iso} for D50C and C102 in SL-Cyt *c*/**Au-TPhe**, but τ_{iso} roughly doubled for both D50C and C102 in SL-Cyt *c*/**Au-TAsp**. These differences suggested that the global motion of SL-Cyt *c*/**Au-TAsp** is slower.

For K79C, both adducts saw an increase in τ_{iso} relative to free SL-Cyt *c*, indicating that **Au-TX** affects heme accessibility. Between the two adducts, SL-Cyt *c*/**Au-TAsp** had the longer τ_{iso} value which was reflective of its larger, more rigid binding interface as defined by both SDSL and the H/D amide exchange data.[19]

The intermolecular ET studies resulted in bimolecular rate constants of 1.95×10^{11} M^{-1} s^{-1} for Cyt *c*/**Au-TPhe** and 0.0870×10^{11} M^{-1} s^{-1} for Cyt *c*/**Au-TAsp** under high salt conditions—a 100-fold difference. The SDSL experiments concluded that the SL-Cyt *c*/**Au-TAsp** adduct was less globally dynamic and had lower heme accessibility, as indicated by the K79C, D50C, and C102 locations. Thus, the heme crevice was likely less accessible and collisions with the redox partner less frequent, reducing the reactivity of the **Au-TAsp** adduct.

3.4. Conclusions

SDSL characterized the dynamic interactions and motion of Cyt *c* with **Au-TX**. Several mutants of Cyt *c* were utilized to extract information about the different dynamics of the Cyt *c*/**Au-TPhe** and Cyt *c*/**Au-TAsp** systems. The Cyt *c*/**Au-TPhe** adduct was more dynamic than Cyt *c*/**Au-TAsp**, as shown by the shorter τ_{iso} values for most SLs. In particular, C102 was located outside of the Cyt *c*/**Au-TPhe** binding interface and reported rapid global movement. The T8C, N92C, and K79C mutants all indicated that Cyt *c* had a dynamic binding interface with **Au-TPhe**, as shown by highly anisotropic motion and multiple component spectra that resulted from the strong interactions between the SL and Phe functional groups.

In contrast, the Cyt *c*/**Au-TAsp** binding interface was more rigid, as indicated by the universal increase in τ_{iso} around the previously identified binding interface and the absence of multiple SL conformations and probe immobilization. C102 also reported that the global dynamics of the Cyt *c*/**Au-TAsp** adducts were slower. These

results coincide with the amide H/D exchange data that showed **Au-TAsp** had the larger binding footprint.

A major goal of these experiments was to relate protein dynamics and reactivity. The intermolecular ET study reported that the Cyt *c*/**Au-TAsp** adduct reacted 100 times slower. This discrepancy could arise from electronic effects or dynamics. The SDSL experiments showed very distinct behavior between the Cyt *c*/**Au-TPhe** and Cyt *c*/**Au-TAsp** adducts. Cyt *c* appeared to have a highly dynamic binding interaction with the surface of **Au-TPhe** while binding to **Au-TAsp** resulted in a more rigid interface. The dynamic interaction of Cyt *c*/**Au-TX** at the heme crevice could promote a gated ET mechanism between Cyt *c* and its redox partner. The transient interactions of **Au-TPhe** and **Au-TAsp** with Cyt *c* at this location are distinct, which could alter ET reactivity. Thus, the reduced reactivity of Cyt *c*/**Au-TAsp** is likely a result of both slower global dynamics and more rigid binding near the heme crevice.

3.5. References Cited

(1) Fanucci, G. E.; Cafiso, D. S. *Curr. Opin. Struct. Biol.* **2006**, *16*, 644-653.

(2) Berliner, L. J. *Spin labeling: theory and applications / edited by Lawrence J. Berliner*; Academic Press: New York, 1976.

(3) Columbus, L.; Hubbell, W. L. *Biochemistry* **2004**, *43*, 7273-87.

(4) Nelson, W. D.; Blakely, S. E.; Nesmelov, Y. E.; Thomas, D. D. *Proc. Natl. Acad. Sci. U. S. A.* **2005**, *102*, 4000-5.

(5) Todd, A. P.; Millhauser, G. L. *Biochemistry* **1991**, *30*, 5515-5523.

(6) Qu, K. B.; Vaughn, J. L.; Sienkiewicz, A.; Scholes, C. P.; Fetrow, J. S. *Biochemistry* **1997**, *36*, 2884-2897.

(7) Cuello, L. G.; Cortes, D. M.; Perozo, E. *Science* **2004**, *306*, 491-5.

(8) Dong, J.; Yang, G.; McHaourab, H. S. *Science* **2005**, *308*, 1023-8.

(9) Buchaklian, A. H.; Klug, C. S. *Biochemistry* **2005**, *44*, 5503-9.

(10) Borbat, P. P.; Surendhran, K.; Bortolus, M.; Zou, P.; Freed, J. H.; McHaourab, H. S. *PLoS Biol.* **2007**, *5*, e271.

(11) Qin, P. Z.; Iseri, J.; Oki, A. *Biochem. Biophys. Res. Commun.* **2006**, *343*, 117-24.

(12) Crane, J. M.; Mao, C. F.; Lilly, A. A.; Smith, V. F.; Suo, Y. Y.; Hubbell, W. L.; Randall, L. L. *J. Mol. Biol.* **2005**, *353*, 295-307.

(13) Hanson, S. M.; Francis, D. J.; Vishnivetskiy, S. A.; Kolobova, E. A.; Hubbell, W. L.; Klug, C. S.; Gurevich, V. V. *Proc. Natl. Acad. Sci. U. S. A.* **2006**, *103*, 4900-5.

(14) Hegde, B. G.; Isas, J. M.; Zampighi, G.; Haigler, H. T.; Langen, R. *Biochemistry* **2006**, *45*, 934-42.

(15) Herrick, D. Z.; Sterbling, S.; Rasch, K. A.; Hinderliter, A.; Cafiso, D. S. *Biochemistry* **2006**, *45*, 9668-74.

(16) Deweerd, K.; Grigoryants, V.; Sun, Y. H.; Fetrow, J. S.; Scholes, C. P. *Biochemistry* **2001**, *40*, 15846-15855.

(17) Snel, M. M. E.; Dekruijff, B.; Marsh, D. *Biochemistry* **1994**, *33*, 7146-7156.

(18) Mchaourab, H. S.; Lietzow, M. A.; Hideg, K.; Hubbell, W. L. *Biochemistry* **1996**, *35*, 7692-7704.

(19) Bayraktar, H.; You, C. C.; Rotello, V. M.; Knapp, M. J. *J. Am. Chem. Soc.* **2007**, *129*, 2732-2733.

(20) You, C. C.; De, M.; Han, G.; Rotello, V. M. *J. Am. Chem. Soc.* **2005**, *127*, 12873-12881.

(21) Marsh, D. In *Biological Magnetic Resonance*; Berliner, L., Ruben, J., Ed.; Plenum: New York, 1989, p 255-303.

(22) Vugman, N. V.; Giannoni, R. A.; Coelho Neto, J. A. *J. Magn. Reson.* **1997**, *124*, 352-354.

(23) Byberg, J. R.; Bech Nielsen, B.; Fanciulli, M.; Estreicher, S. K.; Feddres, P. A. *Physical Review B* **2000**, *61*, 12939-12945.

(24) Hwang, J. S.; Mason, R. P.; Hwang, L. P.; Freed, J. H. *J. Phys. Chem.* **1975**, *79*, 489-511.

(25) Goldman, S. A.; Freed, J. H.; Bruno, G. V.; Polnasze, C. F. *J. Chem. Phys.* **1972**, *56*, 716-735.

(26) Owenius, R.; Osterlund, M.; Lindgren, M.; Svensson, M.; Olsen, O. H.; Persson, E.; Freskgard, P. O.; Carlsson, U. *Biophys. J.* **1999**, *77*, 2237-50.

CHAPTER 4

SURFACE MAPPING PROTEIN/NANOPARTICLE ADDUCTS USING COVALENT LABELING TECHNIQUES

4.1. Introduction

Relating protein structure to function is a major pursuit in biochemistry. Various methods exist to probe protein structure, including NMR spectroscopy, X-ray crystallography, computational methods, and mass spectrometry (MS).[1] These methods are often used to probe protein-protein interactions and our studies extend that to interactions within protein-nanoparticle macromolecules. Among these techniques, the aforementioned H/D amide exchange is a useful noncovalent labeling method when coupled with MS. However, back exchange and small mass shifts limit this approach. Covalent labeling methods similar to SDSL also exist in which a reagent irreversibly modifies specific amino acids. These molecules don't undergo back exchange and have larger mass shifts, but their size can perturb protein structure if left unchecked.[2] We aim to use a covalent label to map the surface of Cyt *c* when bound to **Au-TX**, gaining additional information about Cyt *c*/**Au-TX** interactions and how they relate to function.

Covalent labels have been extensively used to map protein surfaces,[2-4] identify important residues for ligand binding and reactivity,[5-11] probe active site structure and coordination,[12-16] determine solvent accessibility,[15,17,18] and investigate the role of specific residues in conformational changes.[19-25] Diethylpyrocarbonate (DEPC) is a popular reagent and is known to react with His, Cys, Tyr, Lys, Ser, and Thr residues, potentially covering a significant percentage of a typical protein sequence. Certain residues can be targeted by carefully controlling experimental conditions such as concentration or reaction time.[2] This method yields information complementary to SDSL

and H/D amide exchange with the potential of covering even more extensive regions.

In addition to the previously presented H/D amide exchange[26] and SDSL (Chapter 3) experiments, covalent modification affords more extensive surface coverage for mapping the binding interaction between Cyt *c* and **Au-TX**. When bound to **Au-TX**, any Cyt *c* residues blocked from solvent access by a binding interaction will escape labeling, while solvent exposed areas will be labeled. Both are tracked using LC/MS. This method's advantage is that the potentially labeled residues cover a larger surface area of Cyt *c* than SDSL.

DEPC is a covalent labeling agent that reacts most commonly with His, Tyr, Ser, and Thr residues, which account for approximately 25% of the residues found in an typical protein. Under carefully controlled experimental conditions, residues are labeled without compromising the protein's structural integrity.[2] Thus, Cyt *c* can be preincubated with **Au-TX** and DEPC introduced into the system to label any solvent exposed residues, mapping binding interfaces and areas of dynamic movement. Potentially labeled residues are shown in Figure 4.1 in yellow relative to the already presented H/D amide exchange binding interface data. Combined with the SDSL and H/D amide exchange data, DEPC labeling should elucidate the type and locations of interactions of Cyt *c* with **Au-TX**. By surface mapping Cyt *c*/**Au-TPhe** and Cyt *c*/**Au-TPhe**, we aim to further understand the differences in dynamics observed using SDSL and to link these differences to reactivity.

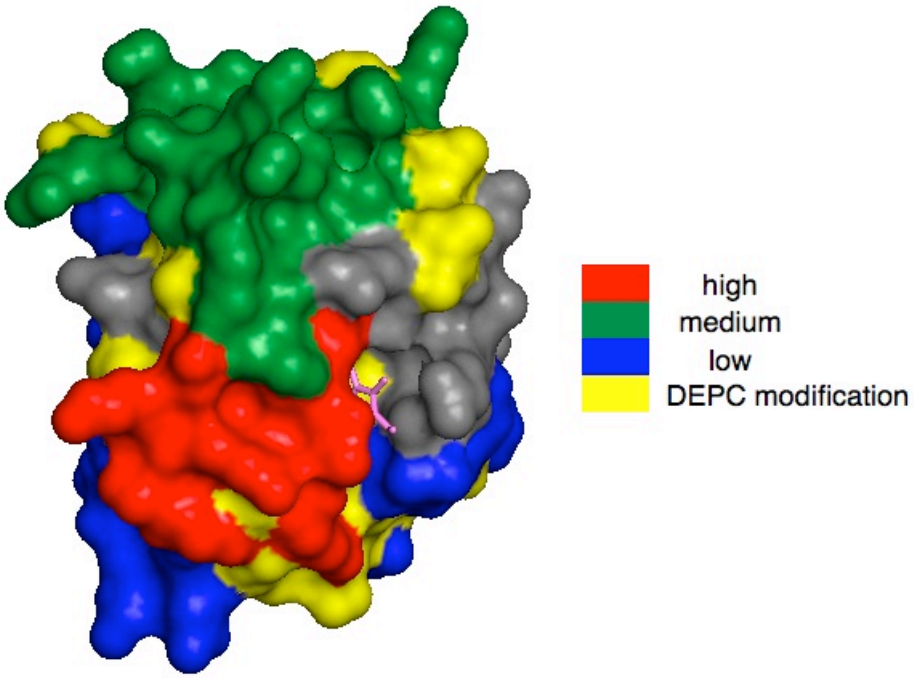

Figure 4.1. Possible sites of DEPC modification (His, Tyr, Ser, Thr) are highlighted in yellow and superimposed upon the solvent protection data of Cyt *c* bound to **Au-TPhe** that was determined using amide H/D exchange. Cyt *c* has been rotated to emphasize the binding interface with **Au-TPhe**.

4.2. Experimental Methods

4.2.1. General considerations

Horse heart Cyt *c*, 3-morpholinopropanesulfonic acid (MOPS), tris(hydroxymethyl)-aminomethane (Tris), and diethylpyrocarbonate (DEPC) were obtained from Sigma-Aldrich. Sequence grade modified trypsin was obtained from Promega. Anionic gold nanoparticles (**Au-TX**) were functionalized with thiol ligands containing the free-carboxylate form of amino acids (Phe and Asp) according to previously published procedures.[27]

4.2.2. DEPC modification

The DEPC modification experiments were performed according to published literature methods[2]. DEPC was reacted with Cyt *c* for one minute to achieve covalent

modification without compromising the overall protein structure. Samples were 500 µL of 100 µM Cyt *c* in MOPS (25 mM, pH 7.4) and were reacted with 0.5 mM DEPC to 1.5mM DEPC for 1 min at 37 °C. A stock solution of DEPC in ACN was prepared so the total ACN added was less than 1%. Reactions were quenched with the addition of 10 mM imidazole. Unreacted DEPC was removed using a 5000 MWCO filter and the samples buffer exchanged into 10 mM Tris for the subsequent proteolytic digestion.

4.2.3. Proteolytic digestion

Cyt *c* was initially denatured by incubating samples with 5 mM $CaCl_2$ and 10 µL ACN for 45 min at 40 °C. Following this, 2 µg of sequence grade modified trypsin was added to 100 µL of 200 µM Cyt *c* and incubated at 37 °C for approximately 20 hours. 2 µL of acetic acid was added to quench the reaction. Samples were immediately frozen and analyzed within 24 hours.

4.2.4. Liquid chromatography mass spectrometry

Mass spectra were acquired on a Bruker Esquire-LC quadrupole ion trap mass spectrometer. LC experiments used a HP1100 HPLC system with a C18 column (15 cm × 2.1 mM, 5 µM particle size). The electrospray needle voltage was set to 3000 kV, skimmer 1 to 35 V, skimmer 2 to 55 V, and the capillary temperature set at 300 °C. Trypsin digested samples were eluted with a linear methanol gradient containing 0.1% acetic acid that increased from 5 to 90% over 45 min while at a flow rate of 0.250 mL/min. Peptide fragments and sequences were determined using PeptideMass and Fragment Ion Calculator (ExPASy), which is based off of de novo sequencing and allows specific amino acid modifications.

4.3. Results and Discussion

The covalent labeling agent DEPC was used to investigate the binding interface and areas of dynamic interactions of Cyt *c*/**Au-TX**. Cyt *c* was covalently labeled using varied concentrations of DEPC, digested with trypsin, and the peptides tracked using LC/MS. Preliminary LC/MS studies showed that the 0.5 mM DEPC sample did not noticeably label any peptides or the undigested protein observed according to the charge state ruler function in Bruker Daltonics DataAnalysis program, while the 1mM DEPC sample displayed a significant mass shift. However, precipitation was observed during the DEPC removal of the 1 mM sample and the literature also states this is outside of the linear range, so further systematic screening is necessary to verify the best working concentration range. Once known, the DEPC modified and unmodified peptides must be identified. All major peptides were observable for unlabeled Cyt *c*, equaling 98% sequence coverage, which was also reported in literature[2]. The modified peptide masses containing residues most likely to be labeled (H, Y >> T, S) must be determined using de novo sequencing and extracted from the total ion chromatogram as shown in Figure 4.2. Since mild labeling conditions are necessary, particular residues never label completely, thus both labeled and unlabeled peptides will be observed. The specifically labeled residue within the peptide can be verified by performing MS/MS on each individual peptide from the resulting b and y ions.

After determining the proper experimental conditions and labeling information of free Cyt *c*, mapping the surface of Cyt *c* when bound to **Au-TX** should quickly follow. Any peptides that completely escape labeling indicate that Cyt *c* has some strong interaction with the surface of **Au-TX** at that location which completely blocks solvent

accessibility. Thus, the primary Cyt *c*/**Au-TX** binding interface can be identified and related to the H/D amide exchange and SDSL data. With these sets of data, the differences in binding and dynamic interactions of Cyt *c*/**Au-TPhe** and Cyt *c*/**Au-TAsp** should be apparent and relatable to the reactivity studies.

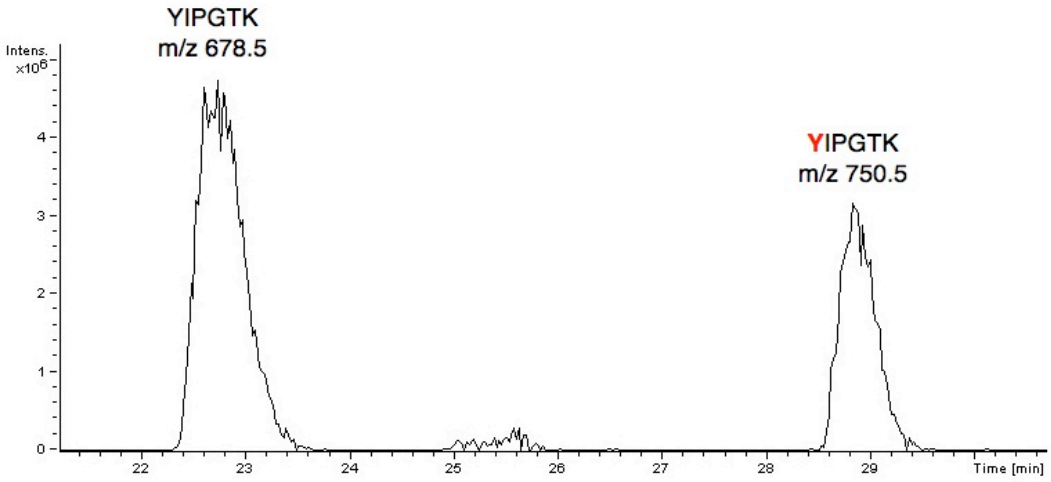

Figure 4.2. An extracted ion chromatogram displaying both the unlabled and DEPC-labeled YIPGTK peptide of Cyt *c*. The electrospray needle voltage was set to 3000 kV, skimmer 1 to 35 V, skimmer 2 to 55 V, and the capillary temperature set at 300 °C. The trypsin digested samples were eluted with a linear methanol gradient containing 0.1% acetic acid that increased from 5 to 90% over 45 min while at a flow rate of 0.250 mL/min.

4.4. Conclusions

These experiments are preliminary work in the development of a surface mapping protocol using covalent labeling coupled with LC/MS to study the interactions within a protein/nanoparticle macromolecule. The labeled residues (His, Tyr, Ser, Thr) cover approximately 25% of a typical protein sequence, making this method highly adaptable to a variety of proteins.[2] We observed and identified both labeled and unlabeled peptides of Cyt *c*, but further work is needed to optimize experimental conditions so we observe labeling while not compromising protein structure. Since data analysis is manually

intense, high confidence and reproducibility is desired before complicating the system with the introduction of a second macromolecule such as **Au-TX**. If these conditions are satisfied, this covalent labeling mapping method would cover a larger surface area than SDSL and offer more stability than amide H/D exchange, yielding more information about the interaction of Cyt *c* with the surface of **Au-TX**.

4.5. References Cited

(1) Juan, H.-F.; Liu, H.-L.; Hsu, J.-P. *Curr. Proteomics* **2004**, *1*, 183-197.

(2) Mendoza, V. L.; Vachet, R. W. *Anal. Chem.* **2008**, *80*, 2895-2904.

(3) Leite, J. F.; Cascio, M. *Biochemistry* **2002**, *41*, 6140-6148.

(4) D'Ambrosio, C.; Talamo, F.; Vitale, R. M.; Amodeo, P.; Tell, G.; Ferrara, L.; Scaloni, A. *Biochemistry* **2003**, *42*, 4430-4443.

(5) Walter, E. D.; Stevens, D. J.; Visconte, M. P.; Millhauser, G. L. *J. Am. Chem. Soc.* **2007**, *129*, 15440-1.

(6) Safarian, S.; Moosavi-Movahedi, A. A.; Hosseinkhani, S.; Xia, Z.; Habibi-Rezaei, M.; Hosseini, G.; Sorenson, C.; Sheibani, N. *J. Protein Chem.* **2003**, *22*, 643-54.

(7) Narindrasorasak, S.; Kulkarni, P.; Deschamps, P.; She, Y. M.; Sarkar, B. *Biochemistry* **2007**, *46*, 3116-3128.

(8) Kipp, B. H.; Kelley, P. M.; Njus, D. *Biochemistry* **2001**, *40*, 3931-7.

(9) Qin, K.; Yang, Y.; Mastrangelo, P.; Westaway, D. *J. Biol. Chem.* **2002**, *277*, 1981-90.

(10) Mailfait, S.; Belaiche, D.; Kouach, M.; Dallery, J.; Chavatte, P.; Formstecher, P.; Sablonniere, B. *Biochemistry* **2000**, *39*, 2183-2192.

(11) de Peredo, A. G.; Saint-Pierre, C.; Adrait, A.; Jacquamet, L.; Latour, J. M.; Michaud-Soret, I.; Forest, E. *Biochemistry* **1999**, *38*, 8582-8589.

(12) Nakanishi, N.; Takeuchi, F.; Park, S. Y.; Hori, H.; Kiyota, K.; Uno, T.; Tsubaki, M. *J. Biosci. Bioeng.* **2008**, *105*, 604-613.

(13) Runquist, J. A.; Miziorko, H. M. *Protein Sci.* **2006**, *15*, 837-842.

(14) Ploemen, J. H. T. M.; Johnson, W. W.; Jespersen, S.; Vanderwall, D.; Vanommen, B.; Vandergreef, J.; Vanbladeren, P. J.; Armstrong, R. N. *J. Biol. Chem.* **1994**, *269*, 26890-26897.

(15) Nuss, J. E.; Sweeney, D. J.; Alter, G. M. *Biochemistry* **2006**, *45*, 9804-9818.

(16) Njus, D.; Wigle, M.; Kelley, P. M.; Kipp, B. H.; Schlegel, H. B. *Biochemistry* **2001**, *40*, 11905-11.

(17) Hartleib, J.; Ruterjans, H. *Biochim. Biophys. Acta* **2001**, *1546*, 312-24.

(18) Bauer, P. J.; Krause, E. *Biochemistry* **2005**, *44*, 1624-1634.

(19) Hesp, J. R.; Raven, N. D.; Sutton, J. M. *Biochem. Biophys. Res. Commun.* **2007**, *362*, 695-9.

(20) Li, C. Y.; Takazaki, S.; Jin, X. R.; Kang, D. C.; Abe, Y.; Hamasaki, N. *Biochemistry* **2006**, *45*, 12117-12124.

(21) Jin, X. R.; Abe, Y.; Li, C. Y.; Hamasaki, N. *Biochemistry* **2003**, *42*, 12927-12932.

(22) Miller, G. J.; Ball, E. H. *J. Biol. Chem.* **2001**, *276*, 28829-34.

(23) Carven, G. J.; Stern, L. J. *Biochemistry* **2005**, *44*, 13625-13637.

(24) Turner, B. T.; Sabo, T. M.; Wilding, D.; Maurer, M. C. *Biochemistry* **2004**, *43*, 9755-9765.

(25) Lennon, C. W.; Cox, H. D.; Hennelly, S. P.; Chelmo, S. J.; McGuirl, M. A. *Biochemistry* **2007**, *46*, 4850-4860.

(26) Bayraktar, H.; You, C. C.; Rotello, V. M.; Knapp, M. J. *J. Am. Chem. Soc.* **2007**, *129*, 2732-2733.

(27) You, C. C.; De, M.; Han, G.; Rotello, V. M. *J. Am. Chem. Soc.* **2005**, *127*, 12873-12881.

CHAPTER 5

ELECTRON AND ENERGY-TRANSFER REACTIONS OF $RU(BPY)_3^{2+*/3+}$ WITH COPPER-PHENOLATES

5.1. Introduction

Redox-active amino acids are increasingly recognized as an important class of redox cofactors[1-3], with cofactors derived from tyrosine residues as the largest class. These are often associated with a transition metal, such as the tyrosyl radicals in ribonucleotide reductase, cytochrome *c* oxidase, and galactose oxidase (GalOx), and the tri-hydroxyphenylalanine quinone (TPQ) found in copper amine oxidase (CAO)[1,4-8]. The tyrosyl-radical cofactors of GalOx and CAO are notable in that each is covalently modified at the phenolic ring and require Cu(II) for normal function[8-11]. GalOx oxidizes primary alcohols to aldehydes while CAO oxidizes primary amines to aldehydes plus ammonia; in each case the synergistic action of the copper and modified-tyrosine supports this chemistry by shuttling the 2 e− and 2 H^+ to O_2, forming H_2O_2[12]. Due to the importance of developing new oxidation catalysts which use O_2 as terminal oxidant, these enzymes have inspired synthetic catalysts based upon a stabilized phenoxyl radical ($PhO^{\bullet}$) directly coordinated to Cu(II)[13-17]. Improving these catalysts will require optimizing the redox reactivity of metal-coordinated phenolates.

It has been shown that both electron-transfer (ET) and proton-coupled electron transfer (PCET) reactions of uncoordinated phenolates are well described by Marcus theory[18-23], in which the rate of ET/PCET is a function of collisional frequency (Z), driving force (ΔG°) and reorganization energy (λ)[24].

$$\ln k_{ET} = \ln Z - \frac{(\Delta G + \lambda)^2}{4\lambda RT} \qquad (5.1)$$

Sjodin, et al., showed that the inner-sphere oxidation of tyrosinate had a moderate intrinsic barrier, with λ = 22 kcal/mol, whereas the PCET oxidation of tyrosine was much slower, λ = 46 kcal/mol (Correcting for the large $\Delta S°$ led to λ = 32 kcal/mol for this PCET)[19]. They suggested that the slower rate for PCET was largely due to the additional inner-sphere reorganization associated with transfer of the proton from the phenolic O-H to bulk[18,19]; The computational study of Carra, et al. suggested that the slower PCET rate is due to a larger outer-sphere reorganization barrier and the Franck-Condon overlap factor for the proton[25]. While the concerted transfer of a proton imparts an additional reorganizational barrier to phenol oxidation, internal hydrogen bonding attenuates this effect[20,26]. For example, Rhile et al. reported λ = 34 kcal/mol for the PCET oxidation of an α-alkyl-amino phenol by tri-aryl aminium cations[20,21], which is significantly smaller than the apparent λ for the related tyrosine oxidation[19]. While the above suggests that the $PhO^{\bullet/-}$ ET reaction is subject to a smaller kinetic barrier than that of protonated phenols, it is unclear how this translates to the redox reactivity of metal-coordinated phenolates.

As the cofactors found in GalOx and CAO are proposed to form via oxidation of a copper-tyrosine precursor[27-30], our work was motivated by a desire to understand the ET reactivity of metal coordinated phenolates[31]. For these studies, the roughly square-planar complexes Cu(salxn) (H_2salxn, bis-salicylidinediamine) were synthesized to vary the planarity of the Cu(O_2N_2) center, as well as the more easily oxidized complexes Cu(bppa) (Hbppa, bis-pyridyl phenolamine) and Cu(icoph) (H_2icoph, bis-iminocatechol *o*-phenylenediamine) (Chart 5.1). Cu(salxn) complexes were observed to be efficient energy-transfer quenchers of $Ru(bpy)_3^{2+*}$, likely due to spectral overlap with a copper ligand-field state. In contrast, Cu(bppa) and Cu(icoph) quenched $Ru(bpy)_3^{2+*}$ by electron

transfer, with observed reorganization energy λ = 22 kcal/mol. While this reactivity difference likely arises from the more favorable driving force for electron transfer in the case of Cu(bppa) and Cu(icoph), the large self-exchange reorganization energy calculated for the Cu-coordinated phenolate suggests that the CAO and GalOx cofactors may be poor 1 e^- redox centers.

5.2. Experimental Methods

5.2.1. General considerations

Chemicals were obtained from commercial sources and used without further purification. For the electrochemical and time-resolved studies, CH_2Cl_2 and CH_3CN were dried over calcium hydride and distilled. ^1H NMR spectra were collected using a Bruker Avance 400 HMz NMR spectrometer. Electronic spectra were recorded using a Hewlett Packard 8453 UV-Visible spectrometer. Elemental analyses were performed at the University of Massachusetts Microanalysis Laboratory.

5.2.2. Synthesis

$Ru(bpy)_3(PF_6)_2$, $Ru(dmbpy)_3(PF_6)_2$, and $Ru(dombpy)_3(PF_6)_3$ were prepared according to literature procedures and recrystallized using CH_3CN/ether; $Ru(bpy)_3(PF_6)_3$ was prepared by oxidizing $Ru(bpy)_3^{2+}$ in 7M H_2SO_4 using MnO_2.[32] The complexes Cu(bppa)[17] and Cu(icoph)[33] were produced and purified following literature methods. H_2salen, H_2salpen, H_2salben, and H_2saloph were synthesized through the condensation reaction of 3,5-di*tert*butyl-2-hydroxybenzaldehyde and the appropriate diamine. Copper(II) complexes were produced by adding $Cu(OAc)_2$ to the ligands in ethanol. The resulting compounds were recrystallized in CH_2Cl_2/ether and characterized using elemental analysis.

Cu(salen), Copper (II) *N,N'*-disalicylidene-1,2-ethylenediamine. Cu(salen)•0.5H_2O. Anal. Calcd. for $C_{32}H_{47}N_2CuO_{2.5}$: C, 68.23; H, 8.41; N, 4.97. Found: C, 68.36; H, 8.21; N, 4.96.

Cu(salben), Copper (II) *N,N'*-disalicylidene-1,4-butylenediamine. Anal. Calcd. for $C_{34}H_{50}N_2CuO_2$: C, 70.13; H, 8.65; N, 4.81. Found: C, 69.98; H, 8.67; N, 4.80.

Cu(salpen), Copper (II) *N,N'*-disalicylidene-1,3-propylenediamine. Cu(salpen) •0.5H_2O. Anal. Calcd. for $C_{33}H_{49}N_2CuO_{2.5}$: C, 68.66; H, 8.56; N, 4.85. Found: C, 68.84; H, 8.52; N, 4.80.

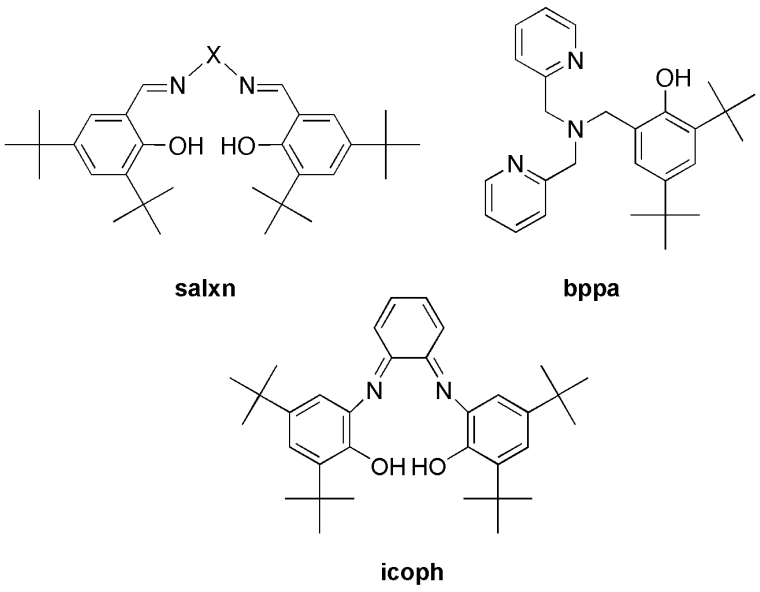

salxn **bppa** **icoph**

Chart 5.1. Ligand structures of bppa, icoph, and salxn, where X = -CH_2CH_2- (salen), -$CH_2CH_2CH_2$- (salpen), or -$CH_2CH_2CH_2CH_2$- (salben).

5.2.3. Electron Paramagnetic Resonance Spectroscopy

X-band (9.764GHz) EPR experiments were performed on a Bruker ESP-300 spectrometer, with a liquid nitrogen finger-dewar used to hold the sample temperature at 77 K. The modulation amplitude was 10 gauss and the frequency 100 kHz. Spectra were collected using 20 mW power. 0.9 mM solutions of Cu(salophen) and Zn(salophen) were

prepared separately in CH_2Cl_2, then combined with an equal volume of 0.9 mM $Ru(bpy)_3^{3+}$ in CH_3CN. The mixtures were immediately transferred to EPR tubes and frozen in liquid nitrogen manually. Simulations were run using XSophe[34].

5.2.4. Electrochemistry

Electrochemical measurements were performed using a Bioanalytical Systems BAS CV-50W potentiostat with a standard three electrode cell. Glassy carbon (working), Pt wire (auxiliary), and Ag/AgCl (reference) electrodes were used. 1 mM solutions of each complex were prepared using CH_3CN or CH_2Cl_2 with 0.1 M of tetra-n-butylammonium hexafluorophosphate (TBA) as the supporting electrolyte and ferrocene as an internal standard. Samples were sparged with Ar before collection.

5.2.5. Emission Lifetimes

Lifetime experiments were performed using a Photon Technology International PL-2300 nitrogen laser at 23 °C. The emission was filtered using a 695 nm filter and detected using a photomultiplier. Decay traces were acquired using a digital oscilloscope triggered by a photodiode. The $Ru(R_2bpy)_3^{2+}$ concentration was approximately 5 μM while the quencher solutions contained $Ru(R_2bpy)_3^{2+}$ with an additional 0.3 mM to 4 mM metal phenolate. Since Cu(bppa) is a positively charged species in solution, 0.1 M TBA was added to attenuate any electrostatic interactions for that sample.

The lifetime of $Ru(R_2bpy)_3^{2+}$ alone, τ_o, was determined for each individual experiment, then aliquots of the quencher solution were transferred via a Hamilton gas-tight syringe to the cuvette, and lifetime measurements taken after each sequential addition. The lifetime values were determined from the slope of semilog plots.[35] The quenching efficiency (K_{SV}) for each quencher was determined from Stern-Volmer plots of

τ_o/τ vs. quencher concentration. The observed quenching rate constants (k_{obs}) were determined from the relationship $k_{obs} = K_{SV} \times \tau_o$ and corrected for the rate of diffusion (k_{diff}) to obtain the diffusion-corrected quenching rate constant, k_q according to the equation $1/k_{obs} = 1/k_{diff} + 1/k_q$.

5.3. Results and Discussion

5.3.1. $Ru(bpy)_3^{3+}$ oxidizes Cu-phenolates

The ET reactivity of metal coordinated phenolates was investigated using EPR as a model for the proposed copper-tyrosine precursors formed in GalOx and CAO. $Ru(R_2bpy)_3^{3+}$ oxidized metal-coordinated phenolates, which was expected from existing literature reports of similar non-coordinated phenolate oxidation.[19-21,36] Cu(salophen) (0.9 mM, CH_2Cl_2) and Zn(salophen) (0.9 mM, CH_2Cl_2) were separately mixed with $Ru(bpy)_3^{3+}$ (0.9 mM, CH_3CN), then added to an EPR tube and quickly frozen in liquid nitrogen. Zn(salophen) exhibited no EPR signal, as expected for this S = 0 ground state (Figure 5.1a); upon reaction with ~1 equivalent of $Ru(bpy)_3^{3+}$, a narrow isotropic signal at g_{eff} ~ 2.01 appeared (Figure 5.1c). This narrow signal is assigned to the phenoxyl radical (S = ½) of $Zn(salophen)^+$. Similarly, Cu(salophen) exhibited an axial signal with fine structure, as expected for a an S = 1/2 Cu^{2+} (Figure 5.1d). This spectrum was simulated with $g_\perp = 2.034$, $g_{||} = 2.196$, and Cu-hyperfine coupling of $A_\perp = 3.0$ mT, $A_{||} = 19.2$ mT (Figure 5.1e) These electronic parameters are similar to those reported for other square-pyramidal Cu(II) complexes with a predominantly $d_{(x2-y2)}$ ground state[37,38]. Oxidation of Cu(salophen) by ~ 1 equivalent of $Ru(bpy)_3^{3+}$ attenuated this Cu^{2+} signal, while a broad g_{eff} ~ 2.1 signal appeared, which we attribute to weak magnetic coupling between Cu^{2+} (S = 1/2) and a phenoxyl radical (S=1/2) on $Cu(salophen)^+$ (Figure 5.1f).

The EPR spectra clearly indicated that $Ru(bpy)_3^{3+}$ oxidized the salophen ligand for both Cu(salophen) and Zn(salophen) to form the metal-coordinated phenoxyl radical. Cyclic voltammetry confirmed that such reactions were exothermic (Table 5.1). As we were interested in the electron-transfer reactivity of metal-phenolates, we attempted to measure the rate constants for metal-phenolate oxidation by stopped-flow methods. These experiments were unsuccessful, largely due to solvent incompatibilities. Rapid mixing of CH_2Cl_2 solutions of Cu-phenolate with CH_3CN solutions of $Ru(R_2bpy)_3^{3+}$ led to extensive turbidity, due to mixing, leading us to abandon this approach in favor of photo-induced experiments.

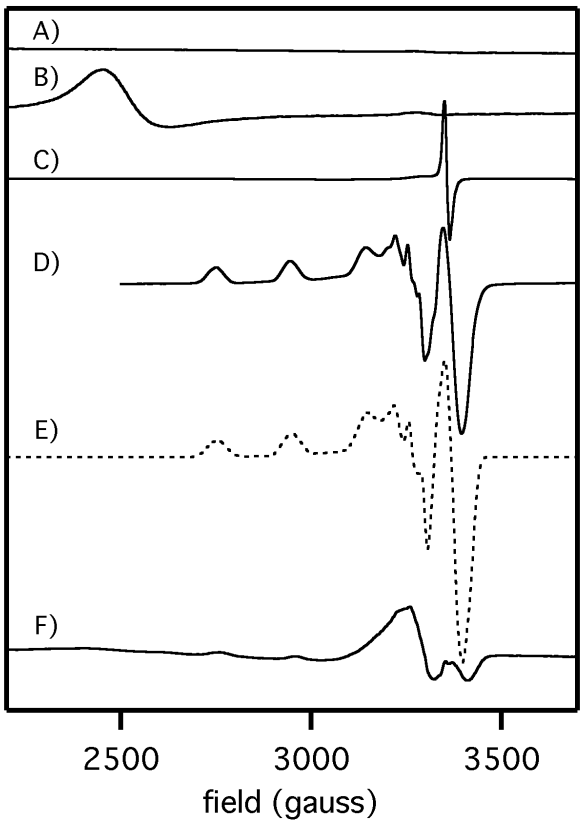

Figure 5.1. 9.764 GHz EPR spectra at 77 K: A) Zn(salophen); B) $Ru(bpy)_3^{3+}$; C) Zn(salophen) mixed with $Ru(bpy)_3^{3+}$ (×0.25); D) Cu(salophen) (×0.75); E) Simulation for Cu(salophen) (×0.75, see text for details); F) Cu(salophen) mixed with $Ru(R_2bpy)_3^{3+}$ (×2).

Table 5.1. Midpoint reduction potentials measured by cyclic voltammetry.

Complex	$E_{1/2}$ (mV)[c]
$Ru(bpy)_3(PF_6)_2$[a]	896
$Ru(dmbpy)_3(PF_6)_2$[a]	737
$Ru(dombpy)_3(PF_6)_2$[a]	566
Cusalen[b]	454
Cusalpen[b]	463
Cusalben[b]	485
Cu(salophen)[b]	549
Zn(salophen)[b]	415
Cu(bppa)[a]	40
Cu(icoph)[b]	-60

[a]CH_3CN, 0.1M TBA; [b]CH_2Cl_2, 0.1M TBA; [c]vs. $Fc^{+/0}$

5.3.2. Quenching of $Ru(bpy)_3^{2+*}$ by Cu(salxn) through energy transfer

The transient fluorescence of $Ru(bpy)_3^{2+*}$ was monitored to determine the mechanism for quenching by Cu(salxn) since the photo-excited has a sufficiently long lifetime. The lowest-lying excited state, $Ru(bpy)_3^{2+*}$, is a charge-separated state conveniently represented as $[Ru(III)(bpy)_2(bpy^-)]^{2+}$ which may be deactivated either by oxidizing Cu(salxn) to form $Ru(bpy)_3^{1+}$, or by energy transfer. As the electron transfer between $Ru(bpy)_3^{2+*}$ and Cu(salxn) would be exothermic, it was expected to form a phenoxyl radical as seen in the oxidation of Cu(salophen) by $Ru(bpy)_3^{3+}$ (Figure 5.1) according to the following reaction (Equation 5.2).

$$Cu(II)(salxn) + Ru(bpy)_3^{2+*} \rightarrow Cu(II)(salxn)^{+\bullet} + Ru(bpy)_3^{1+} \qquad (5.2)$$

The fluorescence lifetime of $Ru(bpy)_3^{2+*}$ was efficiently quenched by Cu(salxn), yielding concentration-dependent quenching data (Figure 5.2). The normalized fluorescence quenching (τ_o/τ) was proportional to the Cu(salxn) concentration, as predicted by the Stern-Volmer equation (Equation 5.3) in which K_{SV} is the quenching efficiency. The linear Stern-Volmer plots indicate a dynamic quenching mechanism, in which a bimolecular collision between Cu(salxn) and $Ru(bpy)_3^{2+*}$ deactivates the excited state.

$$\tau_o/\tau = 1 + K_{SV}[\text{Cu(salxn)}] \qquad (5.3)$$

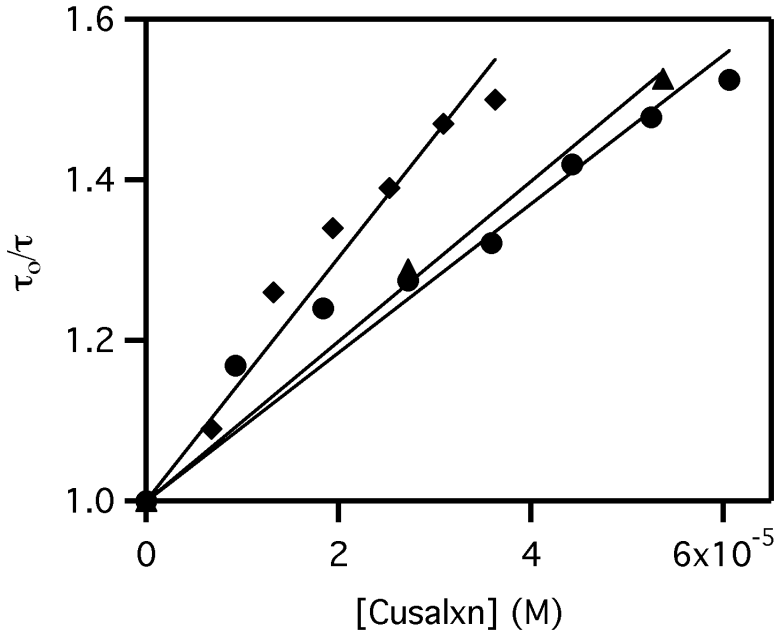

Figure 5.2. Time-resolved Stern-Volmer data of $Ru(bpy)_3^{2+*}$ quenching by Cu(salen) (▲); Cu(salpen) (◆); Cu(salben) (●); see text for details.

Table 5.2 lists the quenching data for Cu(salxn) complexes, indicating that the observed rate constants approach the rate of diffusion. Furthermore, the observed quenching rates for Cu(salxn) displayed no discernable dependence on driving force over the modest range of 4 kcal/mol spanned by this series, suggesting that Cu(salxn)

quenched $Ru(bpy)_3^{2+*}$ either by diffusion-limited electron transfer, or by energy transfer. Treating k_{obs} with Marcus theory (Equation 5.1) indicated that the reorganization energy would need to be very small, $\lambda \sim 10$ kcal/mol, for diffusion limited kinetics. Thus, while thermodynamic arguments indicated that fluorescence quenching could occur by electron transfer, the rates were much faster than anticipated for quenching to occur by bimolecular electron transfer.

Table 5.2. Time-resolved quenching of $Ru(R_2bpy)_3^{2+*}$ by Cu(salxn) in CH_2Cl_2.

Quencher	Sensitizer	k_{obs} ($\times 10^{10}$ M^{-1} s^{-1})	$\Delta G°$ (kcal/mol)
Cusalen	$Ru(bpy)_3^{2+}$	1.7	-3.1
Cusalpen	$Ru(bpy)_3^{2+}$	0.8	-2.9
Cusalben	$Ru(bpy)_3^{2+}$	2.2	-2.4
Cusalen	$Ru(dmbpy)_3^{2+}$	1.7	0.8

Lifetimes in CH_2Cl_2 (μs): $Ru(bpy)_3^{2+}$ (0.6); $Ru(dmbpy)_3^{2+}$ (1.0)

Energy transfer is the more likely mechanism for dynamic quenching of $Ru(bpy)_3^{2+*}$ by Cu(salxn), due to their spectral overlap. Förster and Dexter energy transfer are the two energy transfer mechanisms, with Förster energy transfer requiring spectral overlap between the emission of $Ru(bpy)_3^{2+*}$ and an absorption band of Cu(salxn)[39]. The visible absorption spectra for Cu(salxn) was overlayed with the $Ru(bpy)_3^{2+*}$ emission spectrum (Figure 5.3). A low energy electronic transition in the 570 nm – 670 nm range that is weakly allowed ($\varepsilon \sim 500$ M^{-1} cm^{-1}) is observed for each Cu(salxn), which is appropriate for the ligand-field transition of Cu(II). As the overlap of this absorption with the $Ru(bpy)_3^{2+*}$ emission is considerable, it is likely that this would allow for quenching of $Ru(bpy)_3^{2+*}$ through Förster energy transfer with Cu(salxn).

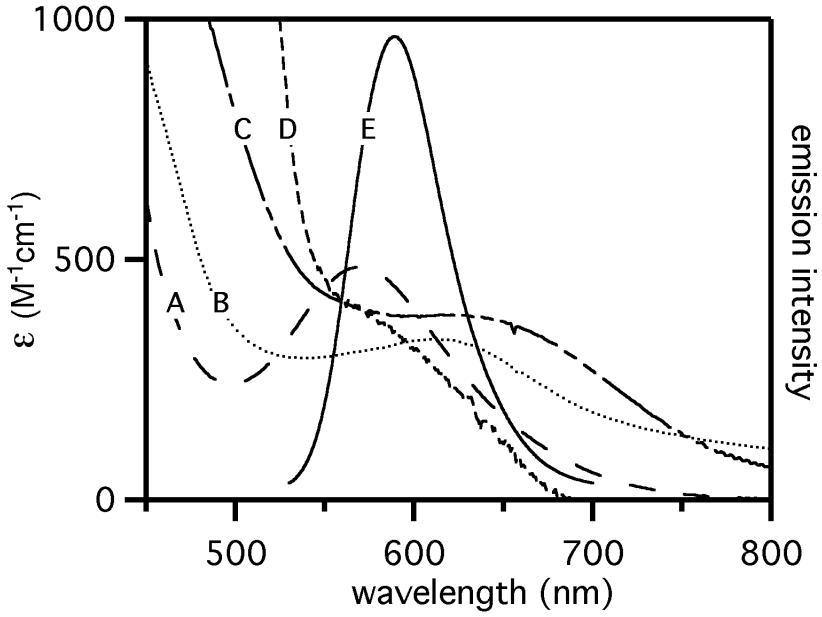

Figure 5.3. Absorption spectrum of Cu(salxn) complexes, A) Cusalen; B) Cusalpen; C) Cusalben; D) Cusalophen; E) Fluorescence of $Ru(bpy)_3^{2+}$.

The excited state lifetime of $Ru(bpy)_3^{2+}$ could have also changed due to complexation with Cu(salxn), as intermolecular aggregation would alter the local solvent environment. Such an effect was observed with phenols, which form a weak adduct with $Ru(bpy)_3^{2+}$ through face-to-face π-π stacking in weakly acidic aqueous solution; binding was enhanced for electron-withdrawing chlorophenols[40]. Complexation with phenol decreased the observed decay rates of $Ru(bpy)_3^{2+*}$, however chlorophenols did not affect the excited-state properties of $Ru(bpy)_3^{2+*}$[41]. We attempted to test for intermolecular complexation by observing the emission spectrum of $Ru(bpy)_3^{2+*}$ in the presence of increasing Cu(salxn) concentrations, and observed no changes in the peak emission wavelength. However, significant inner filter effects due to the absorption of Cu(salxn) would have precluded us from observing small wavelength shifts. As the bulky tert-butyl groups on the Cu(salxn) phenolic rings would strongly disfavor π-π stacking, we consider energy transfer as the more likely mechanism for $Ru(bpy)_3^{2+*}$ quenching by Cu(salxn).

5.3.4. Quenching of $Ru(bpy)_3^{2+*}$ by Cu(bppa), Cu(icoph) through electron transfer

Cu(bppa) and Cu(icoph) are more easily reduced than Cu(salxn), thus their oxidations by $Ru(bpy)_3^{2+*}$ were calculated to be much more favorable (Table 5.3). The reactions of $Ru(bpy)_3^{2+*}$ by Cu(bppa) and Cu(icoph) were monitored by transient fluorescence quenching, with each yielding linear Stern-Volmer plots that indicate a dynamic quenching reaction. The observed quenching rate constants for Cu(bppa) or Cu(icoph) ($k_{obs} \sim 10^9$ $M^{-1}s^{-1}$) were noticeably slower than those observed for Cu(salxn), indicating that diffusion was not rate-limiting in these cases.

Table 5.3. Time-resolved quenching of $Ru(R_2bpy)_3^{2+*}$ by Cu(bppa) and Cu(icoph).

Quencher	Sensitizer	k_{obs} ($\times 10^9$ M^{-1} s^{-1})	k_q ($\times 10^9$ $M^{-1}s^{-1}$)	$\Delta G°$ (kcal/mol)
Cu(icoph)	$Ru(bpy)_3^{2+}$	8.1	18	-14.9
Cu(bppa)	$Ru(bpy)_3^{2+}$	1.1	1.2	-12.6
Cu(icoph)	$Ru(dmbpy)_3^{2+}$	5.8	9.5	-11.1
Cu(bppa)	$Ru(dmbpy)_3^{2+}$	0.95	0.99	-8.8
Cu(bppa)	$Ru(dombpy)_3^{2+}$	1.9	2.1	-5.9

Lifetimes (μs): $Ru(bpy)_3^{2+}$ (0.6, CH_2Cl_2; 1.2; CH_3CN); $Ru(dmbpy)_3^{2+}$ (1.4, CH_2Cl_2; 1.6; CH_3CN); $Ru(dombpy)_3^{2+}$ (0.4; CH_3CN)

The observed rates (k_{obs}) were corrected for the rate of diffusion (k_{diff}) to obtain diffusion-corrected quenching rates (k_q) using $k_q^{-1} = k_{obs}^{-1} - k_{diff}^{-1}$. The diffusion rate was estimated as $k_{diff} = 1.6 \times 10^{10}$ $M^{-1}s^{-1}$ using the Smoluchowski equation (Equation 5.4), in which k_{diff} is a function of the solution viscosity ($\eta = 0.41$ cP for CH_2Cl_2, $\eta = 0.341$ cP for CH_3CN)[42], the radius of $Ru(bpy)_3^{2+}$ ($r_R = 7.1$ Å)[43], and the radius of Cu(bppa) and Cu(icoph) ($r_Q = 5.3$ Å) (Spartan, Wavefunction, Irvine, CA).

$$k_{diff} = \frac{2RT}{3\eta}\left\{2 + \frac{r_R}{r_Q} + \frac{r_Q}{r_R}\right\} \qquad (5.4)$$

The diffusion corrected quenching rates (k_q) of $Ru(bpy)_3^{2+*}$ by Cu(bppa) or Cu(icoph) were correlated with driving force (Table 5.3), as predicted for an electron transfer quenching mechanism. Marcus theory predicts that intermolecular electron transfers will exhibit a parabolic ln k_q vs. $-\Delta G^o$ curve, cresting at $-\Delta G^\circ = \lambda$[24]. Our quenching data (Table 5.3) was fitted to Equation 5.1, yielding λ = 20 (±2) kcal/mol by fixing the collisional rate at $Z = 1.6 \times 10^{10}$ $M^{-1}s^{-1}$. The good fit for the quenching data for Cu(bppa) and Cu(icoph) to the electron transfer model is in direct contrast to the driving-force independent quenching data for Cu(salxn), suggesting that the more favorable driving force for Cu(bppa) and Cu(icoph) makes oxidation much faster than any energy-transfer quenching.

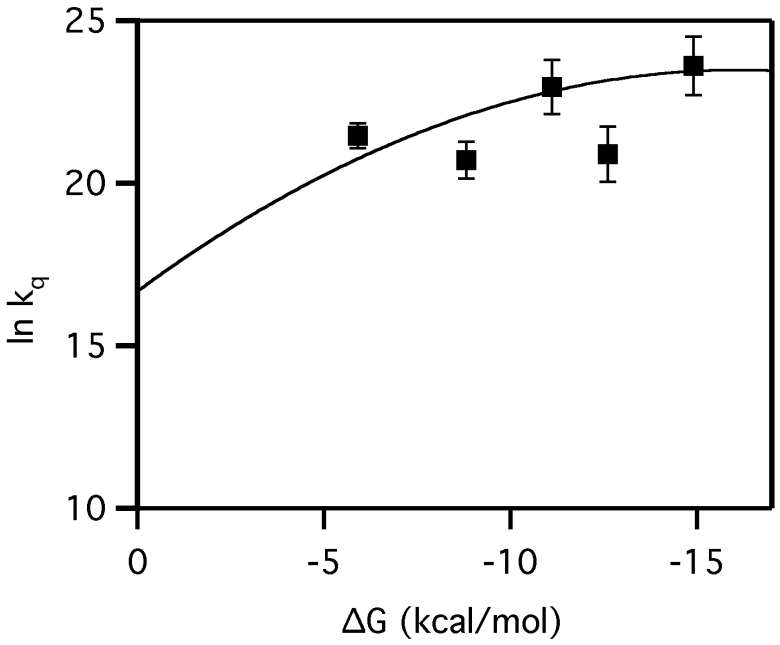

Figure 5.4. Marcus plot for the reaction of Cu(bppa) and Cu(icoph) with $Ru(R_2bpy)_3^{2+*}$; see text for fitting details.

The reorganization energy for the Cu(bppa) and Cu(icoph) oxidations were very similar to those reported for comparable reactions. The oxidation of an appended tyrosine by $Ru(bpy)_3^{3+}$ apparently exhibited λ= 46 kcal/mol[19], however that reaction required the release of a proton to the bulk, leading to a significant additional kinetic barrier[19,25]. At elevated pH, when the tyrosine was deprotonated, the reorganization energy for oxidation by $Ru(bpy)_3^{3+}$ was 22 kcal/mol[19,25]. The oxidation of a substituted phenol with internal hydrogen-bonding by aminium radicals exhibited λ = 34 kcal/mol; while the proton was not released to bulk solvent, the proton-transfer within the internal hydrogen bond would likely impart some additional kinetic barrier[20,21]. The oxidization of substituted phenolates by photo-excited $Ru(NN)_3^{2+*}$ (NN indicates an aromatic diimine) in basic H_2O and H_2O/CH_3CN solution exhibited λ = 25 kcal/mol[22,23]. It is apparent that the reorganization energy for the $Ru(NN)_3^{n+}$ oxidations of deprotonated phenolates by ET are all very similar, with values ranging from λ = 20 – 25 kcal/mol, and much smaller than those for phenol oxidation which require proton transfer in a PCET.

The Marcus cross-relation predicts that the reorganization energy for Cu(bppa) and Cu(icoph) oxidation by $Ru(bpy)_3^{2+*}$ should be the average of the self-exchange reorganization energies: $\lambda = \frac{1}{2}(\lambda_{Ru} + \lambda_{PhO})$[24]. As the reorganization energy for the $Ru(bpy)_3^{2+*}/Ru(bpy)_3^{1+}$ couple is dominantly due to outer-sphere reorganization[32], it is rather small. Marcus described the outer-sphere reorganization energy in terms of a dielectric continuum mode (Equation 5.5)[24,44], in which e is the charge of the electron, r_R is the radius of $Ru(bpy)_3^{2+*}$, and D_{op} and D_S are the optical and static dielectric constants of the solvent. Inserting tabulated values for the dielectric constants into Equation 5.5[42], we calculated that λ_{Ru} = 9 and 12 kcal/mol in CH_2Cl_2 and CH_3CN, respectively.

$$\lambda_{Ru} \approx \lambda_o = e^2\left[\frac{1}{2r_R}\right]\left[\frac{1}{D_{op}}+\frac{1}{D_s}\right] \qquad (5.5)$$

These relationships allow us to estimate the self-exchange reorganization energy for Cu(bppa)$^{+/2+\bullet}$ and Cu(icoph)$^{0+/+\bullet}$ as $\lambda_{PhO\bullet} \approx 30$ kcal/mol, assuming that both complexes have similar values for λ. This implies that, to the extent that these complexes are reasonable models for the Cu-associated tyrosine-derived cofactors found in CAO and GalOx, those proteins may undergo sluggish ET reactions. Typical biological redox proteins, such as those found in cytochromes *c* or azurin, exhibit λ ~ 20 kcal/mol[45], however the specific function of such proteins is to catalyze ET in energy-transformation pathways. As CAO and GalOx catalyze the 2 e^- oxidation of small molecules, one-electron redox reactivity may suppressed to minimize inactivation pathways.

5.4. Conclusions

The reactivity of metal coordinated phenolates was investigated as a model of the proposed copper-tyrosine precursors from the oxidation of GalOx and CAO cofactors. A metal-coordinated phenoxyl radical observable by EPR was formed when Cu(salophen) and Zn(salophen) were oxidized by $Ru(bpy)_3^{3+}$. $Ru(bpy)_3^{2*+}$ was quenched by Cu(salxn) via a dynamic quenching mechanism that was monitored using the transient fluorescence of $Ru(bpy)_3^{2*+}$. Spectral overlap between the photosensitizer and quencher promoted an energy transfer deactivation pathway, as evidenced by observed reaction rates that approached the diffusion limit. In contrast, Cu(bppa) and Cu(icoph) quenched $Ru(bpy)_3^{2+*}$ through electron transfer, as supported by the slower quenching rates that correlated with driving force. Thus, metal phenolates that lack an absorption band in the 500-600 nm region, but are still readily oxidized by $Ru(bpy)_3^{2+*}$ would be ideal

candidates as models for the Cu-associated tyrosine-derived cofactors of GalOx and CAO.

5.5. References Cited

(1) Stubbe, J.; van der Donk, W. A. *Chem. Rev.* **1998**, *98*, 705-762.

(2) Davidson, V. L. *Biochemistry* **2007**, *46*, 5283-5292.

(3) Klinman, J. P. *Biochim. Biophys. Acta, Proteins Proteomics* **2003**, *1647*, 131-137.

(4) Janes, S. M.; Mu, D.; Wemmer, D.; Smith, A. J.; Kaur, S.; Maltby, D.; Burlingame, A. L.; Klinman, J. P. *Science* **1990**, *248*, 981-987.

(5) ITO, N.; Phillips, S. E. V.; Yadav, K. D. S.; Knowles, P. F. *J. Mol. Biol.* **1994**, *238*, 794-814.

(6) Whittaker, M. M.; Whittaker, J. W. *J. Biol. Chem.* **1988**, *263*, 6074-6080.

(7) Rogers, M. S.; Dooley, D. M. *Curr. Opin. Chem. Biol.* **2003**, *7*, 189-196.

(8) Okeley, N. M.; van der Donk, W. A. *Chemistry & Biology* **2000**, *7*, R159-R171.

(9) Rogers, M.; Firbank, S.; Knowles, P.; McPherson, M.; Phillips, S.; Dooley, D. *J. Inorg. Biochem.* **2001**, *86*, 404-404.

(10) Moore, R. H.; Spies, M. A.; Culpepper, M. B.; Murakawa, T.; Hirota, S.; Okajima, T.; Tanizawa, K.; Mure, M. *J. Am. Chem. Soc.* **2007**, *129*, 11524-11534.

(11) Dubois, J. L.; Klinman, J. P. *Biochemistry* **2005**, *44*, 11381-11388.

(12) Klinman, J. P. *Chem. Rev.* **1996**, *96*, 2541-2561.

(13) Itoh, S.; Taki, M.; Takayama, S.; Nagatomo, S.; Kitagawa, T.; Sakurada, N.; Arakawa, R.; Fukuzumi, S. *Angew. Chem. Int. Ed.* **1999**, *38*, 2774-2776.

(14) Wang, Y. D.; DuBois, J. L.; Hedman, B.; Hodgson, K. O.; Stack, T. D. P. *Science* **1998**, *279*, 537-540.

(15) Chaudhuri, P.; Hess, M.; Muller, J.; Hildenbrand, K.; Bill, E.; Weyhermuller, T.; Wieghardt, K. *J. Am. Chem. Soc.* **1999**, *121*, 9599-9610.

(16) Pratt, R. C.; Stack, T. D. P. *Inorg. Chem.* **2005**, *44*, 2367-2375.

(17) Philibert, A.; Thomas, F.; Philouze, C.; Hamman, S.; Saint-Aman, E.; Pierre, J. L. *Chem. Eur. J.* **2003**, *9*, 3803-3812.

(18) Sjodin, M.; Styring, S.; Akermark, B.; Sun, L. C. *Philos. Trans. R. Soc. London, Ser. B* **2002**, *357*, 1471-1478.

(19) Sjodin, M.; Styring, S.; Akermark, B.; Sun, L. C.; Hammarstrom, L. *J. Am. Chem. Soc.* **2000**, *122*, 3932-3936.

(20) Rhile, I. J.; Markle, T. F.; Nagao, H.; DiPasquale, A. G.; Lam, O. P.; Lockwood, M. A.; Rotter, K.; Mayer, J. M. *J. Am. Chem. Soc.* **2006**, *128*, 6075-6088.

(21) Rhile, I. J.; Mayer, J. M. *J. Am. Chem. Soc.* **2004**, *126*, 12718-12719.

(22) Swarnalatha, K.; Rajkumar, E.; Rajagopal, S.; Ramaraj, R.; Lu, Y. L.; Lu, K. L.; Ramamurthy, P. *J. Photochem. Photobiol., A* **2005**, *171*, 83-90.

(23) Thanasekaran, P.; Rajagopal, S.; Srinivasan, C. *J. Chem. Soc., Faraday Trans.* **1998**, *94*, 3339-3344.

(24) Marcus, R. A.; Sutin, N. *Biochim. Biophys. Acta* **1985**, *811*, 265-322.

(25) Carra, C.; Iordanova, N.; Hammes-Schiffer, S. *J. Am. Chem. Soc.* **2003**, *125*, 10429-10436.

(26) Sjodin, M.; Irebo, T.; Utas, J. E.; Lind, J.; Merenyi, G.; Akermark, B.; Hammarstrom, L. *J. Am. Chem. Soc.* **2006**, *128*, 13076-13083.

(27) Mure, M. *Acc. Chem. Res.* **2004**, *37*, 131-139.

(28) Wilce, M. C. J.; Dooley, D. M.; Freeman, H. C.; Guss, J. M.; Matsunami, H.; McIntire, W. S.; Ruggiero, C. E.; Tanizawa, K.; Yamaguchi, H. *Biochemistry* **1997**, *36*, 16116-16133.

(29) Ruggiero, C. E.; Smith, J. A.; Tanizawa, K.; Dooley, D. M. *Biochemistry* **1997**, *36*, 1953-1959.

(30) Dubois, J. L.; Klinman, J. P. *Arch. Biochem. Biophys.* **2005**, *433*, 255-265.

(31) Mahadevan, V.; Gebbink, R. J. M. K.; Stack, T. D. P. *Curr. Opin. Chem. Biol.* **2000**, *4*, 228-234.

(32) Biner, M.; Burgi, H. B.; Ludi, A.; Rohr, C. *J. Am. Chem. Soc.* **1992**, *114*, 5197-5203.

(33) Chaudhuri, P.; Hess, M.; Weyhermuller, T.; Wieghardt, K. *Angew. Chem. Int. Ed.* **1999**, *38*, 1095-1098.

(34) Hanson, G. R.; Gates, K. E.; Noble, C. J.; Griffin, M.; Mitchell, A.; Benson, S. *J. Inorg. Biochem.* **2004**, *98*, 903-916.

(35) Lin, C. T.; Bottcher, W.; Chou, M.; Creutz, C.; Sutin, N. *J. Am. Chem. Soc.* **1976**, *98*, 6536-6544.

(36) Rajendran, T.; Thanasekaran, P.; Rajagopal, S.; Gnanaraj, G. A.; Srinivasan, C.; Ramamurthy, P.; Venkatachalapathy, B.; Manimaran, B.; Lu, K. L. *PCCP* **2001**, *3*, 2063-2069.

(37) Pratt, R. C.; Mirica, L. M.; Stack, T. D. P. *Inorg. Chem.* **2004**, *43*, 8030-8039.

(38) Sokolowski, A.; Leutbecher, H.; Weyhermuller, T.; Schnepf, R.; Both, E.; Bill, E.; Hildebrandt, P.; Wieghardt, K. *J. Biol. Inorg. Chem.* **1997**, *2*, 444-453.

(39) Gilbert, A.; Baggott, J. *Essentials of Molecular Photochemistry*; CRC Press, Inc.: Boca Raton, FL, 1991.

(40) Li, C.; Hoffman, M. Z.; Pizzocaro, C.; Maihot, G.; Bolte, M. *Inorg. Chem.* **1998**, *37*, 3078-3082.

(41) Li, C.; Hoffman, M. Z.; Pizzocaro, C.; Mailhot, G.; Bolte, M. *J. Phys. Chem. A* **1998**, *102*, 7370-7374.

(42) Riddick, J. A.; Bunger, W. B.; Sakano, T. K. *Organic Solvents: Physical Properties and Methods of Purification*; John Wiley and Sons: New York, 1986.

(43) Kitamura, N.; Kim, H. B.; Okano, S.; Tazuke, S. *J. Phys. Chem.* **1989**, *93*, 5750-5756.

(44) Marcus, R. A. *J. Chem. Phys.* **1956**, *24*, 966-978.

(45) Gray, H. B.; Winkler, J. R. *Biological Inorganic Chemistry: Structure and Reactivity*; University Science Books: Sausalito, CA, 2007.

APPENDIX A.

DETERMINATION OF FRACTION BOUND OF CYT *c* TO Au-TX

The fraction of Cyt *c* bound to **Au-TX** was determined from equation X, in which *n* indicates the number of identical, independent binding sites on **Au-TX** and K_D is the dissociation constant of Cyt *c*/**Au-TX**. (*J. Am. Chem. Soc.* **2007**, *129*, 2732-2733)

$$\%bound = \frac{n[Au-TX]+[Cytc]+K_D - \sqrt{(n[Au-TX]+[Cytc]+K_D)^2 - 4n[Au-TX][Cytc]}}{2[Cytc]}$$

For 0.1 M NaCl experiments, K_D and *n* values were determined from previously published ITC data and Table presented later (Appendix D; Table D.1). For experiments with no added salt, K_D and n values were determined from off-exchange experiments: **Au-TAsp** (K_D = 77 nm, n = 5) and **Au-TPhe** (K_D = 137 nm, n = 7). (*J. Am. Chem. Soc.* **2007**, *129*, 2732-2733)

APPENDIX B.

DIFFUSION RATE CALCULATION

The rate of diffusion was calculated using the Smoluchowski equation B.1 (*Coord. Chem. Rev.* **1997**, *159*, 359-373),[2] in which k_{diff} is a function of solution viscosity (η = 0.001 N s m^{-2} at 25 °C), the radius of Co(phen)$_3^{3+}$ (r_A = 0.6 nm), and the radius of **Au-TX** (r_B = 8 nm).

$$k_{diff} = \frac{2RT}{3\eta}\left\{2 + \frac{r_A}{r_B} + \frac{r_B}{r_A}\right\} \qquad \text{(B.1)}$$

Under these experimental conditions, k_{diff} was 2.54×10^{11} M^{-1} s^{-1}. k_{diff} for Cyt *c* (r_A = 1.2 nm) and **Au-TX** was 1.46×10^{11} M^{-1} s^{-1}.

APPENDIX C.

CIRCE EFFECT CALCULATION

The Circe Effect is when enzymes use columbics to electrostatically attract reagents to their surfaces or active sites. (*Advances in Enzymology and Related Areas of Molecular Biology*; John Wiley & Sons, 1975; Vol. 43) The effective reagent concentrations are a function of k_{off} and k_{on}. For this system, k_{off} is ~ 1×10^3 M^{-1} s^{-1} while k_{on} is ~ 1×10^8 M^{-1} s^{-1}. If $k_{on} = k_{off}[\text{Cyt } c][\text{Co(phen)}_3^{3+}]$, each reagent would see an approximate 100-fold concentration increase.

APPENDIX D.

ITC DATA FOR CYT *c* BINDING TO Au-TX

ITC experiments were performed in collaboration with Mrinmoy De et al. Low salt conditions are already published (*J. Am. Chem. Soc.* **2009**, *131*, 3798-9), but high salt conditions are as of yet unpublished and collected here for reference in Table D.1.

Table D.1. Thermodynamics for Cyt *c* binding to **Au-TX** (10 mM Tris, 0.10 M NaCl, pH 7.4) at 30 °C.

Au-TX	K_S (M^{-1})	ΔG (kJ mol^{-1})	ΔH (kJ mol^{-1})	$-T\Delta S$ (kJ mol^{-1})	n
Asp	$3.4 \pm 0.3 \times 10^5$	-32.1	66.3 ± 1.7	-98.3	0.86
Val	$1.0 \pm 0.1 \times 10^5$	-29.0	35.0 ± 2.9	-64.1	1.23
Leu	$1.5 \pm 0.2 \times 10^5$	-30.0	26.6 ± 3.7	-56.6	1.74
Phe	$0.8 \pm 0.1 \times 10^5$	-28.3	25.3 ± 1.1	-53.7	2.54

Complex stability constants (K_S), Gibbs free energy changes (ΔG), enthalpy changes (ΔH), entropy changes ($T\Delta S$), and binding stoichiometries (n) for the complexation of Cyt *c* with **Au-TX**.

APPENDIX E.

MTSSL REACTION WITH A PROTEIN TO FORM A DISULFIDE LINKAGE

Figure E.1. The reaction of MTSSL with a thiol attached to a protein to form a disulfide linkage. (*Biochemistry* **1991**, *30*, 5515-5523)

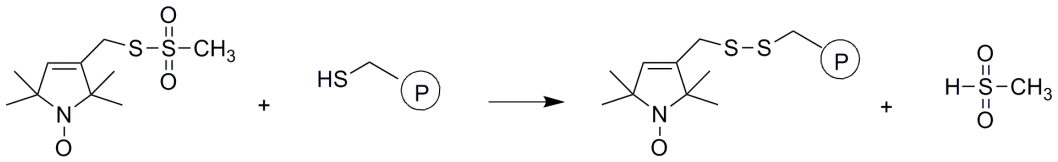

APPENDIX F.

ESTIMATING ERROR OF ROTATIONAL CORRELATION TIMES

Peak intensity and width determine rotational correlation times according to equations 3.1-3.5. The peak intensity and width errors were estimated by recording the small difference in intensities between the individual data points that form the peak. This difference was both added and subtracted from the recorded intensity to give a high (+) and low (-) value of rotational correlation times. A representative set of three different C102 samples and experiments are tabulated below in Table F.1. The high and low values never differed by more than 8%.

Table F.1. Representative data from different C102 samples illustrating the experimental variation in rotational correlation times.

Sample	τ_B (ns)	τ_C (ns)	% error τ_B	% error τ_C
C102-1 (+)	0.880	2.40	8.25	7.65
(-)	0.813	2.23		
C102-2 (+)	0.909	2.51	2.61	6.56
(-)	0.886	2.36		
C102-3 (+)	0.944	2.50	5.30	6.36
(-)	0.896	2.35		

The average rotational correlation times and standard deviations are 0.888 ns (0.0430) and 2.39 ns (0.106) for τ_B and τ_C respectively. Thus, the general error for all rotational correlation times is reported as a generous 0.1 ns.

BIBLIOGRAPHY

Albery, W. J.; Knowles, J. R. *Biochemistry* **1976**, *15*, 5627-31.

Aubin-Tam, M. E.; Hamad-Schifferli, K. *Biomed. Mater.* **2008**, *3*, 034001.

Aubin-Tam, M. E.; Hamad-Schifferli, K. *Langmuir* **2005**, *21*, 12080-4.

Bauer, P. J.; Krause, E. *Biochemistry* **2005**, *44*, 1624-1634.

Bayraktar, H.; Ghosh, P. S.; Rotello, V. M.; Knapp, M. J. *Chem. Commun.* **2006**, 1390-1392.

Bayraktar, H.; You, C. C.; Rotello, V. M.; Knapp, M. J. *J. Am. Chem. Soc.* **2007**, *129*, 2732-2733.

Berliner, L. J. *Spin labeling: theory and applications / edited by Lawrence J. Berliner*; Academic Press: New York, 1976.

Bernhardt, P. V.; Chen, K. I.; Sharpe, P. C. *J. Biol. Inorg. Chem.* **2006**, *11*, 930-936.

Biner, M.; Burgi, H. B.; Ludi, A.; Rohr, C. *J. Am. Chem. Soc.* **1992**, *114*, 5197-5203.

Borbat, P. P.; Surendhran, K.; Bortolus, M.; Zou, P.; Freed, J. H.; McHaourab, H. S. *PLoS Biol.* **2007**, *5*, e271.

Buchaklian, A. H.; Klug, C. S. *Biochemistry* **2005**, *44*, 5503-9.

Byberg, J. R.; Bech Nielsen, B.; Fanciulli, M.; Estreicher, S. K.; Feddres, P. A. *Physical Review B* **2000**, *61*, 12939-12945.

Canters, G. W.; Dennison, C. *Biochimie* **1995**, *77*, 506-15.

Cao, Y. C.; Jin, R.; Nam, J. M.; Thaxton, C. S.; Mirkin, C. A. *J. Am. Chem. Soc.* **2003**, *125*, 14676-7.

Carra, C.; Iordanova, N.; Hammes-Schiffer, S. *J. Am. Chem. Soc.* **2003**, *125*, 10429-10436.

Carven, G. J.; Stern, L. J. *Biochemistry* **2005**, *44*, 13625-13637.

Carver, A. M.; De, M.; Bayraktar, H.; Rana, S.; Rotello, V. M.; Knapp, M. J. *J. Am. Chem. Soc.* **2009**, *131*, 3798-9.

Carver, A. M.; Knapp, M. J. *Polyhedron* **2008**, *27*, 3313-3317.

Cedervall, T.; Lynch, I.; Lindman, S.; Berggard, T.; Thulin, E.; Nilsson, H.; Dawson, K. A.; Linse, S. *Proc. Natl. Acad. Sci. U. S. A.* **2007**, *104*, 2050-5.

Chaudhuri, P.; Hess, M.; Muller, J.; Hildenbrand, K.; Bill, E.; Weyhermuller, T.; Wieghardt, K. *J. Am. Chem. Soc.* **1999**, *121*, 9599-9610.

Chaudhuri, P.; Hess, M.; Weyhermuller, T.; Wieghardt, K. *Angew. Chem. Int. Ed.* **1999**, *38*, 1095-1098.

Clark, C. D.; Hoffman, M. Z. *Coord. Chem. Rev.* **1997**, *159*, 359-373.

Columbus, L.; Hubbell, W. L. *Biochemistry* **2004**, *43*, 7273-87.

Craig, D. B.; Nichols, E. R. *J. Chem. Educ.* **2006**, *83*, 1325-1326.

Crane, J. M.; Mao, C. F.; Lilly, A. A.; Smith, V. F.; Suo, Y. Y.; Hubbell, W. L.; Randall, L. L. *J. Mol. Biol.* **2005**, *353*, 295-307.

Cuello, L. G.; Cortes, D. M.; Perozo, E. *Science* **2004**, *306*, 491-5.

D'Ambrosio, C.; Talamo, F.; Vitale, R. M.; Amodeo, P.; Tell, G.; Ferrara, L.; Scaloni, A. *Biochemistry* **2003**, *42*, 4430-4443.

Daniel, M. C.; Astruc, D. *Chem. Rev.* **2004**, *104*, 293-346.

Davenport, H. E.; Hill, R. *Proc. R. Soc. London, Ser. B* **1952**, *139*, 327-347.

Davidson, V. L. *Acc. Chem. Res.* **2000**, *33*, 87-93.

Davidson, V. L. *Acc. Chem. Res.* **2008**, *41*, 730-738.

Davidson, V. L. *Biochemistry* **2002**, *41*, 14633-6.

Davidson, V. L. *Biochemistry* **2007**, *46*, 5283-5292.

Deweerd, K.; Grigoryants, V.; Sun, Y. H.; Fetrow, J. S.; Scholes, C. P. *Biochemistry* **2001**, *40*, 15846-15855.

Dong, J.; Yang, G.; McHaourab, H. S. *Science* **2005**, *308*, 1023-8.

Dubois, J. L.; Klinman, J. P. *Arch. Biochem. Biophys.* **2005**, *433*, 255-265.

Dubois, J. L.; Klinman, J. P. *Biochemistry* **2005**, *44*, 11381-11388.

Dutton, P. L. *Methods Enzymol.* **1978**, *54*, 411-435.

Fanucci, G. E.; Cafiso, D. S. *Curr. Opin. Struct. Biol.* **2006**, *16*, 644-653.

Fillon, Y.; Verma, A.; Ghosh, P.; Ernenwein, D.; Rotello, V. M.; Chmielewski, J. *J. Am. Chem. Soc.* **2007**, *129*, 6676-6677.

Gilbert, A.; Baggott, J. *Essentials of Molecular Photochemistry*; CRC Press, Inc.: Boca Raton, FL, 1991.

Goldman, S. A.; Freed, J. H.; Bruno, G. V.; Polnasze, C. F. *J. Chem. Phys.* **1972**, *56*, 716-735.

Gray, H. B.; Winkler, J. R. *Annu. Rev. Biochem.* **1996**, *65*, 537-61.

Gray, H. B.; Winkler, J. R. *Biological Inorganic Chemistry: Structure and Reactivity*; University Science Books: Sausalito, CA, 2007.

Gray, H. B.; Winkler, J. R. *Proc. Natl. Acad. Sci. U. S. A.* **2005**, *102*, 3534-9.

Gray, H. B.; Winkler, J. R. *Q. Rev. Biophys.* **2003**, *36*, 341-72.

Guarise, C.; Manea, F.; Zaupa, G.; Pasquato, L.; Prins, L. J.; Scrimin, P. *J. Pept. Sci.* **2008**, *14*, 174-83.

Guarise, C.; Pasquato, L.; De Filippis, V.; Scrimin, P. *Proc. Natl. Acad. Sci. U. S. A.* **2006**, *103*, 3978-82.

Hanson, G. R.; Gates, K. E.; Noble, C. J.; Griffin, M.; Mitchell, A.; Benson, S. *J. Inorg. Biochem.* **2004**, *98*, 903-916.

Hanson, S. M.; Francis, D. J.; Vishnivetskiy, S. A.; Kolobova, E. A.; Hubbell, W. L.; Klug, C. S.; Gurevich, V. V. *Proc. Natl. Acad. Sci. U. S. A.* **2006**, *103*, 4900-5.

Hartleib, J.; Ruterjans, H. *Biochim. Biophys. Acta* **2001**, *1546*, 312-24.

Hazzard, J. T.; Mclendon, G.; Cusanovich, M. A.; Das, G.; Sherman, F.; Tollin, G. *Biochemistry* **1988**, *27*, 4445-4451.

Hegde, B. G.; Isas, J. M.; Zampighi, G.; Haigler, H. T.; Langen, R. *Biochemistry* **2006**, *45*, 934-42.

Herrick, D. Z.; Sterbling, S.; Rasch, K. A.; Hinderliter, A.; Cafiso, D. S. *Biochemistry* **2006**, *45*, 9668-74.

Hesp, J. R.; Raven, N. D.; Sutton, J. M. *Biochem. Biophys. Res. Commun.* **2007**, *362*, 695-9.

Holwerda, R. A.; Knaff, D. B.; Gray, H. B.; Clemmer, J. D.; Crowley, R.; Smith, J. M.; Mauk, A. G. *J. Am. Chem. Soc.* **1980**, *102*, 1142-1146.

Hu, M.; Qian, L.; Brinas, R. P.; Lymar, E. S.; Hainfeld, J. F. *Angew. Chem. Int. Ed.* **2007**, *46*, 5111-4.

Hurst, S. J.; Han, M. S.; Lytton-Jean, A. K.; Mirkin, C. A. *Anal. Chem.* **2007**, *79*, 7201-5.

Hwang, J. S.; Mason, R. P.; Hwang, L. P.; Freed, J. H. *J. Phys. Chem.* **1975**, *79*, 489-511.

Ito, N.; Phillips, S. E. V.; Yadav, K. D. S.; Knowles, P. F. *J. Mol. Biol.* **1994**, *238*, 794-814.

Itoh, S.; Taki, M.; Takayama, S.; Nagatomo, S.; Kitagawa, T.; Sakurada, N.; Arakawa, R.; Fukuzumi, S. *Angew. Chem. Int. Ed.* **1999**, *38*, 2774-2776.

Janes, S. M.; Mu, D.; Wemmer, D.; Smith, A. J.; Kaur, S.; Maltby, D.; Burlingame, A. L.; Klinman, J. P. *Science* **1990**, *248*, 981-987.

Jencks, W. P. *Advances in Enzymology and Related Areas of Molecular Biology*; John Wiley & Sons, 1975; Vol. 43.

Jeuken, L. J. *Biochim. Biophys. Acta* **2003**, *1604*, 67-76.

Jin, X. R.; Abe, Y.; Li, C. Y.; Hamasaki, N. *Biochemistry* **2003**, *42*, 12927-12932.

Juan, H.-F.; Liu, H.-L.; Hsu, J.-P. *Curr. Proteomics* **2004**, *1*, 183-197.

Kang, S. A.; Crane, B. R. *Proc. Natl. Acad. Sci. U. S. A.* **2005**, *102*, 15465-15470.

Katz, E.; Willner, I. *Angew. Chem. Int. Ed.* **2004**, *43*, 6042-6108.

Kellogg, J. A.; Bren, K. L. *Biochim. Biophys. Acta* **2002**, *1601*, 215-221.

Kipp, B. H.; Kelley, P. M.; Njus, D. *Biochemistry* **2001**, *40*, 3931-7.

Kitamura, N.; Kim, H. B.; Okano, S.; Tazuke, S. *J. Phys. Chem.* **1989**, *93*, 5750-5756.

Klein, J. *Proc. Natl. Acad. Sci. U. S. A.* **2007**, *104*, 2029-30.

Klinman, J. P. *Biochim. Biophys. Acta, Proteins Proteomics* **2003**, *1647*, 131-137.

Klinman, J. P. *Chem. Rev.* **1996**, *96*, 2541-2561.

Knowles, J. R. *Nature* **1991**, *350*, 121-4.

Latypov, R. F.; Cheng, H.; Roder, N. A.; Zhang, J.; Roder, H. *J. Mol. Biol.* **2006**, *357*, 1009-25.

Leite, J. F.; Cascio, M. *Biochemistry* **2002**, *41*, 6140-6148.

Lennon, C. W.; Cox, H. D.; Hennelly, S. P.; Chelmo, S. J.; McGuirl, M. A. *Biochemistry* **2007**, *46*, 4850-4860.

Li, C.; Hoffman, M. Z.; Pizzocaro, C.; Maihot, G.; Bolte, M. *Inorg. Chem.* **1998**, *37*, 3078-3082.

Li, C.; Hoffman, M. Z.; Pizzocaro, C.; Mailhot, G.; Bolte, M. *J. Phys. Chem. A* **1998**, *102*, 7370-7374.

Li, C. Y.; Takazaki, S.; Jin, X. R.; Kang, D. C.; Abe, Y.; Hamasaki, N. *Biochemistry* **2006**, *45*, 12117-12124.

Liang, Z. X.; Jiang, M.; Ning, Q.; Hoffman, B. M. *J. Biol. Inorg. Chem.* **2002**, *7*, 580-8.

Liang, Z. X.; Kurnikov, I. V.; Nocek, J. M.; Mauk, A. G.; Beratan, D. N.; Hoffman, B. M. *J. Am. Chem. Soc.* **2004**, *126*, 2785-2798.

Liang, Z. X.; Nocek, J. M.; Huang, K.; Hayes, R. T.; Kurnikov, I. V.; Beratan, D. N.; Hoffman, B. M. *J. Am. Chem. Soc.* **2002**, *124*, 6849-59.

Lin, C. T.; Bottcher, W.; Chou, M.; Creutz, C.; Sutin, N. *J. Am. Chem. Soc.* **1976**, *98*, 6536-6544.

Linse, S.; Cabaleiro-Lago, C.; Xue, W. F.; Lynch, I.; Lindman, S.; Thulin, E.; Radford, S. E.; Dawson, K. A. *Proc. Natl. Acad. Sci. U. S. A.* **2007**, *104*, 8691-6.

Liu, J.; Lu, Y. *Chem. Commun.* **2007**, 4872-4.

Lundqvist, M.; Stigler, J.; Elia, G.; Lynch, I.; Cedervall, T.; Dawson, K. A. *Proc. Natl. Acad. Sci. U. S. A.* **2008**, *105*, 14265-70.

Lynch, I.; Cedervall, T.; Lundqvist, M.; Cabaleiro-Lago, C.; Linse, S.; Dawson, K. A. *Adv. Colloid Interface Sci.* **2007**, *134-135*, 167-74.

Mahadevan, V.; Gebbink, R. J. M. K.; Stack, T. D. P. *Curr. Opin. Chem. Biol.* **2000**, *4*, 228-234.

Mailfait, S.; Belaiche, D.; Kouach, M.; Dallery, J.; Chavatte, P.; Formstecher, P.; Sablonniere, B. *Biochemistry* **2000**, *39*, 2183-2192.

Marcus, R. A. *J. Chem. Phys.* **1956**, *24*, 966-978.

Marcus, R. A.; Sutin, N. *Biochim. Biophys. Acta* **1985**, *811*, 265-322.

Margoliash, E.; Frohwirt, N. *Biochem. J* **1959**, *71*, 570-578.

Marques, H. M. *Dalton Trans.* **2007**, 4371-85.

Marsh, D. In *Biological Magnetic Resonance*; Berliner, L., Ruben, J., Ed.; Plenum: New York, 1989, p 255-303.

Mchaourab, H. S.; Lietzow, M. A.; Hideg, K.; Hubbell, W. L. *Biochemistry* **1996**, *35*, 7692-7704.

Mei, H. K.; Wang, K. F.; Peffer, N.; Weatherly, G.; Cohen, D. S.; Miller, M.; Pielak, G.; Durham, B.; Millett, F. *Biochemistry* **1999**, *38*, 6846-6854.

Mendoza, V. L.; Vachet, R. W. *Anal. Chem.* **2008**, *80*, 2895-2904.

Miller, G. J.; Ball, E. H. *J. Biol. Chem.* **2001**, *276*, 28829-34.

Moore, R. H.; Spies, M. A.; Culpepper, M. B.; Murakawa, T.; Hirota, S.; Okajima, T.; Tanizawa, K.; Mure, M. *J. Am. Chem. Soc.* **2007**, *129*, 11524-11534.

Mure, M. *Acc. Chem. Res.* **2004**, *37*, 131-139.

Myer, Y. P.; Saturno, A. F.; Verma, B. C.; Pande, A. *J. Biol. Chem.* **1979**, *254*, 1202-1207.

Nakanishi, N.; Takeuchi, F.; Park, S. Y.; Hori, H.; Kiyota, K.; Uno, T.; Tsubaki, M. *J. Biosci. Bioeng.* **2008**, *105*, 604-613.

Narindrasorasak, S.; Kulkarni, P.; Deschamps, P.; She, Y. M.; Sarkar, B. *Biochemistry* **2007**, *46*, 3116-3128.

Nelson, W. D.; Blakely, S. E.; Nesmelov, Y. E.; Thomas, D. D. *Proc. Natl. Acad. Sci. U. S. A.* **2005**, *102*, 4000-5.

Niemeyer, C. M. *Angew. Chem. Int. Ed.* **2001**, *40*, 4128-4158.

Njus, D.; Wigle, M.; Kelley, P. M.; Kipp, B. H.; Schlegel, H. B. *Biochemistry* **2001**, *40*, 11905-11.

Nuss, J. E.; Sweeney, D. J.; Alter, G. M. *Biochemistry* **2006**, *45*, 9804-9818.

Oh, E.; Hong, M. Y.; Lee, D.; Nam, S. H.; Yoon, H. C.; Kim, H. S. *J. Am. Chem. Soc.* **2005**, *127*, 3270-1.

Okeley, N. M.; van der Donk, W. A. *Chemistry & Biology* **2000**, *7*, R159-R171.

OhOka, H.; Iwaki, M.; Itoh, S. *Biochemistry* **1997**, *36*, 9267-9272.

Owenius, R.; Osterlund, M.; Lindgren, M.; Svensson, M.; Olsen, O. H.; Persson, E.; Freskgard, P. O.; Carlsson, U. *Biophys. J.* **1999**, *77*, 2237-50.

Peisach, J.; Blumberg, W. E.; Ogawa, S.; Rachmilewitz, E. A.; Oltzik, R. *J. Biol. Chem.* **1971**, *246*, 3342-3355.

Philibert, A.; Thomas, F.; Philouze, C.; Hamman, S.; Saint-Aman, E.; Pierre, J. L. *Chem. Eur. J.* **2003**, *9*, 3803-3812.

Ploemen, J. H. T. M.; Johnson, W. W.; Jespersen, S.; Vanderwall, D.; Vanommen, B.; Vandergreef, J.; Vanbladeren, P. J.; Armstrong, R. N. *J. Biol. Chem.* **1994**, *269*, 26890-26897.

Pollock, W. B. R.; Rosell, F. I.; Twitchett, M. B.; Dumont, M. E.; Mauk, A. G. *Biochemistry* **1998**, *37*, 6124-6131.

Pratt, R. C.; Mirica, L. M.; Stack, T. D. P. *Inorg. Chem.* **2004**, *43*, 8030-8039.

Pratt, R. C.; Stack, T. D. P. *Inorg. Chem.* **2005**, *44*, 2367-2375.

Qin, K.; Yang, Y.; Mastrangelo, P.; Westaway, D. *J. Biol. Chem.* **2002**, *277*, 1981-90.

Qin, P. Z.; Iseri, J.; Oki, A. *Biochem. Biophys. Res. Commun.* **2006**, *343*, 117-24.

Qu, K. B.; Vaughn, J. L.; Sienkiewicz, A.; Scholes, C. P.; Fetrow, J. S. *Biochemistry* **1997**, *36*, 2884-2897.

Rajendran, T.; Thanasekaran, P.; Rajagopal, S.; Gnanaraj, G. A.; Srinivasan, C.; Ramamurthy, P.; Venkatachalapathy, B.; Manimaran, B.; Lu, K. L. *PCCP* **2001**, *3*, 2063-2069.

Redfern, O. C.; Dessailly, B.; Orengo, C. A. *Curr. Opin. Struct. Biol.* **2008**, *18*, 394-402.

Rhile, I. J.; Markle, T. F.; Nagao, H.; DiPasquale, A. G.; Lam, O. P.; Lockwood, M. A.; Rotter, K.; Mayer, J. M. *J. Am. Chem. Soc.* **2006**, *128*, 6075-6088.

Rhile, I. J.; Mayer, J. M. *J. Am. Chem. Soc.* **2004**, *126*, 12718-12719.

Riddick, J. A.; Bunger, W. B.; Sakano, T. K. *Organic Solvents: Physical Properties and Methods of Purification*; John Wiley and Sons: New York, 1986.

Rodkey, F. L.; Ball, E. G. *J. Biol. Chem.* **1950**, *182*, 17-28.

Rogers, M. S.; Dooley, D. M. *Curr. Opin. Chem. Biol.* **2003**, *7*, 189-196.

Rogers, M.; Firbank, S.; Knowles, P.; McPherson, M.; Phillips, S.; Dooley, D. *J. Inorg. Biochem.* **2001**, *86*, 404-404.

Ruggiero, C. E.; Smith, J. A.; Tanizawa, K.; Dooley, D. M. *Biochemistry* **1997**, *36*, 1953-1959.

Runquist, J. A.; Miziorko, H. M. *Protein Sci.* **2006**, *15*, 837-842.

Rush, J. D.; Koppenol, W. H.; Garber, E. A. E.; Margoliash, E. *J. Biol. Chem.* **1988**, *263*, 7514-7520.

Safarian, S.; Moosavi-Movahedi, A. A.; Hosseinkhani, S.; Xia, Z.; Habibi-Rezaei, M.; Hosseini, G.; Sorenson, C.; Sheibani, N. *J. Protein Chem.* **2003**, *22*, 643-54.

Santucci, R.; Reinhard, H.; Brunori, M. *J. Am. Chem. Soc.* **1988**, *110*, 8536-8537.

Schilt, A. A.; Taylor, R. C. *J. Inorg. Nucl. Chem.* **1959**, *9*, 211-221.

Sergi, A.; Ferrario, M.; Polticelli, F.; O'Neill, P.; Desideri, A. *J. Phys. Chem.* **1994**, *98*, 10554-10557.

Sierra-Sastre, Y.; Choi, S.; Picraux, S. T.; Batt, C. A. *J. Am. Chem. Soc.* **2008**, *130*, 10488-9.

Sjodin, M.; Irebo, T.; Utas, J. E.; Lind, J.; Merenyi, G.; Akermark, B.; Hammarstrom, L. *J. Am. Chem. Soc.* **2006**, *128*, 13076-13083.

Sjodin, M.; Styring, S.; Akermark, B.; Sun, L. C. *Philos. Trans. R. Soc. London, Ser. B* **2002**, *357*, 1471-1478.

Sjodin, M.; Styring, S.; Akermark, B.; Sun, L. C.; Hammarstrom, L. *J. Am. Chem. Soc.* **2000**, *122*, 3932-3936.

Snel, M. M. E.; Dekruijff, B.; Marsh, D. *Biochemistry* **1994**, *33*, 7146-7156.

Sokolowski, A.; Leutbecher, H.; Weyhermuller, T.; Schnepf, R.; Both, E.; Bill, E.; Hildebrandt, P.; Wieghardt, K. *J. Biol. Inorg. Chem.* **1997**, *2*, 444-453.

Stubbe, J.; van der Donk, W. A. *Chem. Rev.* **1998**, *98*, 705-762.

Swarnalatha, K.; Rajkumar, E.; Rajagopal, S.; Ramaraj, R.; Lu, Y. L.; Lu, K. L.; Ramamurthy, P. *J. Photochem. Photobiol., A* **2005**, *171*, 83-90.

Thanasekaran, P.; Rajagopal, S.; Srinivasan, C. *J. Chem. Soc., Faraday Trans.* **1998**, *94*, 3339-3344.

Todd, A. P.; Millhauser, G. L. *Biochemistry* **1991**, *30*, 5515-5523.

Turner, B. T.; Sabo, T. M.; Wilding, D.; Maurer, M. C. *Biochemistry* **2004**, *43*, 9755-9765.

Verma, A.; Rotello, V. M. *Chem. Commun.* **2005**, 303-312.

Vugman, N. V.; Giannoni, R. A.; Coelho Neto, J. A. *J. Magn. Reson.* **1997**, *124*, 352-354.

Wade, R. C.; Gabdoulline, R. R.; Ludemann, S. K.; Lounnas, V. *Proc. Natl. Acad. Sci. U. S. A.* **1998**, *95*, 5942-9.

Wallace, C. J. A.; Corradin, G.; Marchiori, F.; Borin, G. *Biopolymers* **1986**, *25*, 2121-2132.

Wallace, C. J. A.; Proudfoot, A. E. I. *Biochem. J* **1987**, *245*, 773-779.

Walter, E. D.; Stevens, D. J.; Visconte, M. P.; Millhauser, G. L. *J. Am. Chem. Soc.* **2007**, *129*, 15440-1.

Wang, Y. D.; DuBois, J. L.; Hedman, B.; Hodgson, K. O.; Stack, T. D. P. *Science* **1998**, *279*, 537-540.

Whittaker, M. M.; Whittaker, J. W. *J. Biol. Chem.* **1988**, *263*, 6074-6080.

Wilce, M. C. J.; Dooley, D. M.; Freeman, H. C.; Guss, J. M.; Matsunami, H.; McIntire, W. S.; Ruggiero, C. E.; Tanizawa, K.; Yamaguchi, H. *Biochemistry* **1997**, *36*, 16116-16133.

You, C. C.; Agasti, S. S.; De, M.; Knapp, M. J.; Rotello, V. M. *J. Am. Chem. Soc.* **2006**, *128*, 14612-14618.

You, C. C.; De, M.; Han, G.; Rotello, V. M. *J. Am. Chem. Soc.* **2005**, *127*, 12873-12881.

You, C. C.; De, M.; Rotello, V. M. *Curr. Opin. Chem. Biol.* **2005**, *9*, 639-46.

Zaupa, G.; Scrimin, P.; Prins, L. J. *J. Am. Chem. Soc.* **2008**, *130*, 5699-5709.

Zheng, G.; Daniel, W. L.; Mirkin, C. A. *J. Am. Chem. Soc.* **2008**, *130*, 9644-5.